

Stefanie Braun

Effect of Impurities on Kinetic Transport Processes in Fusion Plasmas

**IPP 12/7
December, 2010**

EFFECT OF IMPURITIES ON KINETIC TRANSPORT PROCESSES IN FUSION PLASMAS

Inauguraldissertation

zur

Erlangung des akademischen Grades

doctor rerum naturalium (Dr. rer. nat.)

an der Mathematisch-Naturwissenschaftlichen Fakultät

der

Ernst-Moritz-Arndt-Universität Greifswald

vorgelegt von

Stefanie Braun

geboren am 07.04.1983

in Aachen

Greifswald, 24.08.2010

Dekan: Prof. Dr. Klaus Fesser

1. Gutachter: Prof. Dr. Per Helander

2. Gutachter: Prof. Dr. Karl-Heinz Spatschek

Tag der Promotion: 10.12.2010

Abstract

Impurity ions pose a potentially serious threat to fusion plasma performance by affecting the confinement in various, usually deleterious, ways. Due to the creation of helium ash during fusion reactions and the interaction of the plasma with the wall components, which makes it possible for heavy ions to penetrate into the core plasma, impurities can intrinsically not be avoided. Therefore, it is essential to study their behaviour in the fusion plasma in detail. Within the framework of this thesis, different problems arising in connection with impurities have been investigated.

Collisional damping of zonal flows in tokamaks

So-called zonal flows, i.e., poloidally and toroidally symmetric bands of plasma rotation, improve the confinement by reducing radial transport caused by microturbulence. They are subject to a complicated interplay with the turbulence since they are created by the turbulence itself. Other effects, such as collisional damping, can influence the development of this non-linear system significantly. Since the Coulomb collision frequency increases with increasing ion charge, heavy, highly charged impurities play an important role in this process. The effect of such impurities on the linear response of the plasma to an external potential perturbation, as caused by zonal flows, is calculated with analytical methods. The results are compared with numerical simulation, resulting in good agreement. In comparison with a pure plasma, the damping of the flows occurs, as expected, considerably faster; for experimentally relevant parameters, the enhancement exceeds the effective charge Z_{eff} of the plasma.

Impurity transport driven by microturbulence in tokamaks

Fine scale turbulence driven by microinstabilities is a source of particle and heat transport in a fusion reactor. With regard to impurities, it is especially important whether the resulting flows are directed inwards or outwards, since they are deleterious for core energy confinement on the one hand, but on the other hand help protecting plasma-facing components from too high energy fluxes in the edge region. A semi-analytical model is presented describing the resulting impurity fluxes and the stability boundary of the underlying mode. The results are again compared with numerical simulations. The main goal is to bridge the gap between, on the

one hand, costly numerical simulations, which are applicable to a broad range of problems but yield scarcely traceable results, and, on the other hand, analytical theory, which might ease the interpretation of the results but is so far rather rudimentary. The model is based on analytical formulae whenever possible but resorts to a numerical treatment when the approximations necessary for an analytical solution would lead to a substantial distortion of the results. Both the direction of the impurity flux and the stability boundary are found to depend sensitively on the plasma parameters such as the impurity density and the temperature gradient.

Pfirsch-Schlüter transport in stellarators

Due to geometry effects, collisional transport plays a much more prominent role in stellarators than in tokamaks. In the final chapter of this thesis, analytical expressions for the particle and heat fluxes in an impure, collisional plasma are derived from first principles. Contrary to the tokamak case, where collisional transport is exclusively caused directly by friction, in stellarators an additional source of transport exists, namely anisotropy between the pressures parallel and perpendicular to the magnetic field. Whereas this anisotropy term does not contribute much to the overall fluxes at high collisionality since it is then considerably smaller than the friction contributions, it is nonetheless important since it is not ambipolar and therefore of relevance to the ambipolar electric field.

Based on these results, the behaviour of heavy impurity ions under the influence of strong radial temperature and density gradients of the background plasma is studied. It is shown that a redistribution of the impurity ions within each magnetic flux surface arises. This process has previously been found to reduce neoclassical transport in tokamaks, and in this thesis the effect of 3D geometry is studied. Since the resulting partial differential equations are too complicated for an analytical treatment, different limits are considered analytically and the full equation is solved numerically. The redistribution is driven by parallel friction and qualitatively influenced by the radial temperature gradient of the background plasma and the spatially varying $\mathbf{E} \times \mathbf{B}$ rotation due to the radial electric potential. The resulting impurity density patterns on the flux surface are sensitive to the exact geometry of the device and can be determined with the help of numerical databases of the magnetic configurations of different experiments.

Kurzfassung

Verunreinigungen spielen eine wichtige Rolle in Fusionsplasmen, da sie auf verschiedene, üblicherweise schädliche Weise Einfluss auf den Plasmaeinschluss nehmen können. Durch die Entstehung von Heliumasche, die längere Zeit im Plasma verbleibt, während des Fusionsprozesses und die Wechselwirkung des Plasmas mit den Reaktorkomponenten, aufgrund derer schwere Teilchen tief ins Plasma vordringen können, ist die Reinhaltung des Plasmas nahezu unmöglich. Daher ist es wichtig, das Verhalten der vorhandenen Verunreinigungen in Fusionsexperimenten genau zu studieren. In dieser Dissertation wurden verschiedene Effekte, die im Zusammenhang mit Verunreinigungen auftreten, untersucht.

Stoßbehaftete Dämpfung von zonalen Strömungen in Tokamaks

Sogenannte zonale Strömungen, d.h. toroidal und poloidal symmetrische Bänder unterschiedlicher Plasmarotation, begünstigen den Energieeinschluss im Plasma durch Reduktion des durch Mikroturbulenz erzeugten Transports. Sie unterliegen einem komplizierten Wechselspiel, da sie ihrerseits von der Turbulenz, auf die sie rückwirken, erzeugt werden. Andere Einflüsse, wie beispielsweise Stoßdämpfung, können maßgeblich an der Entwicklung dieses nichtlinearen Systems beteiligt sein. Da die Stoßfrequenz für Coulombstöße mit steigender Ionenladung ebenfalls stark ansteigt, spielen schwere, hochgeladene Verunreinigungen eine wichtige Rolle. Der Einfluss solcher Verunreinigungen auf die lineare Antwort des Plasmas auf eine externe Potentialstörung, wie sie durch zonale Strömungen hervorgerufen wird, wird mit Hilfe analytischer Methoden bestimmt und die analytischen Ergebnisse mit numerischen Simulationen verglichen. Im Vergleich zum reinen Plasma erfolgt die Dämpfung, wie erwartet, deutlich schneller. Für experimentell relevante Parameter ist die zu erwartende Dämpfung um einen Faktor, der die effektive Plasmaladung Z_{eff} übersteigt, beschleunigt.

Verunreinigungstransport aufgrund von Mikroinstabilitäten in Tokamaks

Feinskalige Turbulenz, getrieben durch Mikroinstabilitäten, führt zu Teilchen- und Energietransport. Im Bezug auf Verunreinigungen ist es besonders wichtig, ob die Teilchenflüsse nach innen oder außen gerichtet sind, da Verunreinigungen im Kernplasma durch hohe Strahlungsverluste den Energieeinschluss schädigen, während sie durch Abstrahlung am Rand dazu

beitragen, die Reaktorkomponenten vor zu hohen Energieflüssen zu schützen. In dieser Dissertation wird ein semianalytisches Modell für die resultierenden Verunreinigungsflüsse und die Stabilitätsgrenze der zu Grunde liegenden Mode hergeleitet und mit numerischen Simulationen verglichen. Das Hauptziel ist es, eine Brücke zu schlagen zwischen einerseits numerischen Simulationen, die zwar für ein breites Spektrum von Problemen anwendbar sind aber schwer nachvollziehbare Ergebnisse liefern, und andererseits nur ansatzweise vorhandenen analytischen Beschreibungen, welche die Interpretation der Ergebnisse erheblich vereinfachen könnten. Das hergeleitete Modell basiert soweit wie möglich auf analytischen Formeln, greift aber auf numerische Hilfsmittel zurück, wenn die zur Lösung erforderlichen Approximationen die Ergebnisse wesentlich verfälschen würden. Sowohl die Richtung des Verunreinigungsflusses als auch die Stabilitätsgrenze hängen stark von den Plasmaparametern wie Verunreinigungsdichte und Temperaturgradient ab.

Pfirsch-Schlüter-Transport in Stellaratoren

Aufgrund von Geometrieffekten spielt stoßbehafteter Transport in Stellaratoren eine wesentlich größere Rolle als in Tokamaks. In dieser Arbeit werden analytische Ausdrücke für die Teilchen- und Wärmeflüsse in einem stoßdominierten Plasma (Pfirsch-Schlüter-Gebiet) kinetisch hergeleitet. Im Gegensatz zum Tokamak, in dem stoßbehafteter Transport ausschließlich direkt durch Reibung hervorgerufen wird, gibt es im Stellarator eine zusätzliche Transportquelle durch Druckanisotropie parallel und senkrecht zum magnetischen Feld. Obwohl dieser Anisotropieterm bei hohen Stoßfrequenzen deutlich kleiner ist als der Reibungsterm und daher nur geringfügig zum Gesamttransport beiträgt, spielt er aufgrund der Tatsache, dass er im Gegensatz zum Reibungsterm nicht ambipolar ist, eine wichtige Rolle in Bezug auf das ambipolare radiale elektrische Feld.

Aufbauend auf diesen Ergebnissen wird das Verhalten von schweren Verunreinigungen unter dem Einfluss von starken radialen Temperatur- und Dichtegradienten des Hintergrundplasmas untersucht, die zu einer Umverteilung der Verunreinigungen innerhalb der magnetischen Flussflächen führen. In Tokamaks führt diese Umverteilung zu einer Verminderung des neoklassischen Transports, und in dieser Dissertation wird der Effekt von 3D-Geometrie untersucht. Da die resultierenden partiellen Differentialgleichungen für Stellaratoren analytisch nicht mehr lösbar sind, werden verschiedene Grenzwerte analytisch betrachtet und die volle Gleichung numerisch gelöst. Der der Umverteilung zu Grunde liegende Mechanismus ist parallele Reibung. Sowohl der radiale Temperaturgradient des Hintergrundplasmas als auch die durch das radiale elektrische Potential hervorgerufene $\mathbf{E} \times \mathbf{B}$ -Rotation, die auf der Flussfläche variiert, beeinflussen den Prozess qualitativ. Die entstehenden Dichtestrukturen sind stark von der Geometrie der Maschine abhängig und können mit Hilfe numerischer Datenbanken der Magnetfeldkonfigurationen verschiedener Experimente entsprechend bestimmt werden.

Contents

1	Introduction	1
1.1	Nuclear Fusion	1
1.2	Magnetic confinement	2
1.2.1	Tokamaks	2
1.2.2	Stellarators	3
1.2.3	Flux surfaces	4
1.2.4	The high-confinement mode	6
1.3	Transport processes in fusion plasmas	8
1.3.1	Charged particle motion	8
Gyromotion	8	
Drift motion	9	
Guiding centre orbits	10	
1.3.2	Collisional transport	12
1.3.3	Turbulent transport	13
Microinstabilities	14	
Zonal flows	15	
1.4	Role of impurities	15
1.5	Contribution of this thesis	17
2	Basics of kinetic transport theory	19
2.1	Quasi-neutrality	19
2.2	Distribution functions	19
2.3	Kinetic equations	21
2.3.1	Gyro-average	22
2.3.2	Flux-surface average	23
2.3.3	Drift kinetic equation	23
2.3.4	Gyrokinetic equation	25
2.4	Collision operator	29
2.4.1	Linearised collision operator	30
2.4.2	Other approximate collision operators	31
Disparate mass ratio	31	
Self collisions	32	
2.5	Fluid description	33

2.6	Intrinsic ambipolarity	36
2.7	Coordinate systems	36
2.7.1	Coordinates for axisymmetric systems	37
2.7.2	Coordinates for full 3D geometry	38
3	Aspects of impurity transport in Tokamaks	41
3.1	Effect of impurities on collisional zonal-flow damping in tokamaks	41
3.1.1	Rosenbluth-Hinton problem	41
Polarisation of the plasma	42	
Time evolution, Rosenbluth-Hinton test	42	
3.1.2	Basic equations	44
3.1.3	Kinetic equation	44
3.1.4	Neoclassical polarisation	46
3.1.5	Collisionless response	49
3.1.6	Collisional potential response	52
Impurities	53	
Bulk ions	59	
3.1.7	Long-time limit	62
3.1.8	Comparison with numerical simulation	65
3.1.9	Arbitrary source term	69
3.1.10	Physical interpretation and conclusions of section 3.1	72
3.1.11	Appendix: Expression for the drift velocity	73
3.2	Effect of impurities on ITG driven microinstabilities	75
3.2.1	Perturbed density responses	75
Electron response	76	
Perturbed ion response	80	
Perturbed impurity response	81	
3.2.2	Quasilinear impurity flux	81
3.2.3	Stability	83
3.2.4	Conclusions of section 3.2	85
4	Aspects of impurity transport in Stellarators	87
4.1	Impurity Pfirsch-Schlüter transport in Stellarators	88
4.1.1	Expansion of the kinetic equation	89
4.1.2	Radial particle transport	100
4.1.3	Ambipolarity	101
4.1.4	Heat flux	104
4.1.5	Conclusions of section 4.1	105
4.1.6	Appendix: Coefficients of the distribution functions	105
4.2	Pfirsch-Schlüter transport in the presence of large gradients	107
4.2.1	Kinetic equations	108

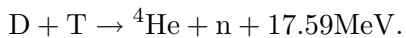
4.2.2	Analytical limits	112
	Weak radial gradients	112
	Large radial gradients, vanishing radial electric field	113
4.2.3	Numerical solution of the full problem	115
4.2.4	Discussion	122
4.2.5	Conclusions & Summary of section 4.2	122
5	Summary & Outlook	125
	List of Figures	135
	List of Symbols	137
	Curriculum Vitae	147
	List of Publications	149
	Acknowledgments	151

1 Introduction

This thesis is concerned with the effect of impurities on transport processes in fusion reactors. The impurities in question are heavy ions that usually originate from the vessel containing the plasma. The present introductory chapter is intended to give a fundamental overview of the physical background of the addressed topics and to enable the reader to place the work into context. A more mathematical treatment of the kinetic theory upon which the following chapters are based is given in chapter 2. The subsequent chapters deal with several different aspects of impurities as further described in section 1.5. In the concluding chapter, the results are summarised and discussed, and an outlook on future work is given.

1.1 Nuclear Fusion

The Sun constantly releases energy at a rate of approximately $3.85 \cdot 10^{17}$ GW [1]. Exploiting the underlying process, nuclear fusion, for harnessing energy provides an extremely powerful but no less challenging option for the solution of mankind's energy problem. Whereas the reaction in the Sun, taking place under conditions of extremely high temperature, density and gravitational force, is fuelled by hydrogen, the reaction with the highest cross section under the circumstances we can reach on Earth is [2]



The released energy corresponds to the difference between the total masses of reactants, the two hydrogen isotopes deuterium and tritium, and the reaction products, helium and a neutron, according to Einstein's famous formula $E = \Delta mc^2$. As this atomic process involves the strong nuclear force, the amount of energy released in a single fusion reaction is six orders of magnitude higher than in chemical reactions, taking place when, e.g., fossil fuels are burned. The reaction cross section for the above mentioned reaction peaks at a temperature between 10–20 keV [2], and under these conditions the fusion reactants form a plasma. However, in order for the fusion reaction to take place, the strong repulsive Coulomb force has to be overcome, which makes ordinary Coulomb collisions the most likely event to happen in a D-T collision. Although quantum-mechanical tunnelling makes the fusion reaction nonetheless possible, it is necessary to confine the plasma long enough for many particle collisions to

1. INTRODUCTION

happen before the particles get lost. In the Sun and other stars, confinement is provided by their huge gravitation, which our experiments on Earth lack. However, as a plasma mainly consists of freely moving charged particles, it is influenced by magnetic fields, forcing the plasma particles to gyrate around the field lines via the Lorentz force, and can therefore be confined in a magnetic cage.

1.2 Magnetic confinement

The simplest conceivable concept for a magnetic geometry confining a plasma is a straight cylinder with homogeneous magnetic field strength. Whereas the gyromotion of the particles around the field lines (see section 1.3.1) provides radial confinement, the particles may move freely along the field lines, and a means has to be found to avoid end losses. Many different concepts have been tried, such as using inhomogeneous magnetic fields so as to exploit the magnetic mirror effect, e.g., closing the ends with so-called *Baseball coils*. However, most of these attempts with linear geometry did not lead to satisfactory confinement or raised other problems (e.g., instabilities), and the great majority of present experiments are based on the far more successful approach of a toroidal device. Incidentally, the naive approach of bending the linear device into torus shape does not work as it leads to radial particle drifts (see section 1.3.1), which spoil confinement. This problem can be overcome by introducing a *rotational transform* ι by superimposing a poloidal magnetic field on the toroidal one¹. This leads to a poloidal shift of the field lines after one toroidal turn, and thus, instead of closing on themselves, they move around the torus, allowing particles to drift towards the centre on one side of the torus and away from the centre on the other. Consequently, the net particle drift vanishes. The two most prominent concepts for creating such magnetic fields that have been proposed and proven successful in experiments are the tokamak and the stellarator.

1.2.1 Tokamaks

The tokamak concept (see fig. 1.1) was proposed by Tamm and Sakharov in 1952 [3], the name being an acronym for the Russian word “toroidal’naya kamera s magnitnymi katushkami” - toroidal chamber with magnetic coils. In this axisymmetric configuration, the toroidal magnetic field is produced by external coils, whereas the poloidal magnetic field is induced by using the plasma itself as the secondary coil of a transformer. A drawback is that, due to the pulsed nature of the transformer, steady-state operation is intrinsically not possible. Furthermore, the vacuum field does not provide confinement as the current in the plasma itself is necessary to create the poloidal component of the magnetic field. Therefore, if the plasma current disappears because of a plasma instability (a so-called disruption), confinement is immediately lost,

¹The toroidal direction is around the major axis of the torus, whereas the poloidal direction describes the direction around the torus’ minor axis.

which can lead to severe damage of the plasma-facing components in a reactor. Nonetheless, the tokamak concept has been proven very successful, mainly due to its simple axisymmetric geometry, and today's leading fusion devices are tokamaks, such as JET (Joint European Torus) at Culham, Great Britain, and the big international project ITER (International Thermonuclear Experimental Reactor) which is currently under construction at Cadarache, France.

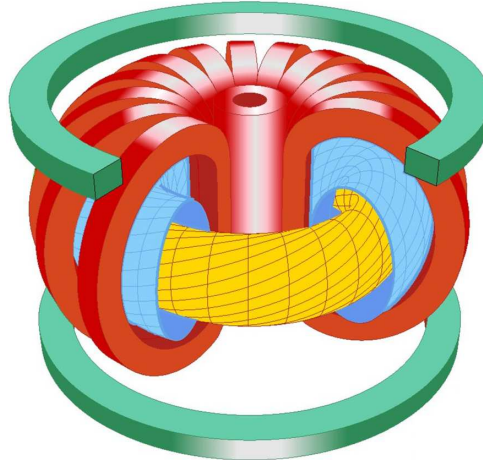


FIGURE 1.1 Schematic sketch of the plasma and coils of a tokamak [4].

1.2.2 Stellarators

The stellarator² concept (see fig.1.2), proposed by Lyman Spitzer in 1951, differs fundamentally from the tokamak in that the entire magnetic field is produced by external coils. Although the geometry of the device is thereby complicated considerably (no axisymmetry, thus full 3D geometry), it does not suffer from the tokamak's drawbacks regarding steady-state operation, which is intrinsic in the stellarator, and current disruptions, as no toroidal current is necessary in the plasma. Although the stellarator looks at first glance like a “cleaner” concept as one needs not worry about these issues, it is lagging behind the tokamak by approximately one generation as much research has focussed almost exclusively on the much-simpler-to-build tokamak. The main stellarator experiment which might play a role in the decision whether DEMO, the first prototype reactor planned for the early mid century, will be a tokamak or a stellarator, is W7-X, which is currently under construction in Greifswald, Germany.

²from Latin stella - the star

1. INTRODUCTION

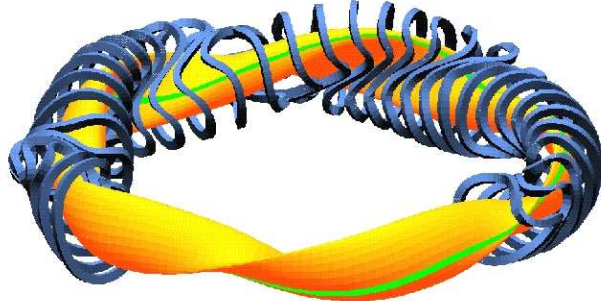


FIGURE 1.2 Plasma and non-planar coils of the future stellarator W7-X [4].

1.2.3 Flux surfaces

In tokamak equilibria, it can be shown that most magnetic field lines ergodically cover surfaces of constant pressure and constant magnetic flux, which are therefore referred to as *flux surfaces*. These flux surfaces form nested tori, and whereas particle and heat transport *within* the flux surface (i.e., along the magnetic field lines) is usually a very fast process, transport *across* flux surfaces occurs on a much slower time scale in well-confined plasmas. The confined region is enclosed by a last closed flux surface (separatrix), leading to the formation of an x point (see fig. 1.3), and the plasma outside this region, the so-called *scrape-off layer* (SOL), is characterised by open field lines. In stellarators, the existence of nested flux surfaces cannot be proven mathematically, although there is numerical and experimental evidence (Poincaré plots) that they usually exist to a very high degree of accuracy. However, this is not always true. The rotational transform is usually not the same on different flux surfaces but varies radially (magnetic shear). Surfaces where ι takes on a rational value, so-called *rational surfaces*, are very sensitive to perturbations which have a resonant symmetry with the flux surface. The consequence is magnetic islands, i.e. structures *within* the confined region, separated from the rest of the plasma via a separatrix. Islands are deleterious for plasma confinement since particles and heat can quickly flow in the radial direction *along* the field lines, thereby degrading the confinement of the system. As both the poloidal and the toroidal magnetic flux lying within one flux surface are constant, they can be used as a label for the corresponding flux surface. Therefore, the *poloidal magnetic flux function* ψ , defined by the magnetic flux passing through a cross section between the magnetic axis and the corresponding flux surface, may serve as a radial coordinate. Functions which only depend on this flux label but do not vary *within* the flux surface are called *flux functions*. The innermost (degenerate) flux surface is called the *magnetic axis*; the major radius R_0 of the device is the distance between the torus axis and the magnetic axis. The minor radius a of the device is the distance between the magnetic axis and the torus edge. In a stellarator, where these distances can vary, appropriate

1.2. MAGNETIC CONFINEMENT

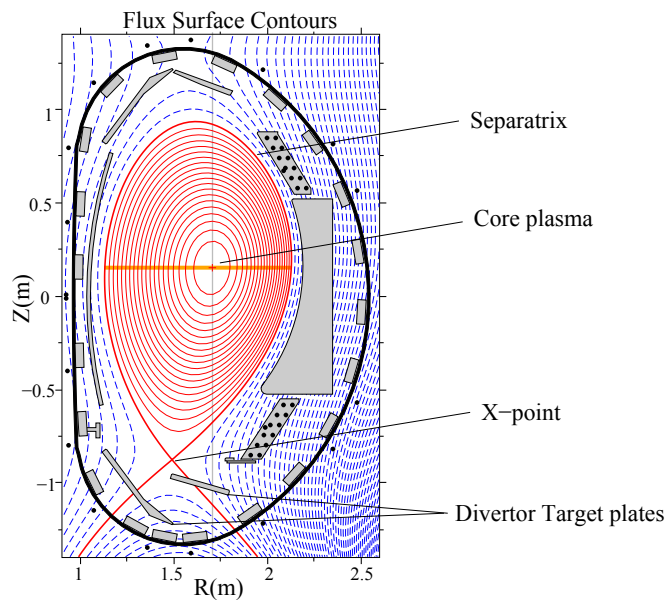


FIGURE 1.3 Nested flux surfaces plus separatrix (red) and scrape-off layer (blue) in a tokamak [4].

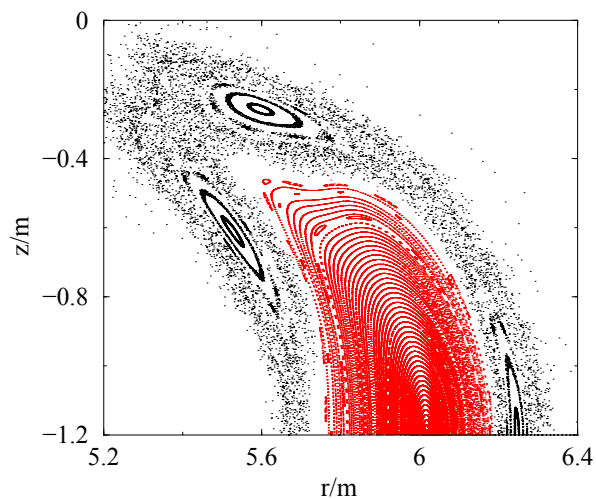


FIGURE 1.4 Magnetic island formation in a stellarator (Source: Michael Drevlak).

1. INTRODUCTION

averages have to be used. Each flux surface is then characterised by a local minor radius r , which defines its distance to the magnetic axis, and a local major radius R defining the distance of the flux surface's mid point to the torus axis. Again, appropriate averages have to be used for stellarators, the exact definition of which is of no importance for the calculations presented in this thesis. The ratio between the minor and the major radius is called the *inverse aspect ratio* $\epsilon \equiv r/R$, which is often used as a small parameter in asymptotic expansions. Depending on the device, the value of ϵ at the edge can range from nearly unity in so-called *spherical tokamaks* to around 0.3 in large aspect-ratio tokamaks and even smaller values in stellarators. In the core of the plasma ϵ is of course smaller and vanishes at the magnetic axis. The toroidal and poloidal angles are usually denoted by φ and θ , respectively (the coordinate system will be discussed in more detail in section 2.7), see fig. 1.5.

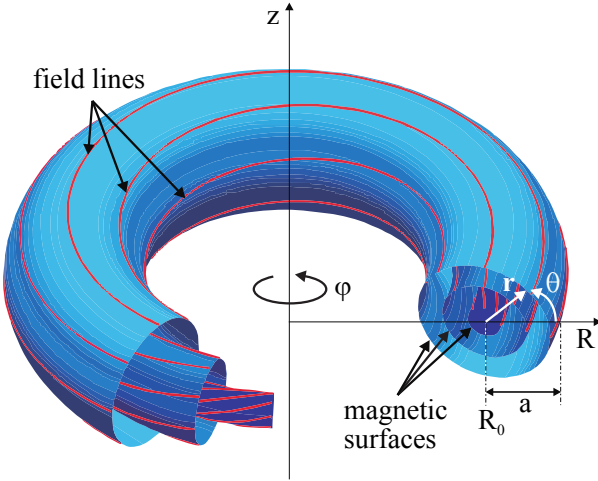


FIGURE 1.5 Illustration of the geometric quantities [4].

1.2.4 The high-confinement mode

Experiments have shown the existence of different operating regimes in magnetic confinement devices. This phenomenon was first discovered on ASDEX (Axial Symmetric Divertor Experiment) at Garching in 1982 [5] and subsequently on various other tokamaks and stellarators. When the heating power exceeds a certain threshold, the plasma may undergo a sudden transition to a higher confinement regime, where the energy confinement time $\tau_E \equiv W_{\text{Plasma}}/P_{\text{heating}}$, defined as the ratio between the energy stored in the plasma and the external heating power, is found to be typically around twice that of the previous regime of low confinement [6]. This high confinement regime is usually referred to as the H-mode, in contrast to the L-mode of low confinement. Although the H-mode was discovered already

more than 25 years ago, the reasons for this phenomenon are as yet mostly unclear, and a fundamental theory on the mechanisms driving the L-H transition is lacking. Nonetheless, many important characteristics of the H-mode have been studied. The most prominent feature is the occurrence of very steep radial density and often also temperature gradients in the edge region, thus forming a pedestal, which acts as a transport barrier. Fig. 1.6 shows such an evolution of the density gradient during L-H transition in the TJ-II stellarator at CIEMAT, Spain. First, the density gradient is rather flat (red curve); the plasma is still in L-mode. Subsequently, the gradient steepens during the L-H transition, until finally, in H-mode, the pedestal has formed (black curve). This occurrence of edge barriers leads to an increase in density over

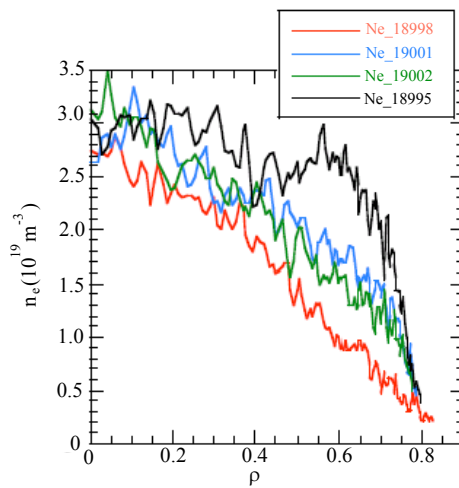


FIGURE 1.6 Evolution of the electron density profile during L-H transition in TJ-II vs. the normalised minor radius ρ . The different curves correspond to different transition states during different shots (the corresponding shot numbers are given in the legend) [7].

the whole plasma with improved confinement properties. Another characteristic feature is a sharp drop of the level of turbulence right at the formation of the transport barrier, leading to a reduction of the turbulent fluxes. Both turbulent and neoclassical effects (see also sections 1.3.2 and 1.3.3) or an interplay of both, are possible candidates in the riddle of the H-mode formation. For a more detailed treatment of the H-mode, see [8]. The H-mode is nowadays the most favoured operating regime, and the most promising experimental results regarding fusion power output have been obtained in this regime. However, there are a couple of difficulties. Apart from the fact that the density increase can lead to a transition back to L-mode, the enhanced confinement also includes impurities, which can start accumulating in the centre

1. INTRODUCTION

and lead to radiation losses (see also section 1.4). This problem is eased by the occurrence of so-called Edge-Localised Modes (ELMs), an instability which manifests itself in sudden bursts from the plasma, leading to large fluxes out of the core region and thus “flushing out” the impurities. However, they are accompanied by immense energy fluxes and might cause severe damage to the plasma facing components, a problem which has yet to be overcome. In this regard, the behaviour of impurities under H-mode operation is a very important issue, and one aspect of this problem will be addressed in section 4.2.

1.3 Transport processes in fusion plasmas

One of the main topics of fusion research is the study of plasma transport processes. This section presents a basic overview of the different mechanisms; a more mathematical treatment of kinetic transport theory will be given in section 2. In principle, there are two fundamentally different sources of transport in plasmas, one being collisional transport, which arises due to Coulomb collisions between the particles, and the other being turbulent fluctuations in the plasma. However, before the different transport processes are described in more detail, a few words have to be said about charged particle motion in fusion plasmas.

1.3.1 Charged particle motion

The collisionless motion of charged particles in fusion devices is in general rather complicated. Effects arising from the toroidicity, such as particle drifts or trapping, and from other inhomogeneities in the magnetic field that occur in stellarators, are superimposed on the gyromotion, which can also be found in cylindrical geometry. These effects become extremely important as they drive so-called *neoclassical transport* (see section 1.3.2), whereas *classical transport* is driven by the gyromotion. The most important mechanisms of particle motion are presented in this section.

Gyromotion

As already mentioned in section 1.1, the most basic mechanism behind radial particle confinement in a magnetic field is the gyromotion of the particles due to the Lorentz force, given by the equation of motion

$$m_a \frac{\partial \mathbf{v}}{\partial t} = e_a \mathbf{v} \times \mathbf{B}, \quad (1.1)$$

where m_a is the mass of a particle of species a , e_a its charge and \mathbf{B} the magnetic field vector. Assuming a homogeneous, constant magnetic field, where without loss of generality

$\mathbf{B} = B_z \mathbf{e}_z$ in a Cartesian coordinate system $\mathbf{e}_x, \mathbf{e}_y, \mathbf{e}_z$, one can identify velocity components parallel and perpendicular to the magnetic field [6]

$$\begin{aligned} v_x &= v_{\perp} \sin(\Omega_a t), \\ v_y &= v_{\perp} \cos(\Omega_a t), \\ v_z &= v_{\parallel}. \end{aligned}$$

This set of equations describes a circular gyromotion around the so-called *guiding centre* of the particle, which moves uniformly along the magnetic field line at the speed v_{\parallel} . Here and throughout the thesis, parallel and perpendicular refer to the directions along and perpendicular to the magnetic field, respectively. The gyration frequency is $\Omega_a = e_a B / m_a$ and the orbit radius $\rho_{L,a} = v_{\perp} / \Omega_a$ is called the *Larmor radius*. For a particle moving at the thermal speed $v_{th,a} \equiv \sqrt{2T_a/m_a}$, where T_a denotes its temperature³, in the perpendicular direction, $\rho_{L,a} = v_{th,a} / \Omega_a \equiv \rho_a$. The guiding-centre position is typically denoted by $\mathbf{R} \equiv \mathbf{r} + \mathbf{v} \times \mathbf{b} / \Omega_a$, where the actual particle position is denoted by \mathbf{r} . The unit vector along the magnetic field is denoted by $\mathbf{b} \equiv \mathbf{B} / B$. The Lorentz force is charge dependent, and electrons gyrate clockwise while positively charged ions gyrate counter-clockwise.

Drift motion

In the presence of external forces or fields perpendicular to the magnetic field, eq. (1.1) has to be extended by adding the corresponding force terms on the right-hand side. The original solution to the equation of motion is then modified in the way that additional drift terms occur, describing a motion of the guiding centre perpendicular to both the magnetic field and the driving force. Inhomogeneities of the magnetic field, which occur naturally in toroidal devices, also give rise to drifts. The most prominent drifts usually kept in kinetic calculations lead to an approximate perpendicular drift velocity

$$\mathbf{v}_d = \frac{\mathbf{E} \times \mathbf{B}}{B^2} + \frac{v_{\perp}^2}{2\Omega_a} \frac{\mathbf{B} \times \nabla B}{B^2} + \frac{v_{\parallel}^2}{\Omega_a} \frac{\mathbf{B} \times \boldsymbol{\kappa}}{B},$$

where \mathbf{E} is the electric field and $\boldsymbol{\kappa} \equiv (\mathbf{b} \cdot \nabla) \mathbf{b}$ is the magnetic curvature. The three terms are usually called $\mathbf{E} \times \mathbf{B}$ drift, grad- B drift and curvature drift, respectively. It is important to note that this expression for the drift velocity is only valid for weak electric fields, since the derivation of the expression is based on the assumption that the perpendicular parts of the gyroorbits nearly close on themselves after one gyration, which is only the case if the $\mathbf{E} \times \mathbf{B}$ drift over one Larmor period is much smaller than the Larmor radius itself.

³Here and throughout the rest of the thesis, temperature is measured in units of energy, thereby implicitly including the Boltzmann factor.

1. INTRODUCTION

Guiding centre orbits

In an inhomogeneous magnetic field, as it naturally occurs in toroidal devices, the guiding-centre motion is more complicated than in a uniform magnetic field. Particles with a sufficiently large parallel velocity component circulate continually around the torus and are usually referred to as *passing* or *circulating particles*. On the other hand, the *mirror force* $F_{\text{mirror}} = -\mu \nabla_{\parallel} B$, $\nabla_{\parallel} B \equiv (\mathbf{B} \cdot \nabla)/B$, caused by variations of the magnetic field strength, leads to a reflection of particles with small parallel velocity as such particles cannot penetrate into regions of high B . This condition is a direct consequence of the conservation of energy and the magnetic moment $\mu_a = m_a v_{\perp}^2 / (2B)$, which can be shown to be an approximate constant of motion (an adiabatic invariant) under certain conditions. Such particles getting caught in the magnetic field wells are called *trapped particles*.

In tokamaks, where the magnetic field is stronger on the inboard side of the torus but is constant in the toroidal direction, this trapping effect leads to the particles bouncing back and forth on the low-field (outer) side of the torus, superimposed by vertical drift of the guiding centre mentioned above. Fig. 1.7 shows a typical bounce orbit. Given their characteristic shape, these orbits are usually called *banana orbits*. The condition for particles to get trapped is that their pitch angle⁴ α exceeds

$$\alpha_c = \arctan \left(\left(\frac{B_{\max}}{B_{\min}} - 1 \right)^{-1/2} \right),$$

where B_{\max} and B_{\min} are the maximum and minimum magnetic field strengths, respectively. Due to axisymmetry, the canonical toroidal angular momentum of the guiding centre is an approximate constant of motion in a tokamak, a property which implies radial particle confinement according to Tamm's theorem [3]. Therefore, the guiding centres perform closed drift orbits, i.e., although they depart slightly from the flux surface they originated from during their motion along the orbit (which does not occur in a uniform magnetic field, where the guiding centre is bound to the same field line at all times), they cannot leave it permanently. For passing particles, the distance the guiding centre may depart from its flux surface can be estimated with

$$\Delta r_{\text{passing}} = \frac{v_{\parallel}}{\Omega_{a\theta}} \sim \epsilon \rho_{a\theta},$$

where $\Omega_{a\theta}$ and $\rho_{a\theta}$ are calculated using only the poloidal magnetic field strength. Trapped particles, whose change in parallel velocity is much more pronounced, depart by the larger

⁴the angle between the particle's velocity vector and the magnetic field

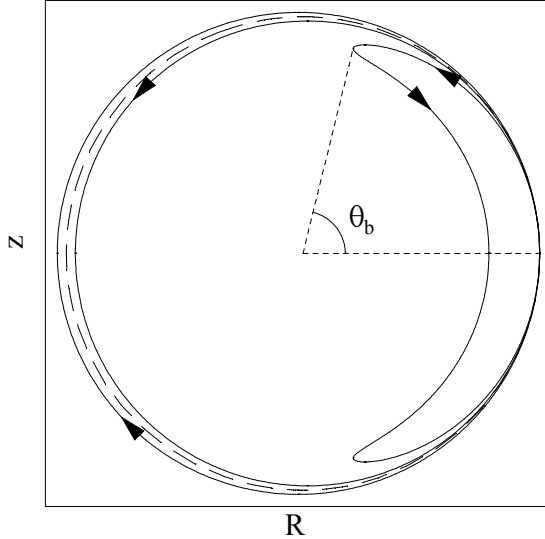


FIGURE 1.7 Trapped and passing orbits in a tokamak. The dashed line shows the corresponding flux surface. R and z correspond to a cylindrical coordinate system, θ_b is the bounce angle (the poloidal location of the turning point) [3].

size of a banana width

$$\Delta r_{trapped} = \frac{v_{\parallel}}{\Omega_{a_\theta}} \sim \sqrt{\epsilon} \rho_{a_\theta}.$$

These departures of the guiding centres from the flux surfaces play an important role in transport theory, as will be discussed in section 1.3. The time it takes a particle to complete a banana orbit is called the *bounce time* [3]

$$\tau_b = \oint \frac{d\theta}{v_{\parallel} \nabla_{\parallel} \theta},$$

which exceeds the time a passing particle needs for one circulation around the torus by roughly a factor $\epsilon^{-1/2}$.

In stellarators, the magnetic field strength varies both in the poloidal and in the toroidal direction, and therefore particles can get trapped not only poloidally but also in the helical magnetic field ripple. The consequence is a large number of different orbits, ranging from ordinary passing particles as can be found in the tokamak and purely helically trapped particles to so-called superbananas, where the whole orbit of a helically trapped particle moves on a banana orbit, and more or less chaotic orbits with particles changing back and forth between

1. INTRODUCTION

different states of trapping. As the stellarator lacks the tokamak's axisymmetry, the canonical toroidal angular momentum of the guiding centre is not a constant of motion, and consequently there is no guarantee that all of these orbits stay close to one flux surface. Indeed, many of them do not. Thus, unlike in a tokamak, trapped particles are *not intrinsically confined* in an arbitrary stellarator. However, the number of unconfined orbits can be greatly reduced by adjusting the configuration of the magnetic field in a suitable way, and thus much of present-day stellarator research is focused on stellarator optimisation.

1.3.2 Collisional transport

As mentioned above, the majority of plasma particle collisions do not lead to a fusion reaction but are instead the source of ordinary Coulomb scattering processes. Upon collision, the particles undergo a random walk, which, in the presence of density, temperature and/or potential gradients, leads to transport. The typical step size is of the order of the deviation of the particles from the field line, which is the Larmor radius of the particle in a straight homogeneous magnetic field, leading to a diffusion coefficient $D_{ab}^{classical} \sim \rho_a^2 / \tau_{ab}$ for collisions between particle species a and b , where τ_{ab} is the collision time. This source of transport, usually referred to as *classical* transport, cannot be avoided and is intrinsically present in all fusion devices. In toroidal devices, inhomogeneities in the magnetic field strength are unavoidable (see section 1.3.1). The corresponding departure of the guiding centres from the flux surfaces, again combined with particle collisions and background gradients, leads to a much stronger transport, the *neoclassical* transport. The exact magnitude depends strongly on the collisionality; whereas classical transport scales linearly with the collision frequency, particle orbit effects lead to a more complicated scaling of the neoclassical diffusion coefficient in toroidal devices. Fig. 1.8 shows the neoclassical diffusion coefficient versus collisionality in a tokamak. When the collisionality is low, particles can complete their orbits, including banana orbits, before they experience a collision with another particle. The characteristic radial diffusion step is of the order of the banana orbit width, and the diffusion coefficient scales linearly with collision frequency ν . The corresponding regime of low collisionality is called the *banana regime*. When collisions get more frequent, such that banana orbits are interrupted by collisions whereas circulating orbits can still be completed (as noted in section 1.3.1, the bounce time exceeds the time a passing particle needs by a factor $\epsilon^{-1/2}$), the diffusion coefficient becomes nearly independent of collisionality as de-trapping effects cancel the effects due to the higher collision frequency. The corresponding regime is called *plateau regime*. When the collision frequency gets yet higher, such that all particle orbits are typically interrupted by collisions before they can be completed, the scaling between collision frequency and diffusion coefficient becomes linear again; this high-collisional regime is usually referred to as the *Pfirsch-Schlüter regime* after the two plasma physicists Dieter Pfirsch and Arnulf Schlüter. In particular, physical effects arising from the particle orbits are completely lost at high collisionality, which clears the way for a fluid treatment of the plasma (see section 2.5).

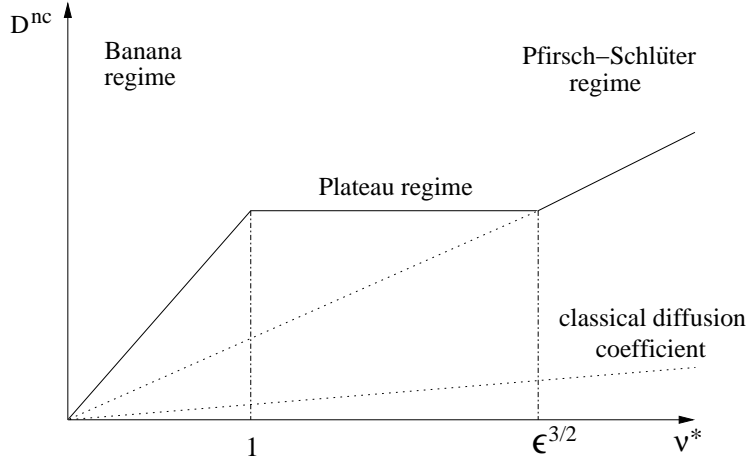


FIGURE 1.8 Neoclassical diffusion coefficient vs. collisionality $\nu^* = \nu/(\epsilon\omega_b)$ in a tokamak. ω_b denotes the bounce frequency (the frequency of the bounce motion).

In a stellarator, the situation is, as usual, more complicated. In the low-collisionality regime, where the collision frequency is small enough to allow particle orbits to be completed, the radial electric field plays a major role. Without a radial electric field, the losses due to helically trapped particles, which are not confined as they do not circulate around the torus, get rather large, leading to the so-called $1/\nu$ -regime where the diffusion coefficient is inversely proportional to the collision frequency ν (see fig. 1.9). However, the presence of a radial electric field causes the helically trapped particles to get convected around the torus by the $E \times B$ velocity, and if this process happens sufficiently fast, these particles are consequently confined. This effect reduces the diffusion coefficient, depending on the strength of the radial electric field E_r , so much as to make it proportional to $\sqrt{\nu}$ or, for even higher E_r , proportional to ν . Accordingly, these regimes are termed $\sqrt{\nu}$ -regime and ν -regime, respectively.

1.3.3 Turbulent transport

Although it exceeds the classical transport considerably, neoclassical transport alone cannot explain the high values for the diffusion coefficients found in experiments. A great part of the transport stems from a completely different cause, namely small-scale turbulent fluctuations of the plasma parameters, such as density, temperature, electrostatic potential and the magnetic field. In a stellarator, turbulent and neoclassical fluxes are often comparable and are both rather high, and thus both mechanisms have to be investigated in detail. However, in a tokamak, due to the simple geometry the neoclassical fluxes tend to be much smaller than in a stellarator and are usually negligible compared with the contribution from turbulence, which is therefore the

1. INTRODUCTION

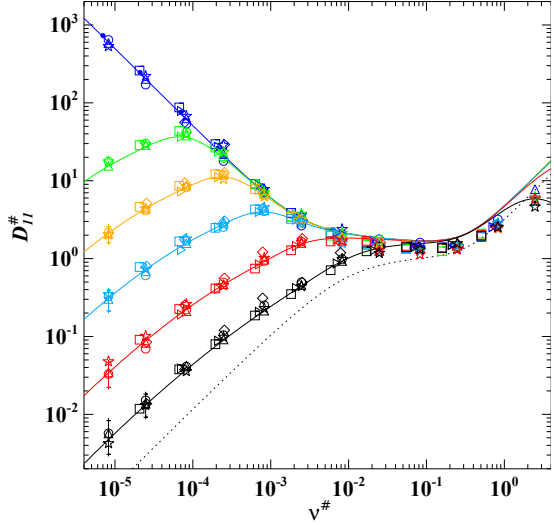


FIGURE 1.9 Neoclassical diffusion coefficient vs. normalised collision frequency in a stellarator for different strengths of the radial electric field (Source: Craig Beidler).

dominant transport mechanism. A lot of research presently aims at understanding the highly nonlinear process of turbulent transport. The driving mechanism is furnished by so-called microinstabilities.

Microinstabilities

The occurrence of fine-scale turbulence in fusion plasmas is often associated with *microinstabilities*, i.e., instabilities with perpendicular wavelengths comparable to the ion Larmor radius. Contrary to long-wavelength instabilities, they are no threat to the plasma equilibrium itself, but they can greatly enhance the radial transport across the flux surfaces and thereby harm the confinement. The primary issue of interest is therefore not whether they are stable or not, as is the case with long-wavelength instabilities, but rather the level of transport caused by the microturbulence. This involves calculations of the nonlinear, saturated state of these microinstabilities, which are usually complicated and not amenable to analytical theory. However, if the microturbulence is sufficiently weak, the correlation time is determined by the growth rate of the underlying microinstability, and the theory can be described by quasilinear diffusion [9]. Furthermore, an analytical linear theory may assist in identifying possible drives and conditions for the turbulence. Different types of microinstabilities include *dissipative* instabilities driven by collisional effects or Landau damping and *reactive* instabilities which do not require dissipation. Two of the most prominent examples are the *trapped-electron mode*

(TEM) carried by the non-equilibrium part of the trapped electron distribution for the former and the *ion-temperature-gradient mode* (ITG) for the latter. This mode is named after the fact that its growth rate depends on the value of $\eta_i = (d\ln T_i/d\psi)/(d\ln n_i/d\psi)$, ψ being a radial coordinate (see section 2.7) and n_a denoting the particle density, driving it unstable above a certain threshold, which is actually rather a critical temperature gradient than a critical η_i if the density profile is sufficiently flat. For a more detailed treatment of microinstabilities, see [6, 9].

Zonal flows

So-called zonal flows have received much attention during the last decade as they can greatly influence fusion performance. A similar phenomenon exists in the Jovian atmosphere, visible from the earth as bands of different colours. Zonal flows in fusion reactors are bands of poloidal (and toroidal) rotation due to an $\mathbf{E} \times \mathbf{B}$ flow associated with a toroidally symmetric electric field perturbation [10]. They are constant on flux surfaces, but vary rapidly in the radial direction, even so much as to reverse the sign of the flow from one band to the next. As a consequence, radial turbulent structures, which can have a greater radial extent than the small-scale zonal flow bands, get “sheared apart” on this smaller scale. Since energy and particles can easily be transported radially along these turbulent structures, this reduction in the radial extent leads to a substantial reduction of the turbulent transport [11, 12] and thereby improves the confinement, a feature which can be crucial for reactor performance. It is therefore necessary to understand the mechanisms involved in the zonal flow creation and destruction in detail. Fig. 1.10 shows a GYRO turbulence simulation demonstrating the shearing process of the turbulent structures. Interestingly, zonal flows are driven by Reynolds stress due to microinstabilities, and therefore a feedback mechanism between, on the one hand, the turbulence creating the flows and, on the other hand, the flows suppressing the turbulence, exists, making the system highly nonlinear (and complicated). Besides the creation process, any mechanism which damps the zonal flows can have a deleterious influence on confinement by letting the level of turbulence rise again. Due to their toroidal symmetry, zonal flows are not subject to *Landau damping* (see, e.g., [6] for a short introduction, or the original paper by Landau [13] for a more detailed derivation), but other damping mechanisms can occur, amongst others collisional damping. This problem will be addressed in section 3.1.

1.4 Role of impurities

Impurities play a crucial role in fusion devices by affecting the confinement in various, usually deleterious, ways [6, 14]. The occurrence of impurities in the plasma can intrinsically not be avoided; on the one hand, during the fusion reaction itself, α -particles (He^{2+} ions) are created, which for some time remain as ash in the plasma. On the other hand, impurity ions

1. INTRODUCTION

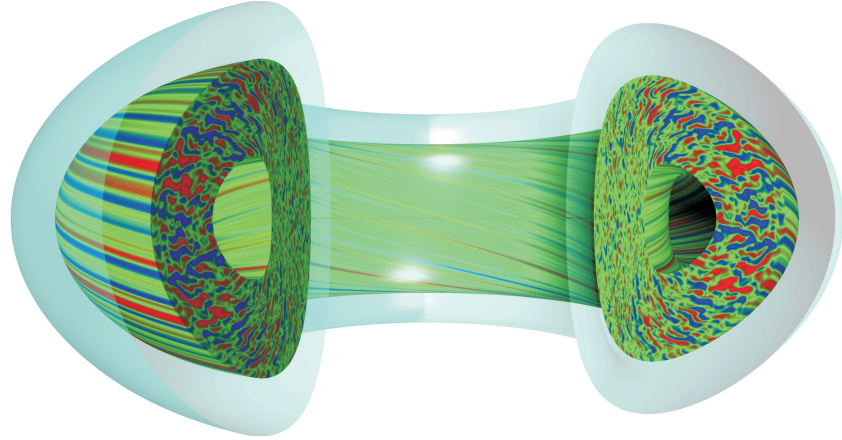


FIGURE 1.10 GYRO simulation of zonal flows
 (Source: <https://fusion.gat.com/theory/Gyromovies>).

are released from the plasma-facing components through interaction with the plasma, and can penetrate deep into the plasma, in the worst case even into the core of the plasma. There, they may degrade the confinement by enhancing the radiated energy, both by increasing the bremsstrahlung in electron-impurity collisions (scaling with a factor Z^2 [2], where $e_z \equiv Ze$), and most severely by line radiation and recombination radiation in the case of high- Z impurities, which are only incompletely stripped even at the very high temperatures reached in the plasma core. If the impurities get too numerous, the radiation losses can become so severe that they lead to a “radiation death” of the plasma, meaning that the plasma radiates away more energy than can be supplied by the heating. Therefore the level, especially of high- Z , impurities must be very small in a reactor. In this respect, the “deleteriousness” of the impurities is often expressed in terms of the *effective ion charge*

$$Z_{\text{eff}} = \frac{\sum_{\text{ions } a} n_a Z_a^2}{\sum_{\text{ions } a} n_a Z_a}.$$

In a fusion reactor, the losses get too high if the condition $Z_{\text{eff}} \lesssim 2$ is violated. Unfortunately, currently considered wall materials include tungsten W⁷⁴, which is, due to its high atomic number, an intrinsic source of strong radiation. Therefore, a lot of research attention is paid to the behaviour and transport of impurities, advantages and disadvantages of different configurations and operation scenarios regarding the accumulation of impurities in the core plasma, etc. Impurities can influence a great number of other important processes in fusion devices, and various aspects are addressed within this thesis.

1.5 Contribution of this thesis

This thesis is concerned with several different problems arising in connection with impurities in fusion plasmas. The first two problems, addressed in section 3, treat turbulence-related issues in tokamaks. The first (see section 3.1) is concerned with the influence of highly charged impurities on collisional zonal-flow damping. Although zonal flows are intrinsically an effect of turbulence, dissipation via collisional damping can be important in the interplay of turbulence and shear flows. As the collision frequency scales with Z^4 , even small amounts of impurities can raise the collision frequency considerably, and the effect of this enhanced damping is studied in detail. The second problem (see section 3.2) deals with the effect of impurities on quasilinear particle fluxes arising due to ITG turbulence. Quantities of interest are the radial impurity flux and scalings of the frequency and growth rate of the underlying microinstability with Z and Z_{eff} . This work attempts to bridge the gap between nonlinear simulations with large numerical codes yielding amounts of parameter-sensitive output on the one hand and analytic theory aiming at explaining basic mechanisms on the other hand. An analytic theory is derived for some limiting cases, and the full problem is solved numerically. Both solutions are compared with quasilinear runs of the GYRO code [15]. The subsequent two chapters shed light on the neoclassical transport of impurities in stellarators, a topic which so far has been not been treated as carefully as tokamak neoclassical transport. In section 4.1, the particle and heat fluxes of heavy impurities in the collisional (Pfirsch-Schlüter) regime, appropriate to cold edge plasmas, are calculated analytically. The following section 4.2 builds upon these results and deals with impurity redistribution within flux surfaces in the presence of steep radial gradients of the bulk ion density, temperature, and the electrostatic potential. These conditions occur, e.g., during H-mode operation, where transport barriers characterised by steep gradients form in the edge region, and the understanding of the redistribution process might be of help for shedding light on the neoclassical processes involved with H-mode operation which has previously been shown to significantly reduce the neoclassical bulk ion transport in tokamaks. The results of the different sections are summarised and discussed in section 5.

1. INTRODUCTION

2 Basics of kinetic transport theory

This chapter introduces the fundamentals of kinetic transport theory, which the following chapters are based upon. Throughout the entire thesis, the plasma will be considered to consist of electrons, whose physical quantities will be indicated by a subscript e , hydrogenic bulk ions with an index i , and a third particle species with index z . Throughout most of the calculations, this species is assumed to be a species of highly charged impurities with charge $Z \gg 1$. However, in principle Z can be arbitrary and could also refer to, e.g., tritium in contrast to the deuterium ions, which are usually considered as bulk ions. Assumptions about Z will be stated explicitly in the relevant chapters.

2.1 Quasi-neutrality

A fusion plasma consists of an enormous number of charged particles, whose trajectories are governed by the interaction with externally applied electromagnetic fields and with other plasma particles via long-range Coulomb forces. It therefore acts as a many-body system and exhibits collective behaviour. On length scales exceeding the *Debye length* λ_D the plasma is charge neutral. This property is called quasi-neutrality, and manifests itself in the fact that, on length scales exceeding a Debye length, the electron density must be approximately equal to the density of positive charges,

$$n_e = n_i + Zn_z.$$

When a deviation from this condition occurs, electric fields start building up, in accordance with the Poisson equation $\nabla \cdot \mathbf{E} = e(n_i + Zn_z - n_e)/\epsilon_0$. The corresponding force drives the particles back towards quasi-neutrality.

2.2 Distribution functions

The most general form of a distribution function describing a plasma with N particles is given by $F_a(\mathbf{r}_1, \dots, \mathbf{r}_N, \mathbf{v}_1, \dots, \mathbf{v}_N, t)$, which describes the probability for a configuration where the exact position and velocity of *each* plasma particle at the given time t are specified. However,

2. BASICS OF KINETIC TRANSPORT THEORY

it is conventional in plasma physics to work with *reduced* distribution functions, which are obtained by integrating the distribution function of an arbitrary particle over the coordinates of the other particles. The resulting distribution function in six-dimensional phase-space, written as $f(\mathbf{r}, \mathbf{v}, t)$, describes the probability density of *any* particle being at the position \mathbf{r} with a velocity \mathbf{v} at the time t , where the other plasma particles can occupy arbitrary states. In this sense, a statistical average over the distribution function can be defined by taking weighted moments over velocity space

$$\langle g \rangle|_f \equiv \frac{\int g(\mathbf{r}, \mathbf{v}, t) f(\mathbf{r}, \mathbf{v}, t) d^3 v}{\int f(\mathbf{r}, \mathbf{v}, t) d^3 v}$$

for any function $g(\mathbf{r}, \mathbf{v}, t)$. In particular, the “zeroth” moment with respect to which the other moments are normalised yields the particle density of species a ,

$$n_a(\mathbf{r}, t) = \int f_a(\mathbf{r}, \mathbf{v}, t).$$

Employing $g = \mathbf{v}$, where \mathbf{v} denotes the velocity of a particular particle, yields the macroscopic flow velocity \mathbf{V}_a of species a ,

$$\mathbf{V}_a(\mathbf{r}, t) = \langle \mathbf{v} \rangle|_f.$$

In a similar way, the temperature T_a can be defined as

$$\frac{3}{2} T_a(\mathbf{r}, t) = \left\langle \frac{m_a (\mathbf{v} - \mathbf{V}_a)^2}{2} \right\rangle|_f,$$

where only the deviation of the particle velocity from the mean flow velocity is taken into account, so that the total energy can be found to equal the sum of the thermal energy and the kinetic energy from the mean flow,

$$\frac{m_a n_a \langle v^2 \rangle_f}{2} = \frac{3 n_a T_a}{2} + \frac{m_a n_a V_a^2}{2}.$$

Furthermore, defining the pressure p_a as

$$p_a \equiv \frac{1}{3} m_a n_a \langle (\mathbf{v} - \mathbf{V}_a)^2 \rangle|_f,$$

one can show the relation $p_a = n_a T_a$.

2.3 Kinetic equations

In a plasma, the movement of each particle is governed by the equations of motion

$$\begin{aligned}\dot{\mathbf{r}} &= \mathbf{v}, \\ \dot{\mathbf{v}} &\equiv \mathbf{a} = \frac{e_a}{m_a}(\mathbf{E} + \mathbf{v} \times \mathbf{B}),\end{aligned}$$

where an overdot denotes a time derivative. Thus, \mathbf{a} is the acceleration the particles experience due to electric and magnetic fields. As the number of particles is conserved, assuming that there are neither sources nor sinks of particles, f_a must obey the continuity equation

$$\frac{\partial f_a}{\partial t} + \frac{\partial}{\partial \mathbf{z}}(\dot{\mathbf{z}} f_a) = 0,$$

$\mathbf{z} = (\mathbf{r}, \mathbf{v})$ being the six-dimensional phase-space variable. Since the phase-space flow velocity is divergence free (Liouville's theorem), this equation can be rewritten, using the equations of motion, as

$$\frac{\partial f_a}{\partial t} + \mathbf{v} \cdot \nabla f_a + \frac{e_a}{m_a}(\mathbf{E} + \mathbf{v} \times \mathbf{B}) \cdot \frac{\partial f_a}{\partial \mathbf{v}} = 0.$$

This equation is known as the *Vlasov equation*. In this representation, \mathbf{E} and \mathbf{B} are the total electric and magnetic fields, including not only externally imposed forces but also the full electromagnetic interactions of all particles in the system. However, the practically relevant forces and distribution functions are not these microscopic ones but instead ensemble-averaged quantities, denoted by $\hat{\mathbf{a}}$ and \hat{f}_a . Ensemble averaging the kinetic equation, one encounters the problem that in general

$$\widehat{\mathbf{a} \cdot \frac{\partial f_a}{\partial \mathbf{v}}} \neq \widehat{\mathbf{a}} \cdot \widehat{\frac{\partial f_a}{\partial \mathbf{v}}},$$

where equality is provided if and only if \mathbf{a} and f_a are statistically independent, i.e., in the absence of interactions. Otherwise, there is a non-zero contribution from the interaction term,

2. BASICS OF KINETIC TRANSPORT THEORY

typically taken into account by introducing a *collision operator*

$$C_a(f_a) \equiv \widehat{\mathbf{a}} \cdot \widehat{\frac{\partial f_a}{\partial \mathbf{v}}} - \mathbf{a} \cdot \widehat{\frac{\partial f_a}{\partial \mathbf{v}}} = \frac{\partial f_a}{\partial t} \Big|_{\text{Collisions}},$$

which accounts for short-scale field fluctuations as they become important during close approaches of particles (on length scales comparable to or smaller than the Debye length) where the fields from the individual particles dominate over the macroscopic large-scale fields. In this way, the usual form of the kinetic equation can be obtained, yielding

$$\frac{\partial f_a}{\partial t} + \mathbf{v} \cdot \nabla f_a + \frac{e_a}{m_a} (\mathbf{E} + \mathbf{v} \times \mathbf{B}) \cdot \frac{\partial f_a}{\partial \mathbf{v}} = C_a(f_a), \quad (2.1)$$

where now \mathbf{E} and \mathbf{B} represent only the large-scale fields, and the overhats have been omitted. In a gas, the collision operator is usually a Boltzmann operator, and the corresponding kinetic equation the *Boltzmann equation*. In a fusion plasma, however, collisional processes are dominated by small-angle scattering events, and thus a Fokker-Planck operator is used, which is described in more detail in section 2.4. Equation (2.1) is therefore usually referred to as the *Fokker-Planck equation*. Obtaining a complete exact solution to this partial differential equation is theoretically possible but usually practically not achievable. Therefore, approximations have to be made in order to simplify the problem. The main trick in kinetic theory is to find a suitable ordering scheme, which, if successful, makes it possible to keep only the terms relevant for the problem of interest and neglect small terms which do not influence the solution much. Which ordering assumptions to use depends on the effect one wishes to study; two particularly beneficial and frequently used ordering concepts, the drift-kinetic ordering and the gyrokinetic ordering, will be introduced in the subsequent sections, after defining two useful averaging procedures which will be used in the derivations and frequently later on.

2.3.1 Gyro-average

Most processes of interest in a fusion plasma occur on time scales much slower than the gyro-motion and on length scales much longer than the Larmor radius. Thus, for these processes, effects due to the gyromotion of the particles are negligible, and it is possible to reduce the number of independent variables in velocity space by taking an average over the gyroangle ϑ ,

$$\bar{a}(\mathbf{r}, v_\perp, v_\parallel, t) = \frac{1}{2\pi} \int_0^{2\pi} a(\mathbf{r}, v_\perp, v_\parallel, \vartheta, t) d\vartheta,$$

where $\mathbf{R} = \mathbf{r} + \mathbf{v} \times \mathbf{b}/\Omega_a$, v_{\parallel} and v_{\perp} are kept fixed and $\mathbf{b} \equiv \mathbf{B}/|\mathbf{B}|$. In this sense, the gyromotion is considered as the motion of a charged ring around the guiding centre.

2.3.2 Flux-surface average

When considering processes where the motion of the particles across the flux surfaces is much slower than the motion within the flux surface, such as, e.g., radial transport processes, the exact dynamics within the flux surface are often unimportant. What matters is the amount of particles, heat, energy etc. that leaves or enters the flux surface. Therefore, the kinetic treatment can be conveniently simplified by taking an average over the flux surface,

$$\langle A \rangle = \frac{\oint A(\psi, \theta, \varphi) \sqrt{g} d\theta d\varphi}{\oint \sqrt{g} d\theta d\varphi},$$

for some set of coordinates where ψ represents a flux label serving as a radial coordinate and θ and φ are some poloidal and toroidal angle coordinates, respectively, \sqrt{g} being the Jacobian for this set of coordinates. An introduction on different sets of coordinates will be given in section 2.7. This average describes a volume average between two neighbouring flux surfaces. A useful property of the flux-surface average is that it annihilates the term $\mathbf{B} \cdot \nabla$, i.e.

$$\langle \mathbf{B} \cdot \nabla F \rangle = 0 \tag{2.2}$$

for all periodic functions $F(\psi, \theta, \varphi)$.

2.3.3 Drift kinetic equation

Drift kinetic theory is concerned with processes occurring on spatial scales large compared with the particle gyroradius scale, for example transport processes. In order for drift kinetic theory to be valid, the plasma has to be strongly *magnetised*, meaning that the magnetic field is sufficiently strong to make the bulk ion Larmor radius much smaller than the plasma dimension L , thus the relation $\delta_a \equiv \rho_a/L \ll 1$ must hold. As the electrons' gyroradius is smaller than that of the ions by a factor of a square root of the mass ratio, electrons are automatically included in this ordering if the ions are. In any reasonable magnetic confinement device, this condition is usually well fulfilled. The kinetic equation can then be expanded in the small parameter δ_a , which, as will become clear in the following, leads to the particle distribution functions being approximately (to lowest order) *Maxwellian* and constant on flux surfaces in toroidal devices. Thus, the problem is *local*, allowing a treatment on each single flux surface separately. If δ_a is not small, the problem becomes non-local and instead involves a large part of the plasma volume, which makes it impossible to look only at processes within one flux

2. BASICS OF KINETIC TRANSPORT THEORY

surface. The derivation of a mathematically rigorous theory becomes extremely challenging in this case.

The ordering assumptions applied to obtain the *drift kinetic equation* from 2.1 are $\delta_a \ll 1$ and $\partial/\partial t \ll \Omega_a$, where the second relation, to be interpreted mathematically in the way that $\partial\alpha/\partial t \ll \alpha\Omega_a$, should hold for all fields and distribution functions α . Furthermore, the flow velocities are ordered to be one order smaller than the thermal speed, $V_a \sim \delta_a v_{th,a}$. Using guiding centre variables $\mathbf{w} = (\mathbf{R}, \varepsilon_a, \mu_a, \vartheta)$, where $\varepsilon_a = m_a v^2/2$ is the kinetic energy, μ_a the magnetic moment and ϑ the gyroangle, the kinetic equation can be written as

$$\frac{\partial f_a}{\partial t} + \dot{\mathbf{R}} \cdot \nabla f_a + \dot{\varepsilon}_a \frac{\partial f_a}{\partial \varepsilon_a} + \dot{\mu}_a \frac{\partial f_a}{\partial \mu_a} + \dot{\vartheta} \frac{\partial f_a}{\partial \vartheta} = C_a(f_a). \quad (2.3)$$

The last term on the left-hand side corresponds to the Larmor rotation of the particle and is the largest in this equation under the given ordering assumptions as the drift term is smaller by a factor δ_a and the two terms $\partial f_a/\partial t$ and $\dot{\varepsilon}_a \partial f_a/\partial \varepsilon_a$ are formally small as the time derivatives are ordered small. The magnetic moment μ_a is approximately conserved, and effects from the term containing $\dot{\mu}_a$ only affect the equation in second order. As the expansion is typically truncated after first order, the μ_a term can be dropped. Additionally, the collision frequency ν_a is usually much smaller than the gyrofrequency, $\Delta_a \equiv \nu_a/\Omega_a \ll 1$, so that the collision term is smaller than the gyroterm by a factor Δ_a . Therefore, the distribution function must be independent of the gyroangle to lowest order in δ_a and Δ_a , and it proves convenient to take a gyro-average of eq. (2.3) to get rid of the last term and thereby reduce the number of variables by one, yielding

$$\frac{\partial f_{a_0}}{\partial t} + \overline{\dot{\varepsilon}_a} \frac{\partial f_{a_0}}{\partial \varepsilon_a} + \dot{\mathbf{R}} \cdot \nabla f_{a_0} = \overline{C_a(f_{a_0})}.$$

A mathematically more accurate derivation of the drift kinetic equation is based on Hamiltonian mechanics, see e.g. [16]. In the following, the overbar will be dropped and f_a is meant to represent the gyroaveraged distribution function.

One can now expand the distribution function in δ_a as $f_a = f_{a_0} + f_{a_1} + \dots$, where $f_{a_j} = \mathcal{O}(\delta_a^j)$. However, it does not make sense to include orders higher than f_{a_1} as the drift-kinetic equation itself is only accurate to first order in δ_a . In lowest order in this expansion, only two terms remain, showing that collisions are balanced by parallel motion,

$$C_a(f_{a_0}) = v_{\parallel} \nabla_{\parallel} f_{a_0}. \quad (2.4)$$

2.3. KINETIC EQUATIONS

It can be shown that the only possible solution to this equation is a *stationary* Maxwellian,

$$f_{a_0} = \frac{n_a}{\pi^{3/2} v_{th,a}^3} \exp^{-v^2/v_{th,a}^2},$$

where $v_{th,a} = 2T_a/m_a \equiv x_a^2$ is the thermal speed. To do so, multiply (2.4) by $\ln f_{a_0}$ and integrate over velocity space. Taking the flux-surface average of the velocity-space integrated eq. (2.4) and exploiting (2.2) yields

$$\left\langle \int (\ln f_{a_0}) C_a(f_{a_0}) d^3 v \right\rangle = 0.$$

But one can show that

$$\frac{\partial n_a s_a}{\partial t} = - \int (\ln f_{a_0}) C_a(f_{a_0}) d^3 v,$$

where s_a is the entropy density. If only self-collisions are considered, the \mathcal{H} -theorem implies that the entropy change is always greater than zero, and a similar argument can be applied for unlike particle collisions by taking a sum over all particle species, which is not shown here. Thus, if $\langle \int (\ln f_{a_0}) C(f_{a_0}) d^3 v \rangle$ is to vanish, it can only do so when the argument itself, i.e., the collision operator, vanishes, which is the case if and only if f_{a_0} is a Maxwellian and the different species have equal equilibrium flow velocities and temperatures. In particular, all lowest-order quantities, such as density and temperature of the different species and, by quasi-neutrality, also the electrostatic potential, are *flux functions*.

The zeroth order solution can now be used to successively derive the higher-order corrections to the Maxwellian, leading to the following equation in first order

$$C(f_{a_1}) = v_{\parallel} \nabla_{\parallel} f_{a_1} + \mathbf{v}_d \cdot \boldsymbol{\nabla} f_{a_0} + \dot{\varepsilon}_a \frac{\partial f_{a_0}}{\partial \varepsilon_a}.$$

A major part of kinetic transport theory consists of solving this first order drift-kinetic equation under different additional assumptions.

2.3.4 Gyrokinetic equation

Another frequently used ordering scheme leads to *gyrokinetic* theory, which applies to situations in which some components of the electromagnetic field are allowed to vary significantly across a particle's Larmor orbit. This is, e.g., often the case in linear stability analyses, in

2. BASICS OF KINETIC TRANSPORT THEORY

which the wavelengths of the perturbed fields perpendicular to the magnetic field may be comparable to the ion Larmor radius. Consequently, so-called *finite Larmor radius* (FOL) effects have to be included, meaning that the movement of the particle is not regarded as that of a particle sitting at the guiding centre but as the movement of a charged ring around the guiding centre. Quantities varying significantly across these short length scales are therefore averaged over this ring (averaged over the gyroangle), as is the whole equation. As in drift kinetics, the zeroth order (in an expansion in δ_a) equation is independent of the gyroangle. It is important to note that a rigorous theory based on such an expansion is only possible if the amplitudes of the perturbed quantities which vary on the Larmor radius scale are small (i.e., of order δ_a), otherwise the full kinetic equation has to be solved.

Averaging the kinetic equation in guiding-centre variables $\mathbf{R}, \varepsilon_a, \mu_a, \vartheta$ (eq. (2.3)) over the gyroangle ϑ leads to

$$\frac{\partial f_a}{\partial t} + (v_{\parallel} \mathbf{b} + \mathbf{v}_d + \bar{\mathbf{v}}_E) \cdot \nabla f_a + \bar{\varepsilon}_a \frac{\partial f_a}{\partial \varepsilon_a} + \dot{\mu}_a \frac{\partial f_a}{\partial \mu_a} = \overline{C_a(f_a)} \quad (2.5)$$

as in drift kinetics, and the term containing μ_a vanishes to lowest order as the magnetic moment is an approximate constant of the motion. Here, f_a denotes only the gyrophase independent part of the distribution function, as the lowest order distribution in the δ_a expansion is again found to be independent of the gyroangle due to the gyration term dominating over all other terms in this ordering. However, whereas the parallel velocity $v_{\parallel} \mathbf{b}$ and the magnetic drift velocity ((4.3) without the $\mathbf{E} \times \mathbf{B}$ term) only contain slowly varying quantities, the $\mathbf{E} \times \mathbf{B}$ velocity

$$\mathbf{v}_E = \frac{\mathbf{b} \times \nabla \tilde{\phi}}{B}$$

contains the perturbed electric potential $\tilde{\phi}$, which is allowed to vary on the gyroscale. Therefore,

$$\bar{\mathbf{v}}_E = \frac{\mathbf{b} \times \nabla \bar{\phi}}{B}.$$

The overbars will be suppressed in the following, and the appearing quantities are to be understood to denote the gyroaveraged quantities. Furthermore, the equation is usually linearised.

The gyrokinetic ordering is

$$\delta_a \sim \frac{k_{\parallel}}{k_{\perp}} \sim \frac{e_a \tilde{\phi}}{T_a} \sim \frac{\partial}{\partial t}/\Omega_a \ll 1,$$

2.3. KINETIC EQUATIONS

where k_{\parallel} and k_{\perp} are the parallel and perpendicular wave numbers, respectively. As for the fluctuations $k_{\perp}\rho_a = \mathcal{O}(1)$ is allowed, this implies in particular that the fluctuation scale length is shorter than the equilibrium scale length L , and the ratio is ordered to be $\mathcal{O}(\delta_a)$, such that

$$\nabla f_{a_0} \sim \nabla_{\perp} f_{a_1}.$$

In this ordering, the zeroth order equation in δ_a becomes

$$v_{\parallel} \nabla_{\parallel} f_{a_0} + \mathbf{v}_d \cdot \nabla f_{a_0} = C_a(f_{a_0}),$$

the solution to which is again a Maxwellian but with finite orbit width (FOW) corrections stemming from the drift term. In first order, one finds

$$\frac{\partial f_{a_1}}{\partial t} + v_{\parallel} \nabla_{\parallel} f_{a_1} + \mathbf{v}_d \cdot \nabla f_{a_1} + \mathbf{v}_E \cdot \nabla f_{a_0} - \dot{\varepsilon}_a \frac{\partial f_{a_0}}{\partial \varepsilon_a} = C_a(f_{a_1}).$$

In the following, a circular, large-aspect-ratio tokamak is considered and an eikonal ansatz for the perturbed electrostatic potential and the perturbed particle distribution functions is used,

$$\begin{aligned} f_{a_1} &= F_{a_1}(\mathbf{r}) e^{iS(\mathbf{r})} \quad \text{and} \\ \tilde{\phi} &= \phi(\mathbf{r}) e^{iS(\mathbf{r})}, \end{aligned}$$

where

$$\begin{aligned} \nabla_{\perp} S &\equiv \mathbf{k}_{\perp} \gg \nabla F_{a_1}, \nabla \phi \quad \text{and} \\ \nabla_{\parallel} S &= 0, \end{aligned}$$

which is valid for perturbations whose longitudinal wavelengths are comparable to the equilibrium scale length L whereas the transverse wavelengths are comparable to the Larmor radius [17]. However, when the magnetic field is sheared, this assumption poses a problem on irrational flux surfaces as it is not compatible with the periodicity of the angles. To overcome this problem, the *Ballooning transform* is applied. The idea is the following: the finite, physical domain, in which periodicity of the poloidal angle is required, is replaced by an infinite domain without this requirement, and the integro-differential equation is solved there. One can show the existence of solutions $g(\theta)$, decaying quickly to zero as $\theta \rightarrow \infty$. Whereas g is not periodic, the integro-differential operator to which it is a solution is, and therefore $g(\theta + 2\pi m)$ is a solution as well for any $m \in \mathbb{N}$. A periodic solution can thus be constructed by summing g over all m . The angle θ occurring in the gyrokinetic equation after ballooning transformation is sometimes referred to as the *extended poloidal angle* [18].

2. BASICS OF KINETIC TRANSPORT THEORY

Using this approach and an ansatz $e^{-i\omega t}$ for the time dependence of the perturbed distribution functions leads to

$$\frac{v_{\parallel}}{qR} \frac{\partial g_a}{\partial \theta} - i(\omega_{D_a} - \omega)g_a - C_a(g_a) = -i \frac{e_a f_{a_0}}{T_a} (\omega - \omega_{*a}^T) \phi J_0 \left(\frac{k_{\perp} v_{\perp}}{\Omega_a} \right), \quad (2.6)$$

where

$$g_a = f_{a_1} + \frac{e_a \phi}{T_a} f_{a_0}$$

is the nonadiabatic part of the perturbed distribution function and q denotes the safety factor. The Bessel function J_0 ,

$$J_n(z) = \frac{1}{2\pi} \oint e^{-in\gamma + iz \sin \gamma} d\gamma,$$

allows for a convenient representation of the gyro-averaged perturbed potential, and, for a circular, large-aspect-ratio tokamak, the different frequencies appearing in the equation are

$$\begin{aligned} \omega_{D_a} &= -\frac{k_{\theta}}{\Omega_a R} (\cos \theta + s \theta \sin \theta) \left(\frac{v_{\perp}^2}{2} + v_{\parallel}^2 \right), \\ \omega_{*a}^T &= \omega_{*a} \left[1 + \left(x_a^2 - \frac{3}{2} \right) \eta_a \right], \\ \omega_{*a} &= -\frac{k_{\theta} T_a}{e_a B L_{n_a}}. \end{aligned}$$

In this notation, k_{θ} is the poloidal wave number, $s = r d \ln q / dr$ is the magnetic shear, r and R the minor and major radius, respectively, and $\eta_a = L_{n_a} / L_{T_a}$, where the inverse radial density and temperature scale lengths are defined as

$$L_{n_a} = - \left(\frac{\partial \ln n_a}{\partial r} \right)^{-1} \quad \text{and} \quad L_{T_a} = - \left(\frac{\partial \ln T_a}{\partial r} \right)^{-1}.$$

Eq. (2.6) is the version of the gyrokinetic equation used in section 3.2. More detailed treatments on the gyrokinetic equation can be found in refs. [17, 19, 20]. For a derivation involving Lie transforms, see [21].

2.4 Collision operator

Although they are rare, collisions play a fundamental role in magnetised fusion plasmas. In the previous section, the operator denoted by C_a is meant to represent the *full* collision operator for species a , consisting of contributions from various two-species collisions,

$$C_a(f_a) = \sum_b C_{ab}(f_a, f_b).$$

The sum has to be taken over all particle species b , including a itself. As mentioned before, the collisions are dominated by small-angle deflections. Physically, the charges in the plasma are shielded on distances exceeding the Debye length, so particles separated by a distance larger than λ_D can be assumed not to interact. Thus, for particle separation $\sim \lambda_D$, small-angle deflections occur. On the other hand, the mean value for the impact parameter of a 90° scattering process can be found to be

$$\lambda_L \equiv \frac{e_a e_b}{4\pi\epsilon_0 T_a},$$

the so-called *Landau length*. Comparing this quantity with the average distance between colliding particles, one finds that they are on average too far away from each other for a 90° scattering if the *Coulomb logarithm* $\ln\Lambda \equiv \lambda_D/\lambda_L$ is much greater than unity. In a typical fusion plasma, $\ln\Lambda \approx 10 - 20$, and thus fusion plasmas are dominated by small-angle collisions. The consequence is that, instead of having to employ the full Boltzmann collision operator, it is possible to use the simpler *Fokker-Planck operator*, which is obtained by an expansion in the smallness of Δv , the change in velocity during a collision. For a full derivation of the Fokker-Planck operator, see [3]. The form of the collision operator found by Landau in 1936 reads

$$C_{ab}(f_a, f_b) = -\frac{m_a v_{th,a}^3}{2n_b} \hat{\nu}_{ab} \frac{\partial}{\partial v_k} \int U_{kl} \left[\frac{f_a(\mathbf{v})}{m_b} \frac{\partial f_b(\mathbf{v}')}{\partial v'_l} - \frac{f_b(\mathbf{v}')}{m_a} \frac{\partial f_a(\mathbf{v})}{\partial v_l} \right] d^3 v',$$

where

$$U_{kl} \equiv \frac{|\mathbf{v} - \mathbf{v}'|^2 \delta_{kl} - (v_k - v'_k)(v_l - v'_l)}{|\mathbf{v} - \mathbf{v}'|^3},$$

2. BASICS OF KINETIC TRANSPORT THEORY

$v - v'$ expressing the relative velocity between the colliding particles, and

$$\hat{\nu}_{ab} \equiv \frac{n_b e_a^2 e_b^2 \ln \Lambda}{4\pi \epsilon_0^2 m_a^2 v_{th,a}^3}$$

denotes the non velocity-dependent part of the collision frequency

$$\nu_D^{ab} = \hat{\nu}_{ab} \frac{\text{Erf}(x_b) - G(x_b)}{x_a^3}.$$

$\text{Erf}(x) \equiv 2/\sqrt{\pi} \int_0^\infty \exp(-t^2) dt$ denotes the error function, and

$$G(x) \equiv \frac{\text{Erf}(x) - x \text{Erf}'(x)}{2x^2}$$

is the so-called *Chandrasekhar function*. Note that the collision frequency is not defined in a way describing the frequency at which every single collision occurs, but rather such that $1/\hat{\nu}_{ab}$ is the time it takes until an average particle has effectively been scattered by a 90° angle. The collision operator above does not include fusion reactions, which are much less frequent than Coulomb scattering, and conserves particles as well as momentum and energy. Furthermore, it is Galilean invariant and can be shown to always lead to positive entropy production [3], thereby driving the system towards thermodynamic equilibrium. As mentioned before, the equilibrium distribution itself is a Maxwellian distribution with equal temperatures and flow velocities for all particle species a .

2.4.1 Linearised collision operator

The full Coulomb collision operator is bilinear, i.e.

$$C_{ab}(\lambda(f_a + g_a), \mu(f_b + g_b)) = \lambda\mu [C_{ab}(f_a, f_b) + C_{ab}(f_a, g_b) + C_{ab}(g_a, f_b) + C_{ab}(g_a, g_b)]$$

for any constants λ, μ and distribution functions f_a, g_a, f_b, g_b . In particular, the self-collision operator is *nonlinear* since

$$C_{aa}(\lambda f_a) = C_{aa}(\lambda f_a, \lambda f_a) = \lambda^2 C_{aa}(f_a),$$

which can complicate any equation involving the collision operator enormously. However, fusion plasmas are usually close to local thermodynamic equilibrium, and thus the distribution

functions deviate only slightly from a Maxwellian,

$$f_a = f_{a_0} + f_{a_1} \quad \text{with} \quad \frac{f_{a_1}}{f_{a_0}} \ll 1.$$

Substituting this expression into the collision operator yields the following expression for the linearised operator,

$$C_{ab}(f_a, f_b) = C_{ab}(f_{a_0} + f_{a_1}, f_{b_0} + f_{b_1}) \simeq C_{ab}(f_{a_1}, f_{b_0}) + C_{ab}(f_{a_0}, f_{b_1}) \equiv C_{ab}^l(f_a, f_b),$$

where the term containing the two Maxwellian distributions vanishes for equal particle temperatures, and the term $C_{ab}(f_{a_1}, f_{b_1})$ is quadratic in the perturbation and thus small. The linearised operator has the same properties regarding particle, momentum and energy conservations as the full operator. Throughout the rest of the thesis, C_{ab} will be understood to denote the linearised collision operator without adding the superscript l .

2.4.2 Other approximate collision operators

When considering collisions between particles of very disparate masses, further significant simplifications of the full collision operator are possible. They will be described in the subsequent sections and frequently be employed throughout the thesis.

Disparate mass ratio

If the speeds at which two colliding different particles move are very disparate, which is usually the case if one species is much heavier than the other as the temperatures do not tend to differ too much, the collision operator can be simplified using the mass ratio as a small parameter. The point is that, as seen from a particle of the lighter (and thus much faster) species, the distribution of the heavy species in velocity space can be approximated with a delta function around the mean flow velocity. If a denotes the lighter species, then the simplified operator becomes

$$C_{ab}(f_a) = \nu_{ab}(v) \left(\mathcal{L}(f_a) + \frac{m_a}{T_a} \mathbf{v} \cdot \mathbf{V}_b f_{a_0} \right).$$

It is accurate in the limit $m_a/m_b \rightarrow 0$. Here, in spherical velocity-space coordinates (r, θ^*, φ^*) ,

$$\mathcal{L}(f_a) = \frac{1}{2} \left[\frac{1}{\sin\theta^*} \frac{\partial}{\partial\theta^*} \left(\sin\theta^* \frac{\partial f_a}{\partial\theta^*} \right) + \frac{1}{\sin^2\theta^*} \frac{\partial^2 f_a}{\partial\varphi^{*2}} \right]$$

2. BASICS OF KINETIC TRANSPORT THEORY

is the so-called *Lorentz scattering operator*, accounting for the fact that in the case of disparate mass ratio pitch-angle scattering is the most important mechanism; it does not alter the magnitude of the velocity but describes diffusion in velocity space on a sphere $v = \text{const}$. Therefore, Legendre polynomials

$$P_n(\xi) = \frac{1}{2^n n!} \frac{d^n}{d\xi^n} [(\xi^2 - 1)^n]$$

are eigenfunctions of this operator, where $\xi \equiv v_{\parallel}/v$. Consequently, as v_{\parallel} is proportional to the first Legendre polynomial, one can derive the useful relation $\mathcal{L}(v_{\parallel}) = -v_{\parallel}$.

Another useful property is the Lorentz operator's self-adjointness in the sense that

$$S[\hat{f}_a, \hat{g}_a] \equiv \int F(v) \hat{g}_a \mathcal{L}(f_{a_0} \hat{f}_a) d^3v = \int F(v) \hat{f}_a \mathcal{L}(f_{a_0} \hat{g}_a) d^3v = S[\hat{g}_a, \hat{f}_a].$$

The collision frequency can be simplified to $\nu_D^{ab} = \hat{\nu}_{ab}/x_a^3$. In particular, for the case of collisions between electrons and ions, the collision operator does not depend on the ion mass but only on the charge, yielding the simple expression for the total electron-ion collision operator (assuming that all ion species are stationary)

$$C_{ei}(f_e) = Z_{\text{eff}} \nu_D^{ei} \mathcal{L}(f_e).$$

On the other hand, for collisions between the heavier and the lighter species, the most dominant effects are friction and energy exchange, yielding

$$C_{ba}(f_b) = \frac{\mathbf{R}_{ab}}{m_b n_b} \cdot \frac{\partial f_b}{\partial \mathbf{v}} + \frac{m_a n_a}{m_b n_b \tau_{ab}} \frac{\partial}{\partial \mathbf{v}} \cdot \left[(\mathbf{v} - \mathbf{V}_b) f_b + \frac{T_a}{m_b} \frac{\partial f_b}{\partial \mathbf{v}} \right],$$

where $\tau_{ab} = 3\sqrt{\pi}/(4\hat{\nu}_{ab})$ and \mathbf{R}_{ab} denotes the friction force between particle species a and b . However, this type of collisions can usually be neglected compared with self collisions of the heavy species as C_{ba} is smaller than C_{aa} by a factor $\sqrt{m_a/m_b} \ll 1$. Energy exchange is usually even smaller than the friction contribution.

Self collisions

Although the linearised collision operator is much simpler than the full one, for many purposes, especially for analytical calculations, it is still far too complicated. Thus, a frequently

employed model operator for self collisions, again based on the observation that, under many circumstances, pitch-angle scattering is the most important process, reads

$$C_{aa}(f_a) = \nu_D^{aa} \left(\mathcal{L}(f_a) + \frac{m_a}{T_a} \mathbf{v} \cdot \mathbf{u}_a f_{a_0} \right).$$

After its inventor, this operator is sometimes also referred to as the *Connor operator* [22]. Here, the term involving

$$u_a = \frac{\int \mathbf{v} \nu_D^{aa}(v) f_a d^3 v}{\int \nu_D^{aa}(v) m_a v^2 / (3 T_a) f_{a_0} d^3 v}$$

is constructed to restore momentum conservation, as the Lorentz operator itself does not have this property. Note that it strongly resembles the operator for disparate mass ratio. However, although it satisfies particle, momentum and energy conservation and is Galilean invariant as the full operator, it has certain drawbacks. Strictly speaking, it is only accurate for weakly-collisional plasmas in the limit of large aspect-ratio, $\epsilon \rightarrow 0$, in tokamaks, as in this case the distribution function has a boundary layer localised to the trapped and barely passing region, where pitch-angle scattering plays the dominant role.

2.5 Fluid description

For most applications, the microscopic behaviour of the plasma is not very relevant; what matters are the *macroscopic* properties. Experimentally measurable quantities are not distribution functions, but rather densities, flow velocities etc. Therefore, it is often sufficient to take moments of the kinetic equation instead of solving it directly. The quantities appearing in these equations are then the different moments of the distribution functions, the first few of which, density, temperature, pressure, and flow velocity, have already been introduced in section 2.2. Higher moments of relevance include the heat flux \mathbf{q}_a and the components of the viscosity tensor, $\pi_{a_{jk}}$,

$$\begin{aligned} \mathbf{q}_a &\equiv n_a \left\langle \frac{m_a |\mathbf{v} - \mathbf{V}_a|^2}{2} (\mathbf{v} - \mathbf{V}_a) \right\rangle \Big|_f, \\ \pi_{a_{jk}} &\equiv m_a n_a \langle (v_j - V_{a_j})(v_k - V_{a_k}) \rangle \Big|_f, \end{aligned}$$

2. BASICS OF KINETIC TRANSPORT THEORY

and the related fluxes of energy and momentum,

$$\begin{aligned} \mathbf{Q}_a &\equiv \frac{m_a n_a}{2} \langle v^2 \mathbf{v} \rangle |_f, \\ \Pi_{a_j k} &\equiv \langle m_a n_a v_j v_k \rangle |_f. \end{aligned}$$

In a similar way, moments can be taken of the entire kinetic equation. Integrating (2.1) over velocity space leads to the continuity equation

$$\frac{\partial n_a}{\partial t} + \nabla \cdot (n_a \mathbf{V}_a) = 0,$$

where the right-hand side vanishes as particles are conserved during Coulomb collisions and thus

$$\int C_a(f_a) d^3 v = 0.$$

Taking the velocity moment of (2.1) yields the momentum equation

$$m_a n_a \frac{\partial \mathbf{V}_a}{\partial t} + \nabla \cdot \mathbf{\Pi}_a = n_a e_a (\mathbf{E} + \mathbf{V}_a \times \mathbf{B}) + \mathbf{R}_a.$$

The friction force \mathbf{R}_a describes the momentum transfer during unlike-particle collisions,

$$\mathbf{R}_a = \int m_a \mathbf{v} C_a(f_a) d^3 v,$$

and, as momentum must be conserved, in particular

$$\int m_a \mathbf{v} C_{ab}(f_a) d^3 v = - \int m_b \mathbf{v} C_{ba}(f_b) d^3 v$$

and

$$\int m_a \mathbf{v} C_{aa}(f_a) = 0.$$

The third equation of importance, the energy equation, is obtained by taking the $m_a v^2 / 2$ moment of (2.1)

$$\frac{\partial}{\partial t} \left(\frac{3n_a T_a}{2} + \frac{m_a n_a V_a^2}{2} \right) + \nabla \cdot \mathbf{Q}_a = e_a n_a \mathbf{E} \cdot \mathbf{V}_a + \int \frac{m_a v^2}{2} C_a(f_a) d^3 v.$$

Again, as energy must be conserved during collisions,

$$\int \frac{m_a v^2}{2} C_{ab}(f_a) d^3 v = - \int \frac{m_b v^2}{2} C_{ba}(f_b) d^3 v$$

and consequently

$$\int \frac{m_a v^2}{2} C_{aa}(f_a) d^3 v = 0.$$

From the equations above, it becomes obvious that solving one of the moment equations requires knowledge of the moments of the distribution function of one order higher, and thus the problem of closure arises, i.e., finding a way of reasonably approximating this infinite hierarchy of equations with a finite number of equations. Entire books have been written on that subject; two principal methods involve *truncation schemes* and *asymptotic schemes*. In truncation schemes, higher-order moments are arbitrarily assumed to vanish or simply expressed through lower moments, which are easy to handle but intrinsically involve uncontrolled approximations. Asymptotic schemes, on the other hand, rely on a mathematically rigorous expansion in a small parameter, having the advantage of providing some error estimates, but tend on the other hand to be mathematically challenging. A classic asymptotic scheme for a collisional neutral gas is the *Chapman-Enskog* [23–25] method, based on an expansion in the smallness of the ratio of the mean-free path to the macroscopic scale length. For fusion applications, i.e., in a magnetised plasma, a rigorous theory is usually derived from an expansion in the small parameter δ_a already introduced, and, further, the shortness of the mean-free path compared with the system size. Applying the Chapman-Enskog method to a collisional plasma leads to the well-known *Braginskii equations* [26]. However, a fluid approach for fusion plasmas is only possible in regions where the mean-free path is indeed short, i.e., the collisional Pfirsch-Schlüter regime. In less collisional regimes, finding an appropriate way of closing the fluid equations becomes extremely challenging, and one usually has to resort to a full solution of the kinetic equation.

2.6 Intrinsic ambipolarity

In the conventional neoclassical ordering described in the previous sections, angular momentum is approximately conserved in axisymmetric systems. This has important consequences for the neoclassical particle flux, making it *intrinsically ambipolar* to lowest order, i.e.,

$$\sum_a e_a \langle \Gamma_a \cdot \nabla \psi \rangle = 0, \quad (2.7)$$

where the sum is taken over all particle species and Γ_a is the particle flux of species a . Consequently, ambipolarity is automatically maintained. Related to this property is the influence of a radial electric field. Applying such a field in a tokamak leads to a purely toroidal rotation of all the particles on one flux surface simultaneously. Due to the Galilean invariance of the system, the radial electric field has little influence on the physics of the system. In particular, eq. (2.7) always holds, independently of the radial electric field. That means in particular that any radial electric field can be applied, which leads to a corresponding rotation, meaning that a tokamak plasma can rotate freely.

The situation is different in a stellarator. The lowest order neoclassical particle fluxes are not ambipolar, i.e., one of the particle species may escape faster than the others. As a consequence, a radial electric field builds up, which enhances the confinement of the fast escaping species until the net transport is ambipolar again. This radial electric field is called the *ambipolar electric field*. Depending on the plasma parameters, in particular on the electron and ion temperatures, different stable equilibrium points exist; for usual parameters, when the electron and ion temperatures do not differ too much, the ions tend to escape faster, leading to negative values for the ambipolar electric field. This scenario is called *ion root operation*. For high electron temperatures, the ambipolar electric field is positive (*electron root*), and in between there exist regimes where several values are possible (*multiple roots*). An important consequence is that the radial electric field is clamped at the value set by ambipolarity, and therefore sets the speed at which the plasma can rotate. Thus, a stellarator plasma cannot rotate freely [27]. Furthermore, as the rotation velocity is not uniform on the flux surface, it is not possible to transform to a system moving with a constant angular velocity without altering the structure of the equations, and consequently the radial electric field does influence stellarator physics. This will become important for the stellarator transport problems addressed in section 4.

2.7 Coordinate systems

In this section, the coordinate systems used in the subsequent sections shall be introduced. As the geometry advantages in axisymmetric systems allow for significant simplifications in the

representation of the magnetic field, it is helpful to use different coordinates for tokamaks and stellarators.

2.7.1 Coordinates for axisymmetric systems

Defining the magnetic field \mathbf{B} as the curl of a vector potential \mathbf{A} , one can find the following representation

$$\mathbf{B} = \nabla \times \mathbf{A} = B_R \mathbf{e}_R + B_\varphi \mathbf{e}_\varphi + B_z \mathbf{e}_z$$

in cylindrical coordinates (R, φ, z) . In an axisymmetric, toroidal system, all derivatives with respect to the toroidal angle φ vanish, and φ is usually defined to vary in the clockwise direction when viewed from above (contrary to the commonly used cylindrical angle). Therefore, $\mathbf{e}_r \times \mathbf{e}_z = \mathbf{e}_\varphi$. The toroidal part of the magnetic field is in the direction of $\nabla\varphi = \mathbf{e}_\varphi/R$ and can be written as [3]

$$\mathbf{B}_t \equiv B_\varphi \mathbf{e}_\varphi = I(R, z) \nabla\varphi,$$

whereas the poloidal field is expressed as

$$\mathbf{B}_p \equiv B_R \mathbf{e}_R + B_z \mathbf{e}_z = \frac{\partial A_\varphi}{\partial z} \mathbf{e}_R - \frac{1}{R} \frac{\partial (RA_\varphi)}{\partial R} \mathbf{e}_z = \nabla\varphi \times \nabla\psi,$$

with

$$\psi \equiv -RA_\varphi(R, z)$$

being the poloidal flux function. From Ampere's law and the equilibrium condition that the magnetic pressure must be balanced by the outer pressure, it is possible to show that $I(R, z) = I(\psi)$ [3]. The two terms can be combined to yield a convenient representation of the magnetic field,

$$\mathbf{B} = I(\psi) \nabla\varphi + \nabla\varphi \times \nabla\psi.$$

This representation will be used in the tokamak calculations in chapter 3. The Jacobian for the set of coordinates (ψ, φ, θ) is

$$\sqrt{g} = \frac{1}{|(\nabla\varphi \times \nabla\psi) \cdot \nabla\theta|} = \frac{1}{|\mathbf{B} \cdot \nabla\theta|}.$$

2.7.2 Coordinates for full 3D geometry

Unfortunately, the magnetic field of a stellarator does not have such a simple representation. The most convenient sets of coordinates are so-called *magnetic coordinates*. The derivation requires the assumptions that the equilibrium condition $\mathbf{j}_0 \times \mathbf{B} = \nabla p_0$, where \mathbf{j}_0 is the equilibrium current and p_0 the equilibrium pressure, is satisfied and that surfaces of constant p_0 form nested toroids. Let θ and φ denote arbitrary poloidal and toroidal angles with period 2π , respectively; from $\mathbf{B} \cdot \nabla p_0$, it follows that the magnetic field can be written as

$$\mathbf{B} = B_1(p_0, \theta, \varphi) \nabla p_0 \times \nabla \theta + B_2(p_0, \theta, \varphi) \nabla \varphi \times \nabla p_0,$$

and, after a bit of algebra, as

$$\mathbf{B} = \nabla \psi \times \nabla \theta + \nabla \varphi \times \nabla \chi$$

for some functions $\psi(p_0)$ and $\chi(p_0)$. Originating from this representation, the *rotational transform* ι is defined as

$$\iota = \frac{(\nabla \varphi \times \nabla \chi) \cdot \nabla \theta}{(\nabla \psi \times \nabla \theta) \cdot \nabla \phi} = \frac{1}{q}$$

where q is the *safety factor* usually used in tokamak literature.

An alternative representation for the magnetic field can be derived exploiting the conditions $\nabla \cdot \mathbf{j} = 0$ and $\mathbf{j} \cdot \nabla p_0 = 0$ as well as Ampère's law, $\mu_0 \mathbf{j} = \nabla \times \mathbf{B}$. One can show that it must then be possible to write \mathbf{B} as

$$\mathbf{B} = I \nabla \theta + J \nabla \varphi + \nu \nabla \psi + \nabla F, \quad (2.8)$$

where $I = I(\psi)$ and $J = J(\psi)$ are flux functions and the two arbitrary functions $\nu(\psi, \theta, \varphi)$ and $F(\psi, \theta, \varphi)$ can be further simplified using the fact that (2.8) does not change its structure when replacing the angle coordinates as

$$\begin{aligned} \theta &\rightarrow \theta' + \iota w \\ \phi &\rightarrow \phi' + w \end{aligned}$$

for any well-behaved function w which is periodic in both angles. As there is the freedom to choose w appropriately, magnetic coordinates are not uniquely defined, and different Ansätze for the choice of w have been tried and found convenient, e.g. so-called *Hamada coordinates*,

where w is chosen such as to make the Jacobian a flux function. Another example are *Boozer coordinates*, where w is chosen in such a way that F vanishes, leading to

$$\mathbf{B} = I(\psi) \nabla \theta + J(\psi) \nabla \varphi + \beta(\psi, \theta, \varphi) \nabla \psi.$$

I and J can be associated with the toroidal and poloidal currents, respectively. The Jacobian becomes

$$\frac{1}{\sqrt{g}} = (\nabla \psi \times \nabla \theta) \cdot \nabla \phi = \frac{B^2}{\iota I + J}.$$

This is the set of coordinates used in the stellarator calculations in chapter 4; note, however, that different normalisations are used for Boozer in the literature.

2. BASICS OF KINETIC TRANSPORT THEORY

3 Aspects of impurity transport in Tokamaks

In this chapter, two turbulence-related problems which arise in axisymmetric devices are studied. The first part deals with the effects of heavy impurity ions on the collisional damping of zonal flows and the consequences for plasma confinement. The second part addresses the topic of microinstabilities and the quasilinear particle fluxes as well as the behaviour of the unstable modes responsible for the production of the turbulence in the presence of impurities.

3.1 Effect of impurities on collisional zonal-flow damping in tokamaks

Zonal flows, which have been introduced in section 1.3.3, are nowadays widely accepted to play a crucial role in reducing turbulent fluxes by shearing apart turbulent eddies, thereby improving the confinement considerably. As they are produced by the turbulence itself, on which they back react to suppress it, they are intrinsically characterised by complicated nonlinear processes involving a multitude of different driving and damping mechanisms, the interplay of which has not yet been fully understood and therefore has attracted a lot of attention. The damping of these flows can be important. One question which arises is thus which damping mechanisms occur and how strong they are. As already mentioned, the poloidal and toroidal symmetry of the zonal flows prevents them from being Landau-damped, which provides a rather strong damping mechanism for any waves with finite wave numbers, and as a consequence the relative importance of collisional damping is enhanced. The presence of heavy, highly charged impurity ions, whose collision frequency exceeds that of hydrogenic bulk ions notably (by a factor $Z^{3/2}$), is therefore expected to influence this delicate balance by speeding up the damping process. The purpose of the work presented in this section was to establish whether and to which extent this is the case, and the results can be found in [28].

3.1.1 Rosenbluth-Hinton problem

In an attempt to understand the fundamental mechanisms and processes involved in the complicated creation and destruction processes of zonal flows, analytical theory can be a powerful tool to accompany numerical simulations, which, while being applicable to a much broader

3. ASPECTS OF IMPURITY TRANSPORT IN TOKAMAKS

range of problems, unavoidably constitute a black box producing results according to the input parameters but without giving any further explanation of why this result was achieved. In the case of the zonal-flow problem, Rosenbluth and Hinton developed a theory to short-circuit the problem of nonlinear feedback between the turbulence and the zonal flows, which of course is far too complicated to be described with analytical theory. The idea is to assume that an initial potential perturbation corresponding to a zonal-flow potential has already been created by turbulence and impose a short-wavelength radial electric field as an initial condition. Then, the linear response of the plasma to this potential perturbation is calculated. As the ion orbits can move radially to some extent, the plasma is polarisable and is thus able to partially shield out the externally applied electric field, and the question is then how the electric field evolves with time. The exact time evolution is not necessarily of importance but rather the state of the plasma after some time has passed. The answer to this question is sufficient to get some first ideas about the relative importance of the damping processes without having to calculate the full nonlinear dynamics; if the potential is quickly shielded out completely or nearly completely, the time scale might be too short for the corresponding zonal flows to have an influence on the turbulence. However, if the shielding is weak and the potential persists for a long time, it may be enough to know how large the influence of such a potential on the turbulence is without having to know the full feedback circle.

Polarisation of the plasma

Polarisation has two different sources, the first being the gyration of the ions around the magnetic field lines, thereby allowing them to leave the corresponding flux surface by a distance of the order of the ion Larmor radius. In accordance with the transport nomenclature, this effect is called *classical polarisation*. The second, dominant part of the polarisation originates from the much greater departure of the guiding centres from the flux surfaces (see section 1.3.1) and is accordingly called *neoclassical polarisation*. It has proven convenient to express the potential response in terms of the neoclassical polarisation.

Time evolution, Rosenbluth-Hinton test

If the plasma is in the “banana” regime, where the collision time exceeds the ion bounce time, the evolution of the initial potential occurs in different stages: on the very fast time scale of the ion gyromotion, the plasma acquires an $\mathbf{E} \times \mathbf{B}$ drift perpendicular to the magnetic field. On the longer time scale of the ion bounce motion, the plasma starts moving in the parallel direction, and this motion is modified again on the yet longer time scale of ion-ion collisions, which damp the flows and compel the plasma ions to be Maxwellian as $t \rightarrow \infty$. A particle-in-cell simulation of the collisionless potential evolution is shown in fig 3.1. The time steps on the x axis are normalised to the ion gyromotion, i.e. to Ω_i^{-1} . The electrostatic

3.1. EFFECT OF IMPURITIES ON COLLISIONAL ZONAL-FLOW DAMPING IN TOKAMAKS

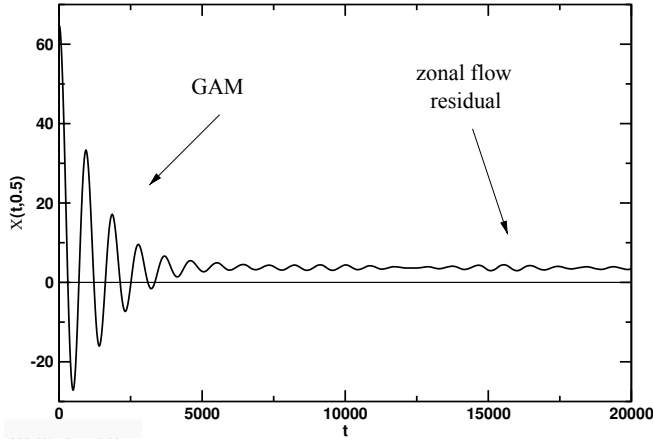


FIGURE 3.1 PIC simulation (EUTERPE) of the collisionless pure-plasma potential response (Source: Ralf Kleiber).

potential on the y axis is given in arbitrary units. As is visible from the figure, the first thing to happen, after some ion gyrations, is that the plasma starts oscillating. These oscillations are called *geodesic acoustic modes*. As they get Landau damped on time scales much faster than that on which collisional damping occurs, they do not influence the considered problem and will therefore not be addressed any further in the following. Superimposed on the Landau damping of the geodesic acoustic modes is a global drop of the potential due to the plasma polarisation. If collisions, which lead to a further global damping on a third, and much longer, time scale, are absent, the electrostatic potential does not decay entirely to zero but instead reaches a finite value, the so-called zonal-flow residual (the fluctuations which are still visible in the figure at these late times are no plasma oscillations but due to numerical noise). This result, found by Rosenbluth and Hinton [29], is of great importance as it shows that zonal flows do not get shielded entirely in a collisionless plasma, with severe consequences for transport and plasma confinement. For gyrokinetic [30] and gyrofluid [31, 32] simulations of zonal flows, this property provides an excellent benchmark, and the procedure has become known as the *Rosenbluth-Hinton test*. When collisions are present, the residual is reduced to a much lower level, as shown analytically for a pure plasma by Hinton and Rosenbluth [33] using a variational principle and later on by Xiao, Catto and Molvig [34] via an eigenfunction expansion technique, which is the method the calculation in this section is based on. The analytic calculation of the collisionless residual is shown in section 3.1.5, followed by the solution of the full multi-species collisional problem, including strongly collisional, highly charged impurities, in the subsequent sections.

3. ASPECTS OF IMPURITY TRANSPORT IN TOKAMAKS

3.1.2 Basic equations

Throughout this section, a plasma in the banana regime consisting of hydrogenic bulk ions and a single species of highly charged impurities is considered, where explicitly $Z \gg 1$ and

$$\frac{Z^2 n_z}{n_i} \sim \frac{Z m_i}{m_z} \sim 1,$$

i.e. $Z_{\text{eff}} - 1 \sim 1$.

3.1.3 Kinetic equation

For each species, the drift kinetic equation introduced in section 2.3.3 reads

$$\frac{\partial f_a}{\partial t} + (\mathbf{v}_{\parallel} + \mathbf{v}_d) \cdot \nabla f_a + \dot{\varepsilon} \frac{\partial f_a}{\partial \varepsilon} = C_a(f_a) \quad (3.1)$$

where $\mathbf{v}_d = \mathbf{b} \times \nabla \phi / B + (v_{\perp}^2/2 + v_{\parallel}^2)\mathbf{b} \times \nabla \ln B / \Omega$ is the drift velocity, $\varepsilon = m_a v^2 / 2$ the kinetic energy of the particles and $\dot{\varepsilon} = -e_a(\mathbf{v}_{\parallel} + \mathbf{v}_d) \cdot \nabla \phi$ represents a drive in form of a given electrostatic zonal flow potential $\phi(\psi, t)$, ψ being the flux surface label. Expanding in the smallness of δ_i as described earlier, one finds the lowest-order time-dependent equation

$$\frac{\partial f_{a_0}}{\partial t} + v_{\parallel} \nabla_{\parallel} f_{a_0} = C(f_{a_0}).$$

In equilibrium (when $t \rightarrow \infty$), the time derivative must vanish, and thus the zeroth-order distribution functions are stationary Maxwellians as shown in section 2. In first order, employing the typical ordering in the banana regime of small effective collision frequency, $(\nu_D^{zz} q R) / (\epsilon^{3/2} v_{thz}) \ll 1$, yields

$$\frac{\partial f_{a_1}}{\partial t} + v_{\parallel} \nabla_{\parallel} \left(f_{a_1} + \frac{I v_{\parallel}}{\Omega_a} \frac{e_a \phi'}{T_a} f_{a_0} \right) = C(f_{a_1}).$$

Here, ν_D^{zz} is the impurity collision frequency, q the safety factor, R the major radius and v_{thz} the impurity thermal velocity. The non-vanishing term $\mathbf{v}_d \cdot \nabla f_{a_0}$ was dropped as it causes ordinary neoclassical transport, which adds linearly to the effect of interest. $\epsilon \equiv r/R_0$ is the inverse aspect ratio with minor radius r and the on-axis value of the major radius R_0 . The term containing the energy derivative has been rewritten as $\dot{\varepsilon} \partial f_{a_0} / \partial \varepsilon = v_{\parallel} f_{a_0} \nabla_{\parallel} (I v_{\parallel} / \Omega_a) e_a \phi' / T_a$, where a prime always denotes derivation with respect to ψ (see appendix at the end of this chapter). This notation suggests splitting off the adiabatic part from

3.1. EFFECT OF IMPURITIES ON COLLISIONAL ZONAL-FLOW DAMPING IN TOKAMAKS

the distribution function by letting

$$f_{a_1} = g_a - \frac{Iv_{\parallel}}{\Omega_a} \frac{e_a \phi'}{T_a} f_{a_0}.$$

If one assumes the distribution function to vary on time scales much longer than the bounce time τ_b and the collision frequency ν to be much smaller than the bounce frequency ω_b , it is possible to further expand g_a to find in zeroth order

$$v_{\parallel} \nabla_{\parallel} g_{a_0} = 0, \quad (3.2)$$

and then in first order

$$\frac{\partial g_{a_0}}{\partial t} - \frac{Iv_{\parallel}}{\Omega_a} \frac{e_a}{T_a} \frac{\partial \phi'}{\partial t} f_{a_0} + v_{\parallel} \nabla_{\parallel} g_{a_1} = C(f_{a_1}). \quad (3.3)$$

Conveniently, only the passing particle distribution has to be calculated, as g_{a_0} can be shown to vanish in the trapped region [3]. To this end, note first that g_{a_0} must be an even function of $\sigma \equiv v_{\parallel}/|v_{\parallel}|$ since this must be true at the bounce points (the points where the trapped particles turn around) where v_{\parallel} vanishes, and consequently everywhere as (3.2) implies that $\partial g_{a_0}/\partial \theta = 0$. Rewriting the parallel gradient in eq. (3.3) in terms of a θ derivative and integrating between the bounce points yields

$$\int_{-\theta_b}^{\theta_b} \frac{d\theta}{\mathbf{B} \cdot \nabla \theta} \frac{B}{\sigma |v_{\parallel}|} \left(C_a(f_{a_1}) + \frac{Iv_{\parallel}}{\Omega} \frac{e_a}{T_a} \frac{\partial \phi'}{\partial t} f_{a_0} - \frac{\partial g_{a_0}}{\partial t} \right) = g_{a_1}(\theta_b) - g_{a_1}(-\theta_b).$$

Taking the difference of the $\sigma = +1$ and the $\sigma = -1$ version annihilates all terms odd in σ (note that this also holds for the parts of f_{a_1} proportional to v_{\parallel} on which the collision operator acts, as the σ dependence is not influenced by this operation), and from the remaining terms one finds

$$\begin{aligned} & \int_{-\theta_b}^{\theta_b} \frac{d\theta}{\mathbf{B} \cdot \nabla \theta} \frac{B}{|v_{\parallel}|} \left(C_a(g_{a_0}(\sigma = 1)) + C_a(g_{a_0}(\sigma = -1)) - \left(\frac{\partial g_{a_0}(\sigma = 1)}{\partial t} + \frac{\partial g_{a_0}(\sigma = -1)}{\partial t} \right) \right) \\ &= 0. \end{aligned}$$

But this relation can only be satisfied if g_{a_0} is odd in σ , and it therefore vanishes identically in the whole trapped region. Thus, only particles with $0 \leq \lambda \leq \lambda_c \equiv B_0/B_{max}$ matter,

3. ASPECTS OF IMPURITY TRANSPORT IN TOKAMAKS

where the pitch-angle variable λ is defined as $\lambda = v_{\perp}^2 B_0 / (v^2 B)$. Furthermore, B_0 is defined via $B_0^2 = \langle B^2 \rangle$, where angular brackets denote the flux-surface average. Multiplying (3.3) by B/ξ , $\xi \equiv v_{\parallel}/v$, and taking the flux surface average annihilates the parallel gradient, so that the differential equation which needs to be solved becomes

$$\left\langle \frac{B}{\xi} \left(\frac{\partial g_{a0}}{\partial t} - C(f_{a1}) \right) \right\rangle = \frac{m_a}{T_a} I v f_{a0} \frac{\partial \phi'}{\partial t}, \quad (3.4)$$

together with the boundary condition $g_{a0}(\lambda_c) = 0$ needed for continuity of the distribution function at the trapped-passing boundary. This equation will be solved in section 3.1.6 for both bulk ions and impurities, taking into account the different collisional behaviour of the two species.

3.1.4 Neoclassical polarisation

In order to study the response of the plasma to a zonal flow potential, the kinetic equation of the previous section can be coupled with the gyrokinetic quasineutrality condition in the limit of small ion gyroradius ($k_{\perp} \rho_i \ll 1$, where k_{\perp} is the perpendicular wave number),

$$en_e = \sum_{a=i,z} e_a \left(N_a + \nabla \cdot \left(\frac{n_a}{\Omega_a B} \nabla \phi \right) \right),$$

where n_a denotes the number density for the respective species and N_a the guiding centre density which is defined by

$$N_a(\mathbf{R}_a) = \int f(\mathbf{R}_a, \mathbf{v}, t) d^3v \Big|_{\mathbf{R}_a \text{fixed}}$$

where $\mathbf{R}_a = \mathbf{r} - \mathbf{b} \times \mathbf{v}/\Omega_a$ is the guiding-centre position of the species a . Since the electrons are frozen into the field, the electron density is conserved and one gets

$$\frac{\partial}{\partial t} \left[N_i + Z N_z + \nabla \cdot \left(\frac{(m_i n_i + m_z n_z) \nabla \phi}{e B^2} \right) \right] = 0. \quad (3.5)$$

Taking the flux surface average and using the relation

$$\langle \nabla \cdot \mathbf{A} \rangle = \frac{1}{V'} \frac{\partial}{\partial \psi} V' \langle \mathbf{A} \cdot \nabla \psi \rangle,$$

3.1. EFFECT OF IMPURITIES ON COLLISIONAL ZONAL-FLOW DAMPING IN TOKAMAKS

which holds for any vector \mathbf{A} and where $V(\psi)$ is the volume within the flux surface ψ , one can rewrite (3.5) as

$$\begin{aligned} \frac{\partial}{\partial t} \left\langle \frac{(m_i n_i + m_z n_z) |\nabla \psi|^2}{B^2} \phi' \right. \\ \left. - \int \frac{I v_{\parallel}}{B} \left(m_i g_{i0} + m_z g_{z0} - \frac{I v_{\parallel}}{B} \phi' \left(\frac{m_i^2}{T_i} f_{i0} + \frac{m_z^2}{T_z} f_{z0} \right) \right) d^3 v \right\rangle = 0, \end{aligned} \quad (3.6)$$

where

$$\begin{aligned} \frac{\partial \langle N_a \rangle}{\partial t} &= -\frac{1}{V'} \frac{\partial}{\partial \psi} V' \left\langle \int f_{a1} \mathbf{v}_d \cdot \nabla \psi d^3 v \right\rangle \\ &= -\frac{1}{V'} \frac{\partial}{\partial \psi} V' \left\langle \int g_a v_{\parallel} \nabla_{\parallel} \left(\frac{I v_{\parallel}}{\Omega_a} \right) d^3 v \right\rangle \\ &= \frac{1}{V'} \frac{\partial}{\partial \psi} V' \left\langle \int \frac{I v_{\parallel}^2}{\Omega_a} \nabla_{\parallel} g_a d^3 v \right\rangle - \frac{1}{V'} \frac{\partial}{\partial \psi} V' \underbrace{\left\langle B \nabla_{\parallel} \left(\int \frac{v_{\parallel}}{B} g_a \frac{I v_{\parallel} m_a}{e B} d^3 v \right) \right\rangle}_{=0} \\ &= -\frac{1}{V'} \frac{\partial}{\partial \psi} V' \left\langle \int \frac{I v_{\parallel}}{\Omega_a} \left(\frac{\partial g_{a0}}{\partial t} - \frac{I v_{\parallel}}{\Omega_a} \frac{e_a}{T_a} \frac{\partial \phi'}{\partial t} f_{a0} - C_a(f_{a1}) \right) d^3 v \right\rangle. \end{aligned}$$

was used. Note that the terms containing the collision operator drop out due to momentum conservation. Noticing that

$$\begin{aligned} \left\langle \frac{I}{B} \int m_a v_{\parallel} f_{a1} d^3 v \right\rangle &= \left\langle m_a n_a R V_{a\parallel} \mathbf{b} \cdot \mathbf{e}_{\varphi} \right\rangle \\ &= L_{\parallel} \end{aligned}$$

is the angular momentum of the parallel motion while that of the perpendicular $\mathbf{E} \times \mathbf{B}$ motion is

$$\begin{aligned} L_{\perp} &= \left\langle m_a n_a \frac{\mathbf{b} \times \nabla \phi}{B} \cdot R \mathbf{e}_{\varphi} \right\rangle = \left\langle m_a n_a \frac{I \mathbf{b} - R B e_{\varphi} \cdot R \mathbf{e}_{\varphi}}{B} \right\rangle \phi' \\ &= m_a n_a \left\langle \frac{I^2}{B^2} - R^2 \right\rangle \phi' = -m_a n_a \left\langle \frac{|\nabla \psi|^2}{B^2} \right\rangle \phi', \end{aligned}$$

one finds that eq. (3.6) represents the conservation of toroidal angular momentum. Here $V_{a\parallel}$ denotes the parallel velocity of the particle species a , \mathbf{b} is the unit vector along the magnetic field and \mathbf{e}_{φ} the unit vector in the φ direction.

3. ASPECTS OF IMPURITY TRANSPORT IN TOKAMAKS

For later calculations, it is convenient to Laplace transform the equations and choose the initial conditions such that there is no initial parallel rotation of the plasma, i.e. $f_{i1}(0) = f_{z1}(0) = 0$, to yield

$$\left\langle - \int \frac{Iv_{\parallel}}{B} \left(m_i \hat{g}_{i0} + m_z \hat{g}_{z0} - \frac{Iv_{\parallel}}{B} \hat{\phi}'(p) \left(\frac{m_i^2}{T_i} f_{i0} + \frac{m_z^2}{T_z} f_{z0} \right) \right) d^3 v + \frac{(m_i n_i + m_z n_z) |\nabla \psi|^2}{B^2} \hat{\phi}'(p) \right\rangle = \frac{1}{p} \left\langle \frac{(m_i n_i + m_z n_z) |\nabla \psi|^2}{B^2} \right\rangle \phi(0),$$

or, using

$$\begin{aligned} \frac{I^2}{B^2} m_a \int \frac{m_a}{T_a} v_{\parallel}^2 f_{a0} d^3 v &= m_a n_a \frac{I^2}{B^2}, \\ \langle (m_i n_i + m_z n_z) R^2 \rangle \hat{\phi}'(p) - \left\langle \int \frac{Iv_{\parallel}}{B} (m_z \hat{g}_{z0} + m_i \hat{g}_{i0}) d^3 v \right\rangle &= \frac{1}{p} \left\langle \frac{(m_i n_i + m_z n_z) |\nabla \psi|^2}{B^2} \right\rangle \phi(0). \end{aligned}$$

Laplace transformed quantities are denoted by a hat. Thus, if defining the neoclassical polarisation \hat{P} as

$$\hat{P} = \sum_{a=i,z} \left\langle \frac{I}{B} \int m_a v_{\parallel} \hat{g}_{a0} d^3 v \right\rangle / \sum_{a=i,z} \langle m_a n_a R^2 \rangle \hat{\phi}',$$

one can represent the potential response as

$$\hat{\phi}'(p) = \frac{1}{p} \phi'(0) \frac{\left\langle \frac{|\nabla \psi|^2}{B^2} \right\rangle}{\langle R^2 \rangle (1 - \hat{P})}.$$

Note that $\hat{g}_{a0}(p)$ was anticipated to be proportional to $\hat{\phi}'(p)$ and the initial condition on the distribution function was taken to be $f_{a1}(t = 0) = 0$. The main remaining task is now to calculate the polarisation \hat{P} , which requires calculating the distribution functions of all the different particle species.

3.1.5 Collisionless response

For the simplest case of a collisionless plasma, (3.4) can easily be integrated without Laplace transforming to yield the circulating part of the distribution

$$g_{a_0} = I v \frac{m_a}{T_a} \left\langle \frac{B}{\xi} \right\rangle^{-1} \phi' f_{a_0}. \quad (3.7)$$

Thus, eq. (3.6) reads

$$\frac{\partial \phi'}{\partial t} \sum_{a=i,z} \left\langle m_a n_a \frac{|\nabla \psi|^2}{B^2} - I^2 \frac{m_a^2}{T_a} \int \frac{v_{\parallel}}{B} f_{a_0} \left(\left\langle \frac{B}{v_{\parallel}} \right\rangle^{-1} H \left(1 - \lambda \frac{B}{B_0} \right) - \frac{v_{\parallel}}{B} \right) d^3 v \right\rangle,$$

where the Heaviside step function H accounts for the fact that g_{a_0} must vanish in the trapped region, and, with the same initial condition as before, namely $f_{a_0}(0) = 0$, the ratio between the potential at time t and the initial potential becomes

$$\frac{\phi'(t)}{\phi'(0)} = \frac{\sum_{a=i,z} \left\langle m_a n_a \frac{|\nabla \psi|^2}{B^2} \right\rangle}{\sum_{a=i,z} \left(\left\langle m_a n_a \frac{|\nabla \psi|^2}{B^2} \right\rangle - I^2 \frac{m_a^2}{T_a} \int \frac{v_{\parallel}}{B} f_{a_0} \left(\left\langle \frac{B}{v_{\parallel}} \right\rangle^{-1} H \left(1 - \lambda \frac{B}{B_0} \right) - v_{\parallel}/B \right) d^3 v \right)}.$$

For a large-aspect-ratio tokamak with circular flux surfaces one can calculate the integrals in the denominator by expressing them through elliptic functions:

$$\begin{aligned} & \left\langle \int \frac{v_{\parallel}}{B} \frac{m_a}{T_a} \left(\left\langle \frac{B}{v_{\parallel}} \right\rangle^{-1} H \left(1 - \lambda \frac{B}{B_0} \right) - \frac{v_{\parallel}}{B} \right) f_{a_0} d^3 v \right\rangle \\ &= \int_0^\infty 2\pi \frac{m_a v^2}{T_a} f_{a_0} v^2 dv \left\langle \int \left(\left\langle \frac{B}{\xi} \right\rangle^{-1} H \left(1 - \lambda \frac{B}{B_0} \right) - \frac{\xi}{B} \right) d\lambda \right\rangle \\ &= \frac{3n_a}{2B_0} \left[\underbrace{\int_0^{\lambda_c} \left(\left\langle \frac{B}{\xi} \right\rangle^{-1} - \left\langle \frac{\xi}{B} \right\rangle \right) d\lambda}_{I_1} - \underbrace{\int_{\lambda_c}^{\frac{B_0}{B}} \frac{\xi}{B} d\lambda}_{I_2} \right], \end{aligned}$$

where $\lambda_c \equiv B_0/B_{max}$.

3. ASPECTS OF IMPURITY TRANSPORT IN TOKAMAKS

Note that the first term vanishes in the trapped region as it is odd in σ . Starting with the second integral and using the cylinder approximation $\mathbf{B} \cdot \nabla\theta \approx B_p/r$, which holds approximately in a large-aspect-ratio tokamak and where B_p denotes the poloidal magnetic field, one gets

$$\begin{aligned} I_2 &= \oint \frac{d\theta}{\mathbf{B} \cdot \nabla\theta} \int_{\lambda_c}^{B_0/B(\theta)} \frac{\xi}{B} d\lambda / \oint \frac{d\theta}{\mathbf{B} \cdot \nabla\theta} \\ &\approx \frac{1}{2\pi B_0} \int_{\lambda_c}^{B_0/B_{min}} d\lambda \int_{-\theta_b}^{\theta_b} \sqrt{1 - \lambda(1 - \epsilon \cos\theta)} d\theta \\ &= \frac{1}{\pi B_0} \int_{\lambda_c}^{B_0/B_{min}} d\lambda \int_{-\theta_b/2}^{\theta_b/2} \sqrt{\frac{2\epsilon}{2\epsilon k^2 + 1}} \sqrt{k^2 - \sin^2\vartheta} d\vartheta \end{aligned}$$

where $\vartheta = \theta/2$, $k^2 \equiv \sin^2\theta_b/2 = (1 - \lambda(1 - \epsilon))/(2\epsilon\lambda)$ is the so-called trapping parameter and the change in the order of integration has been accounted for by taking the second integral between the bounce points θ_b and $-\theta_b$ only. Changing again the integration variable according to $\sin\vartheta = ks\sin x$, one can rewrite this expression as

$$I_2 = \frac{2}{\pi B_0} \int_{\lambda_c}^{B_0/B_{min}} d\lambda \sqrt{\frac{2\epsilon}{2\epsilon k^2 + 1}} [(k^2 - 1)K(k) + E(k)],$$

where E and K are the complete elliptic integrals of first and second kind, respectively, defined as

$$E(k) \equiv \int_0^{\pi/2} \sqrt{1 - k^2 \sin^2 x} dx \quad \text{and} \quad K(k) \equiv \int_0^{\pi/2} \frac{dx}{\sqrt{1 - k^2 \sin^2 x}},$$

3.1. EFFECT OF IMPURITIES ON COLLISIONAL ZONAL-FLOW DAMPING IN TOKAMAKS

and, finally, as

$$\begin{aligned} & \frac{4(2\epsilon)^{3/2}}{\pi B_0} \int_0^1 [(k^2 - 1)K(k) + E(k)] k dk \\ &= \frac{4(2\epsilon)^{3/2}}{\pi B_0} \int_0^1 k^3 K(k) + k^2 \frac{d}{dk} E(k) dk \end{aligned}$$

where $E(k) - K(k) = kd/dk E(k)$ was used. These integrals can be found in tables, and

$$I_2 = \frac{8}{9\pi} \frac{(2\epsilon)^{3/2}}{B_0} + \mathcal{O}(\epsilon^2).$$

For the calculation of I_1 , one needs

$$\begin{aligned} \left\langle \frac{\xi}{B} \right\rangle &= \oint \frac{\xi}{B} \frac{d\theta}{B \cdot \nabla \theta} / \oint \frac{d\theta}{B \cdot \nabla \theta} \\ &\approx \frac{1}{2\pi B_0} \int_0^{2\pi} \sqrt{1 - \lambda(1 - \epsilon \cos \theta)} d\theta \\ &= \frac{2}{\pi B_0} \sqrt{\frac{2\epsilon}{2\epsilon + k^2}} E(k), \end{aligned}$$

where now $k^2 = 2\epsilon\lambda/(1 - \lambda(1 - \epsilon))$, and

$$\left\langle \frac{B}{\xi} \right\rangle^{-1} \approx \frac{2\pi}{\oint B/\xi d\theta} = \frac{\pi}{2B_0} \sqrt{\frac{2\epsilon}{2\epsilon + k^2}} \frac{1}{K(k)}.$$

Thus,

$$I_1 \approx \frac{(2\epsilon)^{3/2}}{B_0} \int_0^1 \left[\frac{\pi}{2K(k)} - \frac{2E(k)}{\pi} \right] \frac{dk^2}{k^5},$$

3. ASPECTS OF IMPURITY TRANSPORT IN TOKAMAKS

which can be calculated numerically to yield

$$I_1 \approx -0.1028 \frac{(2\epsilon)^{3/2}}{B_0} + \mathcal{O}(\epsilon^2).$$

Consequently, the full integral equals

$$\frac{3}{2B_0} n_a (I_1 - I_2) \approx -1.64 n_a \frac{\epsilon^{3/2}}{B_0^2} + \mathcal{O}(\epsilon^2),$$

a value which appears repeatedly in neoclassical transport theory. Inserting this value into the formula for the potential response, one gets

$$\begin{aligned} \hat{\phi}'(p) &= \frac{\sum_a \left\langle m_a n_a \frac{|\nabla \psi|^2}{B^2} \right\rangle}{\sum_a \langle m_a n_a R^2 \rangle (1 - \hat{P})} \frac{\phi'(0)}{p} \\ &\approx \frac{\sum_a m_a n_a R^2 \frac{B_p^2}{B^2}}{\sum_a m_a n_a \frac{r^2}{q^2} \left(1 + 1.64 \frac{q^2}{\sqrt{\epsilon}}\right)} \frac{\phi'(0)}{p} \\ &= \frac{1}{1 + 1.64 \frac{q^2}{\sqrt{\epsilon}}} \frac{\phi'(0)}{p}, \end{aligned}$$

which is the classical Rosenbluth-Hinton result [29] for the collisionless potential response and the same result as in a pure plasma.

In the next sections, the potential response is calculated for the case where collisions are included.

3.1.6 Collisional potential response

In order to obtain the collisional potential response, it is necessary to solve the drift kinetic equations for both particle species. It is slightly easier to do so for the impurities, as impurity-ion collisions are less frequent than impurity self collisions by a factor of $1/\sqrt{Z}$ and can therefore be neglected. Thus, the impurity problem is analogous to the problem in a pure plasma. The solution can afterwards be used to solve for the ion distribution.

Impurities

Self collisions are included in the model derived in section 3.1.3 using the linearised model operator introduced in section 2.4,

$$C_{zz}(f_{z_1}) = \nu_D^{zz} \left(\mathcal{L}(f_{z_1}) + \frac{m_z}{T_z} v_{\parallel} u_{z_{\parallel}} f_{z_0} \right),$$

where the term containing $u_{z_{\parallel}}$ has been added to restore momentum conservation and can be calculated from the constraint

$$\int v_{\parallel} C_{zz}(f_{z_1}) d^3v = 0.$$

In order to solve eq. (3.4), an eigenfunction expansion technique [35] is used for the Lorentz operator, which can be expressed in terms of the pitch angle variable λ as

$$\mathcal{L} = \frac{2\xi B_0}{B} \frac{\partial}{\partial \lambda} \lambda \xi \frac{\partial}{\partial \lambda},$$

and the distribution function is expanded in eigenfunctions $\Lambda_n(\psi, \lambda)$, determined by the eigenvalue problem

$$\left\langle \frac{B}{\xi} \mathcal{L}(\Lambda_n) \right\rangle = 2B_0 \frac{\partial}{\partial \lambda} \lambda \langle \xi \rangle \frac{\partial \Lambda_n}{\partial \lambda} = -\chi_n \left\langle \frac{B}{\xi} \right\rangle \Lambda_n$$

in the domain $0 < \lambda < \lambda_c$. The boundary conditions are chosen such that the transition at the trapped-passing boundary is continuous, and thus $\Lambda_n(\lambda = \lambda_c) = 0$. Note that the equation has a regular singular point at $\lambda = 0$ and it is therefore necessary to demand $\Lambda_n(\lambda = 0)$ to stay finite as a natural boundary condition. As the Lorentz operator is self-adjoint and the weight $\langle B/\xi \rangle \geq 0$, Sturm-Liouville theory applies and the eigenfunctions form a complete and orthogonal set in the sense that

$$\int_0^{\lambda_c} \Lambda_m \Lambda_n \left\langle \frac{B}{\xi} \right\rangle d\lambda = 0 \quad \text{if} \quad m \neq n.$$

This can easily be seen from the following relation, using self-adjointness of the Lorentz

3. ASPECTS OF IMPURITY TRANSPORT IN TOKAMAKS

operator and integration by parts:

$$\begin{aligned}
\int_0^{\lambda_c} \Lambda_m \Lambda_n \left\langle \frac{B}{\xi} \right\rangle d\lambda &= -\frac{1}{\chi_n} \int_0^{\lambda_c} \Lambda_m \left\langle \frac{B}{\xi} \mathcal{L}(\Lambda_n) \right\rangle d\lambda \\
&= -\frac{2B_0}{\chi_n} \int_0^{\lambda_c} \Lambda_m \frac{\partial}{\partial \lambda} \lambda \langle \xi \rangle \frac{\partial \Lambda_n}{\partial \lambda} d\lambda \\
&= -\frac{2B_0}{\chi_n} \int_0^{\lambda_c} \Lambda_n \frac{\partial}{\partial \lambda} \lambda \langle \xi \rangle \frac{\partial \Lambda_m}{\partial \lambda} d\lambda \\
&= \frac{\chi_m}{\chi_n} \int_0^{\lambda_c} \Lambda_m \Lambda_n \left\langle \frac{B}{\xi} \right\rangle d\lambda.
\end{aligned}$$

For $m \neq n$, this relation can only hold if the integral vanishes. For convenience, the normalisation

$$\int_0^{\lambda_c} \Lambda_n d\lambda = \frac{2}{3}$$

is chosen. The functions g_{a_0} can be expanded in an eigenfunction series as

$$g_{a_0} = \sigma \sum_{n=1}^{\infty} b_{an}(\psi, v) \Lambda_n(\psi, \lambda).$$

In principle, the eigenfunctions can be calculated numerically by expanding them in a series of Legendre polynomials, which are exact solutions in a circular flux-surface geometry when ϵ vanishes, albeit the result is rather poor when it does not, even in a large aspect ratio tokamak, as Hsu, Catto and Sigmar noted [35]. The idea is to express the Lorentz operator in terms of the variable $\eta \equiv \sqrt{1 - \lambda/\lambda_c}$, yielding

$$\frac{\partial}{\partial \eta} (1 - \eta^2) \frac{\langle \xi \rangle}{\eta} \frac{\partial}{\partial \eta} \Lambda_n = -2\chi_n \frac{\partial \langle \xi \rangle}{\partial \eta} \Lambda_n$$

with the boundary conditions $\Lambda_n(\eta = 0) = 0$ in order to guarantee the proper behaviour at

3.1. EFFECT OF IMPURITIES ON COLLISIONAL ZONAL-FLOW DAMPING IN TOKAMAKS

the untrapped boundary, and then expand according to

$$\Lambda_n(\eta) = \frac{\eta}{\langle \xi \rangle} \sum_{m=1}^{\infty} a_{nm} P_{2m-1}(\eta)$$

where P_i denotes the i 'th Legendre polynomial. Employing numerical values for $\langle \xi \rangle$, $\langle B/\xi \rangle$ and $\langle B^2/\xi^3 \rangle$, one can calculate the eigenfunctions and eigenvalues for different geometries. Fortunately, in the long-time limit, it is not necessary to employ these inaccurate values, as will become clear later on, and therefore the numerical values are not given here.

Eq. (3.4) is now solved for the impurities. Inserting the model collision operator yields

$$\left\langle \frac{B}{\xi} \right\rangle \frac{\partial g_{z_0}}{\partial t} - \nu_D^{zz} \left\langle \frac{B}{\xi} \mathcal{L}(f_{z_1}) \right\rangle = \frac{m_z}{T_z} v f_{z_0} \left(I \frac{\partial \phi'}{\partial t} + \nu_D^{zz} \left\langle B u_{z_\parallel} \right\rangle \right),$$

and, after using the eigenfunction expansion and Laplace transforming,

$$\begin{aligned} p \hat{b}_{zn} - b_{zn}(t \ll \tau_a) + \chi_n \nu_D^{zz} \hat{b}_{zn} &= \beta_n \frac{m_z}{T_z} v f_{z_0} \left(I p \hat{\phi}' - I \phi'(t \ll \tau_a) \right. \\ &\quad \left. + I \hat{\phi}' \nu_D^{zz} + \nu_D^{zz} \langle B \hat{u}_{z_\parallel} \rangle \right) \end{aligned}$$

with

$$\beta_n \equiv \frac{\sigma B_0 \int_0^{\lambda_c} \Lambda_n d\lambda}{\int_0^{\lambda_c} \left\langle \frac{B}{\xi} \right\rangle \Lambda_n^2 d\lambda} = \frac{2\sigma B_0}{3 \int_0^{\lambda_c} \left\langle \frac{B}{\xi} \right\rangle \Lambda_n^2 d\lambda}.$$

As g_{a_0} changes rapidly on the bounce time scale but afterwards relaxes much more slowly on the collision time scale, it is not possible to use the initial condition $f_{a_1} = 0$ at $t = 0$ used in section 3.1.4 for studying the effect on the slower time scale as this initial condition would violate the condition (3.2) due to the expansion in ω_b . Therefore, the initial condition is taken at $t \ll \tau_a$, which shall express a time later than a few bounce times but much earlier than the collision time, to be consistent with the employed ordering. This initial condition for g_{a_0} can be obtained from the collisionless limit (3.7), which gives

$$g_{a_0}(t \ll \tau_a) = \frac{m_a}{T_a} f_{a_0} \left\langle \frac{B}{v_\parallel} \right\rangle^{-1} I \phi'(t \ll \tau_a),$$

3. ASPECTS OF IMPURITY TRANSPORT IN TOKAMAKS

where τ_a denotes the collision time. Thus, the two terms in eq. (3.8) containing the initial conditions cancel each other.

The distribution function \hat{f}_{z_1} is then given by the following expression

$$\hat{f}_{z_1} = \frac{m_z}{T_z} f_{z_0} \left[\sigma v \sum_{n=1}^{\infty} \frac{\beta_n \Lambda_n}{B_0(p + \chi_n \nu_D^{zz})} (I\hat{\phi}'(p + \nu_D^{zz}) + \nu_D^{zz} \langle B\hat{u}_{z_\parallel} \rangle) - \frac{Iv_\parallel}{B} \hat{\phi}' \right].$$

To conserve momentum in like-particle collisions, \hat{u}_{z_\parallel} is calculated from

$$\int v_\parallel C_{zz}(\hat{f}_z) d^3v \stackrel{!}{=} 0.$$

Exploiting the self-adjointness of the Lorentz operator and the relation $\mathcal{L}(v_\parallel) = -v_\parallel$, one arrives at the following expression [3]

$$\hat{u}_{z_\parallel} = \frac{\int v_\parallel \nu_D^{zz} \hat{f}_{z_1} d^3v}{n_z \{ \nu_D^{zz} \}},$$

with the velocity-space average defined as

$$\{F(v)\}_a \equiv \int F(v) \frac{m_a v_\parallel^2}{n_a T_a} f_{a_0} d^3v = \frac{8}{3\sqrt{\pi}} \int_0^\infty e^{-x_a^2} x_a^4 F(x_a) dx_a.$$

The index a at the curly brackets will be dropped when there is no risk of ambiguity. Using

$$\begin{aligned} \int v_\parallel \nu_D^{zz} \hat{f}_{z_1} d^3v &= \int v_\parallel \nu_D^{zz} \left(\hat{g}_{z_0} - \frac{m_z v_\parallel}{T_z} \frac{I\hat{\phi}'}{B} f_{z_0} \right) d^3v \\ &= \int v_\parallel \nu_D^{zz} \hat{g}_{z_0} d^3v - \frac{I\hat{\phi}'}{B} n_z \{ \nu_D^{zz} \} \end{aligned}$$

and

$$\begin{aligned} \int v_\parallel \nu_D^{zz} \hat{g}_{z_0} d^3v &= \sum_{n=1}^{\infty} \int v_\parallel \hat{b}_{zn} \Lambda_n \sigma f_{z_0} \nu_D^{zz} d^3v \\ &= \frac{B}{B_0^2} n_z \sum_{n=1}^{\infty} \beta_n \left\{ \nu_D^{zz} \frac{p I\hat{\phi}'}{p + \chi_n \nu_D^{zz}} + \nu_D^{zz} (I\hat{\phi}') \right\}, \end{aligned}$$

3.1. EFFECT OF IMPURITIES ON COLLISIONAL ZONAL-FLOW DAMPING IN TOKAMAKS

one can multiply by B and take the flux surface average to find

$$\begin{aligned}\langle B\hat{u}_{z\parallel} \rangle &= -I\hat{\phi}' + \frac{1}{\{\nu_D^{zz}\}} \sum_{n=1}^{\infty} \beta_n \left\{ \nu_D^{zz} \frac{pI\hat{\phi}' + \nu_D^{zz}(I\hat{\phi}' + \langle B\hat{u}_{z\parallel} \rangle)}{p + \chi_n \nu_D^{zz}} \right\} \\ &= -I\hat{\phi}' \left(1 - \frac{\frac{p}{\{\nu_D^{zz}\}} \sum_{n=1}^{\infty} \beta_n \left\{ \frac{\nu_D^{zz}}{p + \chi_n \nu_D^{zz}} \right\}}{1 - \frac{1}{\{\nu_D^{zz}\}} \sum_{n=1}^{\infty} \beta_n \left\{ \frac{(\nu_D^{zz})^2}{p + \chi_n \nu_D^{zz}} \right\}} \right),\end{aligned}$$

which, in the long-time limit (small p), simplifies to

$$\langle B\hat{u}_{z\parallel} \rangle = -I\hat{\phi}'(1 - p\tau_0 + \mathcal{O}(p^2))$$

where

$$\tau_0^{-1} \equiv \{\nu_D^{zz}\} \left(\left(\sum_{n=1}^{\infty} \frac{\beta_n}{\chi_n} \right)^{-1} - 1 \right). \quad (3.8)$$

To ensure the well-definedness of τ_0 , one can show $\sum_{n=1}^{\infty} \beta_n / \chi_n$ to equal the “effective” fraction of circulating particles introduced in [36], and thus always to be smaller than one by the following argument: consider the problem

$$\left\langle \frac{B}{\xi} \mathcal{L}(h) \right\rangle = -B_0, \quad h(\lambda_c) = 0, \quad h(0) < \infty. \quad (3.9)$$

Inserting the expansion $h(\lambda) = \sigma \sum_{n=1}^{\infty} h_n \Lambda_n(\lambda)$ in eq. (3.9) yields

$$\sigma \sum_{n=1}^{\infty} \chi_n h_n \Lambda_n = B_0 \left\langle \frac{B}{\xi} \right\rangle^{-1} = \sum_{n=1}^{\infty} \beta_n \Lambda_n,$$

and thus

$$h(\lambda) = \sigma \sum_{n=1}^{\infty} \frac{\beta_n}{\chi_n} \Lambda_n.$$

3. ASPECTS OF IMPURITY TRANSPORT IN TOKAMAKS

Consequently,

$$\int_0^{\lambda_c} h(\lambda) d\lambda = \sigma \sum_{n=1}^{\infty} \frac{\beta_n}{\chi_n} \int_0^{\lambda_c} \Lambda_n d\lambda = \frac{2}{3} \sigma \sum_{n=1}^{\infty} \frac{\beta_n}{\chi_n}.$$

On the other hand, straight-forward integration of (3.9) leads to

$$h(\lambda) = \frac{\sigma}{2} \int_{\lambda}^{\lambda_c} \frac{d\lambda'}{\left\langle \sqrt{1 - \lambda' \frac{B}{B_0}} \right\rangle},$$

and combining both equations yields

$$\begin{aligned} \sum_{n=1}^{\infty} \frac{\beta_n}{\chi_n} &= \frac{3\sigma}{2} \int_0^{\lambda_c} h(\lambda) d\lambda = \frac{3}{4} \int_0^{\lambda_c} \frac{\lambda d\lambda}{\left\langle \sqrt{1 - \lambda \frac{B}{B_0}} \right\rangle} \\ &\equiv f_c \end{aligned}$$

where f_c is the “effective” fraction of circulating particles and is obviously always smaller than or equal to 1 since, due to Hölder’s inequality,

$$\begin{aligned} f_c &\equiv \frac{3}{4} \int_0^{\lambda_c} \lambda \frac{d\lambda}{\left\langle \sqrt{1 - \lambda \frac{B}{B_0}} \right\rangle} \\ &\leq \frac{3}{4} \int_0^{\lambda_c} \lambda \left\langle \frac{1}{\sqrt{1 - \lambda \frac{B}{B_0}}} \right\rangle d\lambda = \frac{3}{4} b^2 \left\langle \int_0^1 \frac{x dx}{\sqrt{1 - xb}} \right\rangle \end{aligned}$$

with $\lambda_c = b \equiv B_0/B_{max} \leq 1$. But

$$1 = \frac{3}{4} \int_0^1 \frac{x dx}{\sqrt{1 - x}},$$

and as

$$\frac{b^2}{\sqrt{1-xb}} \leq \frac{1}{\sqrt{1-x}},$$

it follows that

$$\begin{aligned} f_c &= 1 - \frac{3}{4} \left\langle \int_0^1 \left(\frac{1}{\sqrt{1-x}} - \frac{b^2}{\sqrt{1-xb}} \right) x dx \right\rangle \\ &\geq 0 \end{aligned}$$

with equality if and only if $B = B_{max} = \text{const}$, which is not the case in a toroidal device. Thus, τ_0 and therefore the momentum restoring term $\langle B \hat{u}_{i\parallel} \rangle$ are both well-defined. For a large aspect-ratio tokamak with circular flux surfaces, $f_c \cong 1 - 1.46\sqrt{\epsilon}$.

Bulk ions

In this section, the slightly more challenging task of calculating the distribution function of the bulk ions is addressed. Decomposing the collision operator into a self collision part, for which the same operator as in the previous section is used, and an operator describing ion-impurity collisions, which can be approximated with the operator for disparate mass ratio from section 2.4, one finds the bulk ion collision operator

$$C_i(f_{i1}) = (\nu_D^{ii} + \nu_D^{iz}) \mathcal{L}(f_{i1}) + \frac{m_i}{T_i} v_{\parallel} f_{i0} \left(\nu_D^{ii} u_{i\parallel} + \nu_D^{iz} V_{z\parallel} \right).$$

Note that, within the ordering applied, ν_D^{ii} and ν_D^{iz} are of the same order of magnitude as $\hat{\nu}_D^{iz}/\hat{\nu}_D^{ii} \sim Z^2 n_z/n_i \sim 1$. The differential equation (3.4) then becomes

$$\begin{aligned} &\left\langle \frac{B}{\xi} \right\rangle \frac{\partial g_{i0}}{\partial t} - (\nu_D^{ii} + \nu_D^{iz}) \left\langle \frac{B}{\xi} \mathcal{L}(f_{i1}) \right\rangle \\ &= \frac{m_i}{T_i} v f_{i0} \left(I \frac{\partial \phi'}{\partial t} + \nu_D^{ii} \langle B u_{i\parallel} \rangle + \nu_D^{iz} \langle B V_{z\parallel} \rangle \right). \end{aligned}$$

3. ASPECTS OF IMPURITY TRANSPORT IN TOKAMAKS

After the same steps as in the calculation for the impurities, one arrives at

$$\hat{f}_{i1} = \frac{m_i}{T_i} f_{i0} \left[\sigma v \sum_{n=1}^{\infty} \frac{\beta_n \Lambda_n}{B_0(p + \chi_n(\nu_D^{ii} + \nu_D^{iz}))} \left(I p \hat{\phi}' + \nu_D^{ii} (I \hat{\phi}' + \langle B \hat{u}_{i\parallel} \rangle) \right. \right. \\ \left. \left. + \nu_D^{iz} (I \hat{\phi}' + \langle B V_{z\parallel} \rangle) \right) - \frac{I v_{\parallel}}{B} \hat{\phi}' \right].$$

The two terms on the right that remain to be calculated are the momentum restoring coefficient $u_{i\parallel}$ and additionally the term containing the impurity flow speed $V_{z\parallel}$. As this second term is needed for the calculation of $u_{i\parallel}$, it is convenient to start by multiplying this term by B/v_{\parallel} and take the flux surface average, yielding

$$\langle B V_{z\parallel} \rangle = \left\langle \frac{B}{n_z} \int v_{\parallel} \hat{f}_{z1} d^3 v \right\rangle \\ = \sum_{n=1}^{\infty} \beta_n \left\{ \frac{p I \hat{\phi}' + \nu_D^{zz} (I \hat{\phi}' + \langle B \hat{u}_{z\parallel} \rangle)}{p + \chi_n \nu_D^{zz}} \right\} - I \hat{\phi}'$$

which, in the long-time limit, becomes

$$\left\langle \frac{B}{n_z} \int v_{\parallel} \hat{f}_{z1} d^3 v \right\rangle = -I \hat{\phi}' \left(1 - \sum_{n=1}^{\infty} \beta_n p \left\{ \frac{1 + \nu_D^{zz} \tau_0}{p + \chi_n \nu_D^{zz}} \right\} \right) \\ = -I \hat{\phi}' (1 - p \tau_1 + \mathcal{O}(p^2))$$

where

$$\tau_1 \equiv f_c \left(\left\{ \frac{1}{\nu_D^{zz}} \right\} + \tau_0 \right)$$

and τ_0 was already defined in (3.8). To calculate

$$\hat{u}_{i\parallel} = \frac{\int v_{\parallel} \nu_D^{ii} \hat{f}_{i1} d^3 v}{n_i \{ \nu_D^{ii} \}},$$

3.1. EFFECT OF IMPURITIES ON COLLISIONAL ZONAL-FLOW DAMPING IN TOKAMAKS

one can use

$$\int v_{\parallel} \nu_D^{ii} \hat{f}_{i_1} d^3v = \frac{B}{B_0^2} n_i \sum_{n=1}^{\infty} \beta_n \left\{ \nu_D^{ii} \frac{pI\hat{\phi}' + \nu_D^{iz} (I\hat{\phi}' + \langle B\hat{u}_{i\parallel} \rangle) + \nu_D^{iz} (I\hat{\phi}' + \langle BV_{z\parallel} \rangle)}{p + \chi_n(\nu_D^{ii} + \nu_D^{iz})} \right\} - \frac{I\hat{\phi}'}{B} n_i \{\nu_D^{ii}\}$$

to obtain

$$\langle B\hat{u}_{i\parallel} \rangle = -I\hat{\phi}' + \frac{\sum_{n=1}^{\infty} \beta_n \left\{ \nu_D^{ii} \frac{pI\hat{\phi}' + \nu_D^{iz} (I\hat{\phi}' + \langle BV_{z\parallel} \rangle)}{p + \chi_n(\nu_D^{ii} + \nu_D^{iz})} \right\}}{\{\nu_D^{ii}\} - \sum_{n=1}^{\infty} \beta_n \left\{ \frac{(\nu_D^{ii})^2}{p + \chi_n(\nu_D^{ii} + \nu_D^{iz})} \right\}} \quad (3.10)$$

and in the approximation $p\tau_{ii} \ll 1$

$$\langle B\hat{u}_{i\parallel} \rangle = -I\hat{\phi}'(1 - p\tau_2 + \mathcal{O}(p^2))$$

with

$$\tau_2 = \frac{f_c \left\{ \frac{\nu_D^{ii}(1 + \nu_D^{iz}\tau_1)}{\nu_D^{ii} + \nu_D^{iz}} \right\}}{\{\nu_D^{ii}\} - f_c \left\{ \frac{(\nu_D^{ii})^2}{\nu_D^{ii} + \nu_D^{iz}} \right\}}.$$

Note that, as

$$\frac{1}{\{\nu_D^{ii}\}} \left\{ \frac{(\nu_D^{ii})^2}{\nu_D^{ii} + \nu_D^{iz}} \right\} \leq \frac{1}{\{\nu_D^{ii}\}} \left\{ \frac{(\nu_D^{ii})^2}{\nu_D^{ii}} \right\} = 1,$$

the denominator of this expression is larger than the fraction of trapped particles, i.e. non-zero, and the momentum restoring term is again well-defined. Before finally calculating the plasma polarisation, one should note that the impurity and bulk ion distribution functions, eqs. (3.8) and (3.10), respectively, adjust to the radial electric field on very different time scales. The impurity ions adjust on the time scale $\tau_0 \sim \tau_1 \sim 1/\nu_D^{zz}$ but the bulk ions do so only on the time scale $\tau_2 \sim 1/\nu_D^{ii}$, which is a factor $Z^{3/2}(Z_{\text{eff}} - 1) \gg 1$ longer. Exploiting this property

3. ASPECTS OF IMPURITY TRANSPORT IN TOKAMAKS

and the fact that $m_z n_z \sim m_i n_i / Z$ in the large- Z approximation, one finds that

$$\left\langle \int \frac{I v_{\parallel}}{B} (m_i \hat{g}_{i0} + m_z \hat{g}_{z0}) d^3v \right\rangle = \left\langle \frac{I}{B_0^2} \sum_{n=1}^{\infty} \beta_n m_i n_i \left\{ \frac{p I \phi' (1 + \tau_2 \nu_D^{ii})}{p + \chi_n (\nu_D^{ii} + \nu_D^{iz})} \right\} \right\rangle,$$

which can, in the long-time limit, be simplified to yield

$$\left\langle \int \frac{I v_{\parallel}}{B} (m_i \hat{g}_{i0} + m_z \hat{g}_{z0}) d^3v \right\rangle = \left\langle \frac{I^2}{B_0^2} p \hat{\phi}' f_c m_i n_i \left\{ \frac{1 + \tau_2 \nu_D^{ii}}{\nu_D^{ii} + \nu_D^{iz}} \right\} \right\rangle.$$

Thus, in leading order, the expression for the polarisation \hat{P} becomes

$$\hat{P} = \frac{I^2}{\langle R^2 \rangle B_0^2} f_c p \left(\left\{ \frac{1}{\nu_D^{ii} + \nu_D^{iz}} \right\} + \frac{f_c \left\{ \frac{\nu_D^{ii}}{\nu_D^{ii} + \nu_D^{iz}} \right\}^2}{\left\{ \nu_D^{ii} \right\} - f_c \left\{ \frac{(\nu_D^{ii})^2}{\nu_D^{ii} + \nu_D^{iz}} \right\}} \right) + \mathcal{O}(Z^{-1/2}) + \mathcal{O}(p^2).$$

In a large-aspect-ratio equilibrium, $I^2 / (R^2 B_0^2) \approx 1$.

3.1.7 Long-time limit

The results from the previous section show that the detailed geometry of the flux surfaces matters little to the zonal flow response in the long-time limit (small p), since the only information from the eigenfunction expansion that survives this limit is the quantity $f_c = \sum_{n=1}^{\infty} \beta_n / \chi_n$. This suggests that the response on time scales longer than the bulk ion collision time can be obtained more easily. To this end, eq. (3.3) is reconsidered but the small term containing the time derivative (in this limit, $\partial g_a / \partial t \sim p g_a \ll \nu_D^{aa} g_a$) is neglected. Thus, instead of having to solve a partial differential equation depending on time, one arrives at the much simpler equation

$$v_{\parallel} \nabla_{\parallel} g_a - \frac{e_a E_a v_{\parallel}}{T_a} f_{a0} = C_a(f_a)$$

with

$$E_a = \frac{I}{\Omega_a} \frac{\partial \phi'}{\partial t}$$

3.1. EFFECT OF IMPURITIES ON COLLISIONAL ZONAL-FLOW DAMPING IN TOKAMAKS

regarded as given. This resembles a neoclassical Spitzer problem, except that the “electric field” E_a is different for different species, and one can solve straightforwardly for both impurities and ions to find

$$\hat{g}_{z_0} = \frac{1}{2B_0} \frac{m_z}{T_z} \sigma v f_{z_0} \left(I\hat{\phi}' \left(1 + \frac{p}{\nu_D^{zz}} \right) + \langle B\hat{u}_{z_\parallel} \rangle \right) \int_{\lambda}^{\lambda_c} \frac{d\lambda'}{\langle \sqrt{1 - \lambda' \frac{B}{B_0}} \rangle} + \mathcal{O}(p^2)$$

and

$$\begin{aligned} \hat{g}_{i_0} &= \frac{1}{2B_0} \frac{m_i}{T_i} \sigma v f_{i_0} \left(I\hat{\phi}' \frac{p}{\nu_D^{ii} + \nu_D^{iz}} + \left(I\hat{\phi}' + \langle B\hat{u}_{i_\parallel} \rangle \right) \frac{\nu_D^{ii}}{\nu_D^{ii} + \nu_D^{iz}} \right. \\ &\quad \left. + \left(I\hat{\phi}' + \langle BV_{z_\parallel} \rangle \right) \frac{\nu_D^{iz}}{\nu_D^{ii} + \nu_D^{iz}} \right) \int_{\lambda}^{\lambda_c} \frac{d\lambda'}{\langle \sqrt{1 - \lambda' \frac{B}{B_0}} \rangle} + \mathcal{O}(p^2). \end{aligned}$$

Thus,

$$\begin{aligned} \hat{P} &= \frac{I^2}{\langle R^2 \rangle B_0^2} f_c p \left(\left\{ \frac{1}{\nu_D^{ii} + \nu_D^{iz}} \right\} + \frac{f_c \left\{ \frac{\nu_D^{ii}}{\nu_D^{ii} + \nu_D^{iz}} \right\}^2}{\left\{ \nu_D^{ii} \right\} - f_c \left\{ \frac{(\nu_D^{ii})^2}{\nu_D^{ii} + \nu_D^{iz}} \right\}} \right) \\ &\quad + \mathcal{O}(Z^{-1/2}) + \mathcal{O}(p^2), \end{aligned}$$

which is the same result as with the eigenfunction expansion method.

As the inverse Laplace transform involves not only small p , it is not possible to formally transform the expression for the long-time limit back to t -space. Nonetheless, one can extract important information about the zonal flow damping time by considering how the potential approaches its final value. In the long-time limit, when $p \rightarrow 0$, the neoclassical polarisation vanishes, and as $1/p$ transforms back to t -space as a constant, one can conclude

$$\lim_{t \rightarrow \infty} \phi'(t) = \frac{\langle \frac{|\nabla \psi|^2}{B^2} \rangle}{\langle R^2 \rangle} \phi'(0) \equiv \phi'_\infty.$$

A suitable measure for the time scale on which $\phi'(t)$ approaches ϕ'_∞ is

$$\tau_p \equiv \int_0^\infty \frac{\phi'(t) - \phi'_\infty}{\phi'_\infty} dt. \tag{3.11}$$

3. ASPECTS OF IMPURITY TRANSPORT IN TOKAMAKS

Using (3.7), one find

$$\begin{aligned}
\tau_p &= \lim_{p \rightarrow 0} \int_0^\infty \frac{\phi'(t) - \phi'_\infty}{\phi'_\infty} e^{-pt} dt \\
&= \lim_{p \rightarrow 0} \left(\frac{\hat{\phi}(p)}{\phi'_\infty} - 1 \right) = \lim_{p \rightarrow 0} \left(\frac{1}{p(1 - P(p))} - \frac{1}{p} \right) \\
&= \lim_{p \rightarrow 0} \frac{P(p)}{p(1 - P(p))} = \frac{d\hat{P}}{dp}(0).
\end{aligned}$$

The effective zonal-flow damping time, τ_p , thus corresponds exactly to the term that was calculated explicitly in the polarisation (3.11). This expression is a simple function of f_c but depends in a complicated way on Z_{eff} , as it involves velocity-space averages $\{\dots\}$ of ν_D^{ii} and ν_D^{iz} . In order to further simplify eq. (3.11), consider the limits of $Z_{\text{eff}} \rightarrow 1$ and $Z_{\text{eff}} \rightarrow \infty$: in a pure plasma, the damping time becomes

$$\tau_p|_{Z_{\text{eff}}=1} = \frac{I^2}{\langle R^2 \rangle B_0^2} \frac{f_c}{\hat{\nu}_{ie}} \left(\left\{ \frac{x_a^3}{\text{Erf}(x_a) - G(x_a)} \right\} + \frac{f_c}{1 - f_c} \frac{1}{\left\{ \frac{\text{Erf}(x_a) - G(x_a)}{x_a^3} \right\}} \right),$$

whereas for $Z_{\text{eff}} \rightarrow \infty$

$$\tau_p|_{Z_{\text{eff}} \rightarrow \infty} \approx \frac{I^2}{\langle R^2 \rangle B_0^2} f_c \frac{\{x_a^3\}}{\hat{\nu}_{ie}} \frac{1}{Z_{\text{eff}}},$$

where the relation that $\hat{\nu}_{ie} \approx \hat{\nu}_{ii}$ for large Z was used and [3]

$$\begin{aligned}
\nu_D^{iz} &\approx \frac{\hat{\nu}_{iz}}{x_a^3} = \frac{Z^2 n_z}{n_i} \frac{\hat{\nu}_{ii}}{x_a^3} = \frac{Z_{\text{eff}} - 1}{1 - \frac{1}{Z}} \frac{\hat{\nu}_{ii}}{x_a^3} \\
&\approx (Z_{\text{eff}} - 1) \frac{\hat{\nu}_{ie}}{x_a^3},
\end{aligned}$$

where $Z_{\text{eff}} = \sum_j (Z_j^2 n_j) / \sum_j (Z_j n_j)$ and the sum is taken over all ion species j . The normalisation to $\hat{\nu}_{ie}$ is chosen to account for the electron density being the quantity typically measured in experiment, and, furthermore, this normalisation is also used for the numerical simulations in the next chapter in order to avoid singular behaviour when Z is close to Z_{eff} , as it would be when normalising with respect to $\hat{\nu}_{ii}$ while keeping n_e , Z and Z_{eff} fixed. With the help of

3.1. EFFECT OF IMPURITIES ON COLLISIONAL ZONAL-FLOW DAMPING IN TOKAMAKS

these values, one can construct the following interpolation formula for the damping time

$$\begin{aligned}\tau_p &= \frac{I^2}{\langle R^2 \rangle B_0^2} \frac{f_c}{\hat{\nu}_{ie}} \left[\frac{\{x_a^3\}}{Z_{\text{eff}}} + \left(\left\{ \frac{x_a^3}{\text{Erf}(x_a) - G(x_a)} \right\} + \frac{f_c}{1-f_c} \frac{1}{\left\{ \frac{\text{Erf}(x_a) - G(x_a)}{x_A^3} \right\}} - \{x_a^3\} \right) \frac{1}{Z_{\text{eff}}^4} \right] \\ &\approx \frac{I^2}{\langle R^2 \rangle B_0^2} \frac{f_c}{\hat{\nu}_{ie}} \left[\frac{4.51}{Z_{\text{eff}}} + \left(0.87 + 2.49 \frac{f_c}{1-f_c} \right) \frac{1}{Z_{\text{eff}}^4} \right],\end{aligned}$$

which is exact in the limits and sufficiently accurate for intermediate values of Z_{eff} . Fig. 3.2 shows the interpolation formula, together with the exact solution, for different values of f_c .

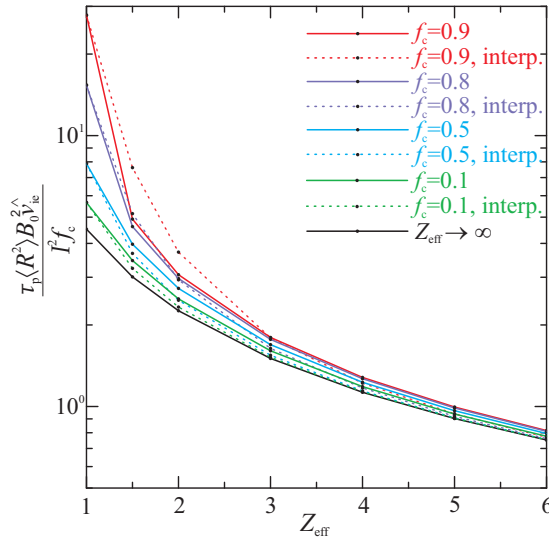


FIGURE 3.2 Damping time: interpolation formula and exact solution.

3.1.8 Comparison with numerical simulation

Since the calculation of τ_p only requires solving a standard equation from neoclassical transport theory, a number of existing codes can be used for this purpose. In this section, the obtained analytical results are compared with the results of the NEO code [15]. In standard form, NEO solves the multi-species, steady-state first-order drift-kinetic equation using an Eulerian numerical scheme. Here it was modified to solve the Laplace-transformed eq. (3.11) for f_{a1} , i.e. the usual neoclassical driver source term was set to zero in the drift-kinetic equation and the term $-I(e_a/T_a)v_{\parallel}f_{0a}\hat{\phi}'[-p/\Omega_a + \nabla_{\parallel}(v_{\parallel}/\Omega_a)]$ was added as the new right-hand side source term. Given as input $\hat{\phi}'$ and p , the discretised kinetic equation is solved as a

3. ASPECTS OF IMPURITY TRANSPORT IN TOKAMAKS

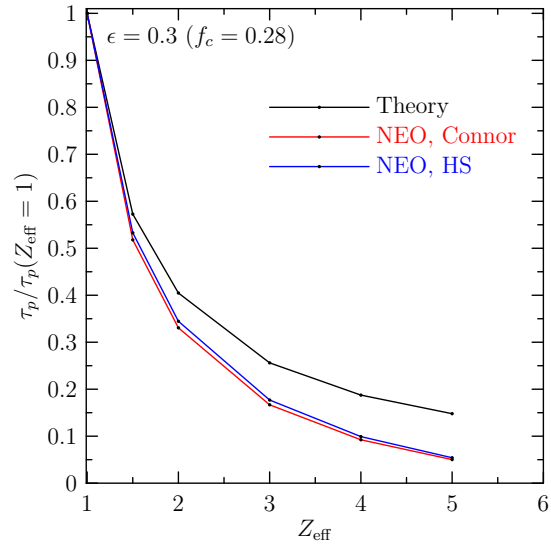


FIGURE 3.3 Normalised damping time vs. effective charge.

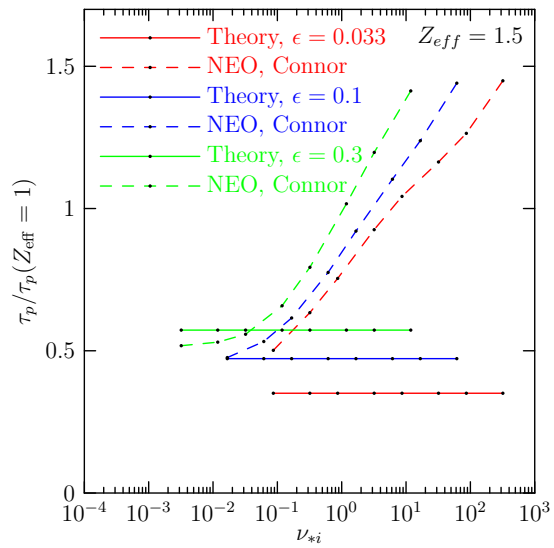


FIGURE 3.4 Normalised damping time vs. ν_{*i} .

matrix problem for f_{a1} and the polarisation \hat{P} is computed from eq. (3.7). For these simulations, a deuterium species and a carbon species are considered in a tokamak plasma with s- α geometry and the parameters $\alpha = q^2 R_0 d\beta/dr = 0$, $R_0/a = 3$, $q=2$, $T_{0i} = T_{0c}$ (s- α geometry refers to unshifted circular flux surfaces with $R = R_0 + r \cos \theta$, magnetic field variation $B = B_0/(1 + r \cos \theta/R_0)$, and constant flux function $I(\psi) = R_0 B_0$). The electron parameters are assumed to be fixed, with $\tau_{ee}^{-1}/(c_s/a) = 10^{-2}$, where $c_s = \sqrt{T_e/m_i}$ and $\tau_{ee}^{-1} = (\sqrt{2}\pi e^4 n_e \ln \Lambda)/(m_e^{1/2} T_e^{3/2})$. For given n_e , Z and Z_{eff} , the ion and impurity densities are determined from quasi-neutrality and the relative ion and impurity collision frequencies are varied accordingly. To be consistent with the theory, in the NEO calculations the kinetic electron dynamics are neglected, which are small. With NEO, the zonal-flow damping time τ_p has been calculated using various collision operators, namely the Connor operator used in section 3.1.7, and the more advanced full Hirshman-Sigmor operator [37]. Unlike the Connor operator, which consists of just a Lorentz scattering operator and simple momentum-restoring term, the full Hirshman-Sigmor operator also includes energy diffusion and models for heating friction effects and for the deceleration effect arising from dynamic friction, which has been shown to be important for modelling the neoclassical transport of multi-ion plasmas [15]. Fig. 3.3 shows the damping time versus effective charge at $\epsilon = 0.3$ for both theory and simulation. In order to emphasise the role of the impurities, the ratio of the damping time to that in a pure plasma has been plotted. It is clearly visible that the use of different collision operators does not have any significant influence on the damping time as the curves hardly deviate from each other. This suggests that the form of the momentum correction term is not playing a large role in the dynamics. Moreover, one finds, for regimes in which the theory is valid, numerical simulation and analytical theory to be in fairly good agreement. The larger discrepancy for larger Z_{eff} is due to the fact that the effective charge approaches the impurity charge, i.e. violation of the ordering assumptions as the impurities stop being a minority. The agreement improves for smaller ϵ ; however, it is not possible to reasonably compare simulation and theory for much smaller ϵ as the simulation is carried out keeping the collision frequency fixed, which leads to a failure of the banana regime assumption of small effective collision frequency compared with the bounce frequency. In order to further illustrate for which parameters the theory is valid, fig. 3.4 shows the dependence of τ_p on $\nu_{*i} \equiv \nu_i/(\epsilon \omega_b)$. Obviously, $\epsilon = 0.1$ or smaller would require going to much smaller collision frequencies than done here in order to keep the theory valid, which is difficult numerically. In figs. 3.5, the damping time has been plotted versus ϵ for different values of Z , where in fig. 3.5(b) the aspect ratio has been changed to $R/a_0 = 1.5$ to allow for higher values of ϵ . Clearly visible is the asymptotic behaviour for $Z \rightarrow \infty$, which was assumed in the theory, and again the theory fails for small ϵ as the plasma leaves the banana regime.

3. ASPECTS OF IMPURITY TRANSPORT IN TOKAMAKS

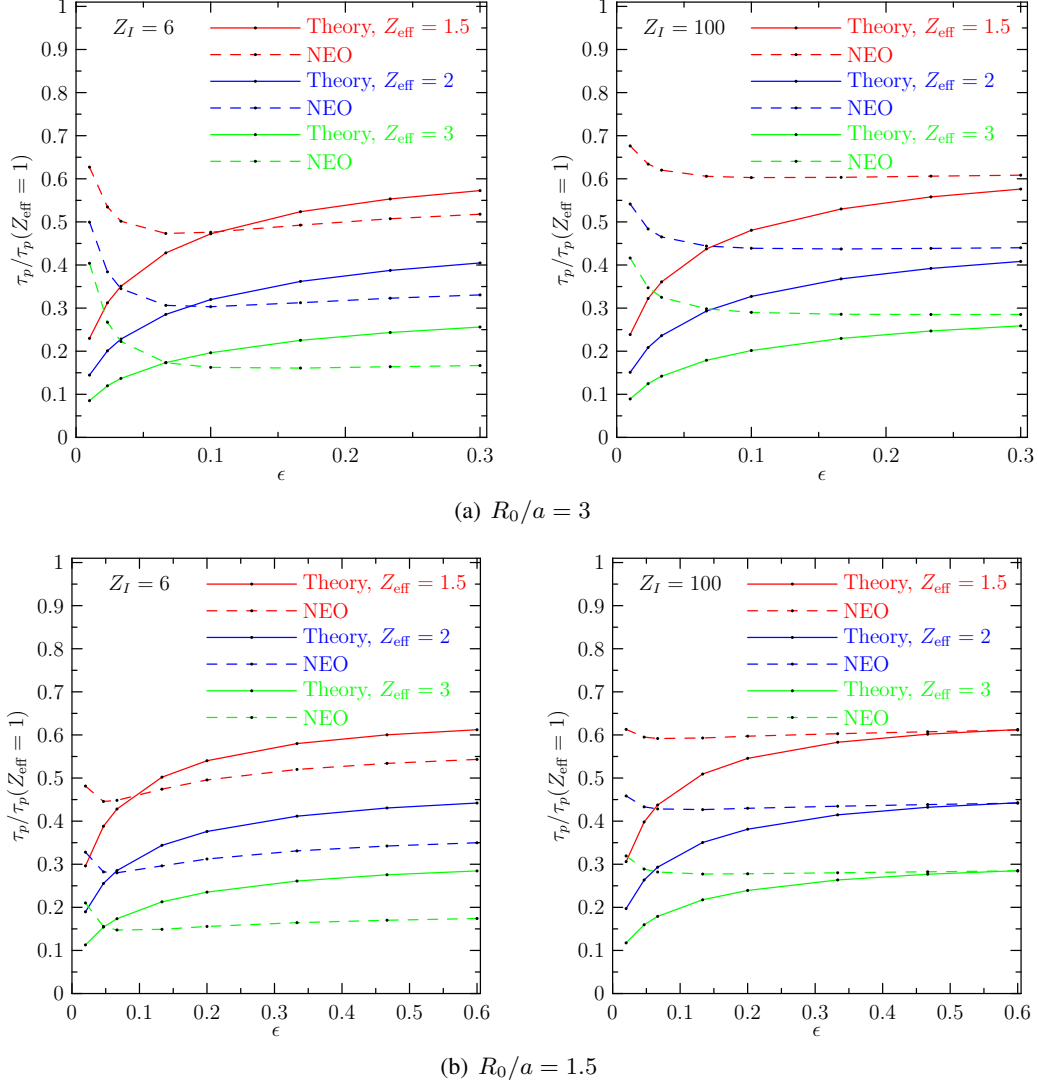


FIGURE 3.5 Normalised damping time vs. ϵ .

3.1.9 Arbitrary source term

In a plasma with electrostatic turbulence, the actual problem of interest is not (3.1), but rather

$$\frac{\partial f_a}{\partial t} + (\mathbf{v}_\parallel + \mathbf{v}_d + \tilde{\mathbf{v}}_E) \cdot \nabla f_a + \dot{w} \frac{\partial f_a}{\partial w} = C_a(f_a),$$

where $\tilde{\mathbf{v}}_E = \mathbf{b} \times \nabla \tilde{\phi}/B$ denotes the fluctuating $\mathbf{E} \times \mathbf{B}$ velocity, averaged over gyromotion. Following Hinton and Rosenbluth [33], one can take an average over the toroidal angle to isolate the axisymmetric component, \bar{f}_a , and obtain

$$\frac{\partial \bar{f}_a}{\partial t} + (\mathbf{v}_\parallel + \mathbf{v}_d) \cdot \nabla \bar{f}_a + \dot{w} \frac{\partial \bar{f}_a}{\partial w} - C_a(\bar{f}_a) = S_a, \quad (3.12)$$

where the source term

$$S_a = -\frac{1}{2\pi B} \oint (\mathbf{b} \times \nabla \tilde{\phi}) \cdot \nabla f_a d\varphi$$

only has relatively weak contributions from the axisymmetric components of either $\tilde{\phi}$ or f_a . The point is that the axisymmetric components only contribute through the term

$$(\mathbf{b} \times \nabla \tilde{\phi}) \cdot \nabla \bar{f}_a = I \left(\frac{\partial \bar{f}_a}{\partial \psi} \nabla_\parallel \tilde{\phi} - \frac{\partial \tilde{\phi}}{\partial \psi} \nabla_\parallel \bar{f}_a \right),$$

involving parallel gradients, whilst the non-axisymmetric components of $\tilde{\phi}$ and f_a also contribute through their perpendicular gradients, which are much larger in gyrokinetic theory. Hinton and Rosenbluth therefore took S_a to be given when calculating the axisymmetric components. Since the resulting equation (3.12) is linear, it can be solved as an initial value problem. If one calculates the response to an initial perturbation, the general solution can be obtained by convoluting the solution of the initial-value problem with the source term S_a (see appendix). The latter can be arbitrary, and it does not matter, for instance, whether its auto-correlation time is long or short compared with the collision time.

The problem (3.12) with an arbitrary source term amounts to finding the functions G_a and

3. ASPECTS OF IMPURITY TRANSPORT IN TOKAMAKS

Φ' , which satisfy

$$\begin{aligned} M_a[\hat{G}_a] &= \hat{S}_a \\ \Phi'(t) &= \sum_a \left\langle \frac{I}{B} \int m_a v_{\parallel} G_a d^3 v \right\rangle / \sum_a \langle m_a n_a R^2 \rangle \\ G_a(0) &= 0, \quad \Phi'(0) = 0 \end{aligned} \tag{3.13}$$

where the operator M_a is defined as

$$M_a[h] \equiv ph + v_{\parallel} \nabla_{\parallel} h - \frac{Iv_{\parallel}}{\Omega_a T_a} e_a f_{a0} p \sum_a \left\langle \frac{I}{B} \int m_a v_{\parallel} h d^3 v \right\rangle / \sum_a \langle m_a n_a R^2 \rangle.$$

The solutions \hat{g}_a and $\hat{\phi}'$ to

$$\begin{aligned} M[g_a] &= k \frac{Im_a v_{\parallel}}{B} f_{a0} = L_a[g_a] \\ \phi'(t) &= \sum_a \left\langle \frac{m_a n_a |\nabla \psi|^2}{B^2} \phi'(0) + \frac{I}{B} \int m_a v_{\parallel} g_a d^3 v \right\rangle / \sum_a \langle m_a n_a R^2 \rangle \\ g_a(0) &= \frac{Iv_{\parallel}}{\Omega_a T_a} e_a \phi'(0) f_{a0}, \quad \phi'(0) = \phi'_0 \end{aligned}$$

are already known, where

$$L_a[h] \equiv ph - v_{\parallel} \nabla_{\parallel} h - \frac{Iv_{\parallel}}{\Omega_a T_a} e_a f_{a0} p \sum_a \left\langle \frac{I}{B} \int m_a v_{\parallel} h d^3 v \right\rangle / \sum_a \langle m_a n_a R^2 \rangle$$

only differs from M_a in the reversed sign in front of the term containing the parallel gradient. As g_a was found to be odd in σ , it is also a solution to the problem including the operator L_a . When all ion temperatures are equilibrated, the constant

$$k \equiv \frac{1}{T_a} \frac{\sum_a \left\langle \frac{m_a n_a |\nabla \psi|^2}{B^2} \right\rangle \phi'(0)}{\sum_a \langle m_a n_a R^2 \rangle}$$

is independent of the particle species.

3.1. EFFECT OF IMPURITIES ON COLLISIONAL ZONAL-FLOW DAMPING IN TOKAMAKS

Since, for the unlike-species collision operator, the relation

$$\sum_{a,b} \int d^3v \frac{g_a}{f_{a0}} C_{ab}(f_a, f_b) = \sum_{a,b} \int d^3v \frac{f_a}{f_{a0}} C_{ab}(g_a, g_b)$$

holds for any pair of distributions g_a, f_a [38], the operators M_a and L_a are adjoint in sense that

$$\sum_a \left\langle \int \frac{\hat{G}_a}{f_{a0}} L_a[\hat{g}_a] d^3v \right\rangle = \sum_a \left\langle \int \frac{\hat{g}_a}{f_{a0}} M_a[\hat{G}_a] d^3v \right\rangle.$$

Thus, to calculate the potential response (3.13), one can use

$$\begin{aligned} \sum_a \left\langle \frac{I}{B} \int m_a v_{\parallel} \hat{G}_a d^3v \right\rangle &= \frac{1}{k} \sum_a \left\langle \int \frac{\hat{G}_a}{f_{a0}} L_a[\hat{g}_a] d^3v \right\rangle \\ &= \frac{1}{k} \sum_a \left\langle \int \frac{\hat{g}_a}{f_{a0}} M_a[\hat{g}_a] d^3v \right\rangle \\ &= \frac{1}{k} \sum_a \left\langle \int \frac{\hat{g}_a \hat{S}_a}{f_{a0}} d^3v \right\rangle. \end{aligned}$$

As mentioned as well in [33], the response to a source is thus obtained by convoluting this source with the solution of the initial value problem.

However, in practice the source term S_a is not known and *does* contain contributions from the axisymmetric part \bar{f}_a . One might then ask the question whether the turbulent transport may carry particles across a radial wavelength of the zonal flow in a time shorter than the collision time. The zonal flow would then be damped by diffusion caused by the fluctuating $E \times B$ drift (turbulent viscosity) rather than collisions. If the global confinement time is denoted by τ_E , then the time required for diffusion across a fraction $\Delta r/a$ of the cross section is

$$\tau_D \sim \tau_E \left(\frac{\Delta r}{a} \right)^2,$$

and collisional damping is only important for zonal flows with a radial wavelength longer than

$$\frac{\Delta r}{a} > \left(\frac{\tau_p}{\tau_E} \right)^{1/2},$$

3. ASPECTS OF IMPURITY TRANSPORT IN TOKAMAKS

where τ_p is the neoclassical polarisation time (3.11) due to collisions. Depending on plasma parameters, this condition may or may not be satisfied – a limitation that seems not to have been pointed out in literature on collisional damping of zonal flows.

It should perhaps be mentioned that there is another application of these results, which has to do with the question of how the plasma responds to a sudden change of the pressure profile. Conventional neoclassical theory predicts the level of poloidal plasma rotation in steady state. In the LH-transition, the pressure gradient changes very rapidly, and one may ask the question of how quickly a new steady state is attained. This is of interest when trying to resolve the “chicken-and-egg” problem of whether sheared rotation causes the H-mode or is merely a consequence of the increased gradients in the pedestal. Since the pressure gradient in f_{a_0} enters in exactly the same way as the radial electric field in the kinetic equation (3.2), this problem is identical to the zonal flow damping problem, and it can be concluded that the new equilibrium is established on the time scale (3.11).

3.1.10 Physical interpretation and conclusions of section 3.1

The effect of heavy, highly charged impurity ions on zonal-flow damping in tokamaks was considered. Although such impurities do not affect the first, collisionless stage of the damping, they do accelerate the collisional damping since they increase the effective collisionality of the bulk ions roughly by a factor Z_{eff} . It is possible to calculate the time history of the damping by expanding the pitch-angle dependence of the distribution function in eigenfunctions of the orbit-averaged pitch-angle-scattering operator. However, in the long-time limit, i.e. at late times during the damping process, the problem can be reduced to solving a neoclassical Spitzer problem, and this is also sufficient to calculate the overall damping time defined by eq. (3.11).

Collisional damping of zonal flows occurs as a result of friction between the circulating and trapped particles. The latter are locked in the magnetic well on the outboard side of the torus and are therefore unable to rotate poloidally. The circulating ions experience friction against this stationary, trapped population, which damps the rotation. The damping time (3.11) therefore increases with the effective fraction of circulating particles. In the limit of very tight aspect ratio (the edge region in a spherical tokamak), where the circulating particle fraction is small, $f_c \rightarrow 0$, the damping becomes instantaneous, independently of whether impurities are present in the plasma. In the opposite limit of very few trapped particles, $f_c \rightarrow 1$, the damping occurs much more quickly if impurity ions are present than otherwise. This has to do with the fact that the time it takes for the trapped and passing populations to reach a mutual collisional equilibrium is much shorter for the impurities than for the bulk ions, because of the shorter collision time of the former. Therefore, as soon as the poloidal impurity rotation has been damped, the bulk ions experience friction against the *entire* impurity population, not just the trapped impurities. This is much more effective than the friction against just the trapped bulk

3.1. EFFECT OF IMPURITIES ON COLLISIONAL ZONAL-FLOW DAMPING IN TOKAMAKS

ions when f_c is close to unity. Mathematically, this is reflected by the fact that the denominator of eq. (3.11) does not vanish in the limit $f_c \rightarrow 1$. Physically, it has the effect that the zonal flow damping is enhanced by more than a factor Z_{eff} when the aspect ratio is large.

These analytical predictions, which are made using a simple pitch-angle-scattering collision operator with a momentum-restoring term, seem largely insensitive to the choice of collision operator. Indeed, because the zonal flow damping time can be reduced to a neoclassical Spitzer problem, it can be calculated by neoclassical transport codes, which makes it possible to use still more accurate collision operators and to treat cases of finite collisionality. As long as the particles are in the low-collisionality banana regime, the results are in very good agreement.

It is clear from these results that, when a realistic amount of impurities are present in a tokamak plasma, the collisional damping of zonal flows occurs significantly faster than otherwise. Insofar as this damping mechanism is important, this would suggest that impurities inhibit zonal flows and could have a deleterious effect on confinement.

3.1.11 Appendix: Expression for the drift velocity

It is to show that

$$\begin{aligned} \mathbf{v}_d \cdot \nabla \psi &= \left(\frac{\mathbf{b} \times \nabla \phi}{B} + \left(\frac{v_{\perp}^2}{2} + v_{\parallel}^2 \right) \frac{\mathbf{b} \times \nabla \ln B}{\Omega} \right) \cdot \nabla \psi \\ &\stackrel{!}{=} v_{\parallel} \nabla_{\parallel} \left(\frac{I v_{\parallel}}{\Omega} \right). \end{aligned}$$

Starting from the right-hand side, one finds

$$\begin{aligned} v_{\parallel} \nabla_{\parallel} \left(\frac{I v_{\parallel}}{\Omega} \right) &= v_{\parallel} \frac{I m_a}{e_a} \nabla_{\parallel} \left(\frac{v_{\parallel}}{B} \right) \\ &= -\frac{I}{\Omega} v_{\parallel}^2 \nabla_{\parallel} (\ln B) + \frac{I}{\Omega} v_{\parallel} \nabla_{\parallel} \left(\sigma v \sqrt{1 - \lambda B} \right) \\ &= -\frac{I}{\Omega} v_{\parallel}^2 \nabla_{\parallel} (\ln B) + \frac{I}{\Omega} v_{\parallel} \nabla_{\parallel} \left(\frac{-\sigma v \lambda \nabla_{\parallel} B}{2\sqrt{1 - \lambda B}} \right) \\ &= -\frac{I}{\Omega} \left(v_{\parallel}^2 + \frac{v_{\perp}^2}{2} \right) \nabla_{\parallel} \ln B. \end{aligned}$$

But

$$\frac{\mathbf{b} \times \nabla \phi}{\Omega} \cdot \nabla \psi = 0$$

3. ASPECTS OF IMPURITY TRANSPORT IN TOKAMAKS

as $\phi \approx \phi(\psi)$, and

$$\begin{aligned}
\mathbf{B} \times \nabla\psi \cdot \nabla \ln B &= \frac{1}{B} \left(I(\psi) \nabla\varphi \times \nabla\psi + \underbrace{\nabla\varphi \times \nabla\theta \times \nabla\psi}_{=0} \right) \cdot \nabla \ln B \\
&= \frac{I}{B} \nabla\varphi \times \nabla\psi \cdot \nabla\theta \frac{\partial}{\partial\theta} (\ln B) = \nabla_{\parallel} \ln B.
\end{aligned}$$

□

3.2 Effect of impurities on ITG driven microinstabilities

The work presented in this chapter has been carried out in collaboration with Dr Tünde Fülöp and Istvan Pusztai, Chalmers University of Technology, Gothenburg, Sweden. The results can be found in [39].

Turbulent fluctuations are the main source of particle and heat transport in present-day tokamak experiments. Of special importance is the question of the direction of the impurity flux. If impurities are transported from outside into the core of the plasma, they can harm plasma performance. However, if they instead can be brought to reside at the edge in a stable steady state, they may help protect the divertor from the strong heat fluxes by creating a radiation belt. Although various models for microinstability-driven impurity transport exist [40–46], there are still many open questions regarding the sign and magnitude of the flux and its parametric dependences. The basic problem is that the process is highly nonlinear, thereby making it necessary to resort to complicated gyrokinetic simulations or to use simplified, but controversial, models. However, the plasma density and temperature profiles usually adjust to be close to the threshold predicted by linear theory [6], and quasilinear electrostatic approximations have been proven to retain much of the relevant physics and reproduce the results of nonlinear simulations satisfactorily for a wide range of parameters [47]. The simplified treatment makes it easier to identify and interpret the connections between different drives and sources. In this section, a quasilinear semi-analytical model for impurity transport driven by ion-temperature-gradient (ITG) modes based on a boundary layer solution of the gyrokinetic equation is derived. Analytical expressions for the perturbed densities of the electrons, ions and impurities are obtained by employing a model electrostatic potential, motivated by gyrokinetic simulations, and used in the quasi-neutrality equation, which is solved numerically for the frequencies and growth rates of the unstable modes. The results are compared with quasilinear simulations using the GYRO code [48]. The remainder of the section is organised as follows: in section 3.2.1, the perturbed density responses are calculated, and the resulting quasilinear fluxes are derived in section 3.2.2. Section 3.2.3 addresses the stability of the modes, and scalings of the growth rates and eigenfrequencies with various parameters, such as charge number, impurity density scale length and the fraction of impurities, are shown. The results of section 3.2 are summarised in section 3.2.4.

3.2.1 Perturbed density responses

In this section, an axisymmetric, large aspect-ratio torus with circular flux surfaces is considered. The plasma consists of electrons, ions and a single species of impurities with arbitrary charge Z , where the electrons are assumed to be in the low collisional (banana) regime, i.e. the collisionality $\nu_{e*} \equiv \nu_e / (\epsilon \omega_{be})$ is a small parameter, ϵ being the inverse aspect ratio, ν_e the total electron collision frequency and ω_{ba} the bounce frequency of particle species a . The frequency

3. ASPECTS OF IMPURITY TRANSPORT IN TOKAMAKS

ω of the ITG mode considered is assumed to obey the ordering constraint $\omega_{bi} \ll \omega \ll \omega_{be}$. In order to calculate the distribution functions of the different particle species, the linearised gyrokinetic equation

$$\frac{v_{\parallel}}{qR} \frac{\partial g_a}{\partial \theta} - i(\omega - \omega_{Da})g_a - C_a(g_a) = -i \frac{e_a f_{a0}}{T_a} (\omega - \omega_{*a}^T) \phi J_0(z_a), \quad (3.14)$$

introduced in section 2.3.4 has to be solved. As usual, q denotes the safety factor and R the major radius of the torus. g_a is the nonadiabatic part of f_{a1} , whereas f_{a0} denotes the equilibrium Maxwellian distribution, and θ the poloidal angle in ballooning space. The magnetic drift frequency $\omega_{Da} = -k_{\theta}(v_{\perp}^2/2 + v_{\parallel}^2)(\cos \theta + s\theta \sin \theta)/(\Omega_a R)$, k_{θ} being the poloidal wave number and s the magnetic shear, and $\omega_{*a}^T = \omega_{*a} [1 + (x_a^2 - 3/2) \eta_a]$, written in terms of the diamagnetic frequency $\omega_{*a} = -k_{\theta} T_a / (e_a B L_{na})$ where $\eta_a = L_{na}/L_{Ta}$, $L_{na} = -[\partial(\ln n_a)/\partial r]^{-1}$ and $L_{Ta} = -[\partial(\ln T_a)/\partial r]^{-1}$ being the radial density and temperature scale lengths, respectively. J_0 denotes the zeroth-order Bessel function, and the argument $z_a = k_{\perp} v_{\perp} / \Omega_a$ with k_{\perp} the perpendicular wave number and Ω_a the cyclotron frequency of species a . z_a represents the finite Larmor radius (FLR) effects which have to be kept in the gyrokinetic equation. It is difficult to solve this equation self-consistently for both the perturbed electrostatic potential ϕ and the distribution functions, and thus ϕ is assumed to be given externally and then fed into the equation for the distribution functions. It has proven convenient [49] to use

$$\phi(\theta) = \phi_0 \left(\frac{1 + \cos \theta}{2} + i f_s \sin^2 \theta \right) [H(\theta + \pi) - H(\theta - \pi)],$$

where H is the Heaviside function, ϕ_0 the overall amplitude of the electrostatic potential and f_s can be approximated by $f_s = -0.6s + s^2 - 0.3s^3$. This ansatz is based on the experience from GYRO simulations and is satisfactorily accurate in the moderate shear region but breaks down outside the region $0.2 \lesssim s \lesssim 1.7$. In the subsequent sections, (3.14) is solved for the different species.

Electron response

The electron response in a pure plasma has been calculated in [49], where the circulating electrons were assumed to be adiabatic. Including impurities affects the collision operator as electron-impurity collisions have to be taken into account. Due to their small mass compared with the other species, it is justifiable to approximate the electron collision operator with a pitch-angle scattering operator,

$$C_e(f_e) = \nu_e(v) \mathcal{L}(f_e)$$

3.2. EFFECT OF IMPURITIES ON ITG DRIVEN MICROINSTABILITIES

where \mathcal{L} is the Lorentz operator introduced in section 2.4, and thus including impurities only alters the collision frequency,

$$\begin{aligned}\nu_e &= (\hat{\nu}_{ee} + \hat{\nu}_{ei} + \hat{\nu}_{ez})/x_e^3 = (1 + n_i/n_e + Z^2 n_z/n_e) \hat{\nu}_{ee}/x_e^3 \\ &= (1 + Z_{\text{eff}}) \hat{\nu}_{ee}/x_e^3,\end{aligned}$$

with $\hat{\nu}_{ee} = 4\pi n_e e^4 \ln \Lambda / (m_e^2 v_{Te}^3)$, but does not affect the structure of the collision operator. Therefore, it is possible to follow closely the derivation in [49], and only a rough sketch of the basic ideas is given here. Expanding the trapped part of the nonadiabatic electron distribution g_e in the smallness of ω/ω_{be} and the smallness of the collisionality ν_{e*} yields in lowest order

$$\frac{\partial g_{e0}}{\partial \theta} = 0,$$

and therefore bounce averaging (3.14) between the reflection points leads to the constraint

$$(\omega - \langle \omega_{De} \rangle_b) g_{e0} - \frac{i\nu_e}{\epsilon K(\kappa)} \frac{\partial}{\partial \kappa} \hat{J}(\kappa) \frac{\partial g_{e0}}{\partial \kappa} = -\frac{e \langle \phi \rangle_b}{T_e} (\omega - \omega_{*e}^T) f_{e0}, \quad (3.15)$$

where the bounce average is defined as

$$\langle A \rangle_b = \frac{1}{\tau_b} \oint \frac{Ad\theta}{v_{\parallel} \mathbf{b} \cdot \nabla \theta}.$$

Here, the Lorentz operator, rewritten in terms of the trapping parameter

$$\kappa = \frac{1 - \lambda B_0(1 - \epsilon)}{2\epsilon \lambda B_0},$$

where B_0 is defined via $\langle B^2 \rangle = B_0^2$ as usual, can conveniently be expressed with elliptic functions using $\hat{J} = E(\kappa) + (\kappa - 1)K(\kappa)$ and

$$K(\kappa) = \int_0^{\pi/2} \frac{d\theta}{\sqrt{1 - \kappa \sin^2 \theta}}$$

3. ASPECTS OF IMPURITY TRANSPORT IN TOKAMAKS

and

$$E(\kappa) = \int_0^{\pi/2} \sqrt{1 - \kappa \sin^2 \theta} d\theta$$

are the complete elliptic integrals of the first and second kind, respectively. Note that κ differs from the trapping parameter k^2 used in section 3.1 by some normalisation constants. The bounce-averaged potential and the orbit-averaged precession frequency are given by

$$\langle \phi \rangle_b = \phi_0 \left\{ \frac{E(\kappa)}{K(\kappa)} + i \frac{4f_s}{3} \left[(2\kappa - 1) \frac{E(\kappa)}{K(\kappa)} + 1 - \kappa \right] \right\}$$

and

$$\langle \omega_{De} \rangle_b = \omega_{D0} \left[\frac{E(\kappa)}{K(\kappa)} - \frac{1}{2} + 2s \left(\frac{E(\kappa)}{K(\kappa)} + \kappa - 1 \right) \right], \quad (3.16)$$

where $\omega_{D0} = -k_\theta v^2 / (\Omega_e R)$. Introducing the parameter $\hat{\nu} \equiv \nu_e / (\omega_0 \epsilon)$, ω_0 is the absolute value of the real part of the eigenfrequency, so that $\omega = \sigma \omega_0 + i\gamma = (\sigma + i\hat{\gamma})\omega_0 \equiv y\omega_0$, $\sigma = \text{sign}(\Re\{\omega\})$ denotes the sign of the real part of the eigenfrequency and $\hat{\gamma} = \gamma/\omega_0$ is the normalised growth rate, one can solve eq. (3.15) analytically in the limit of small collisionality, i.e., $\hat{\nu} \ll 1$. It should be noted that the smallness of $\hat{\nu}$ depends strongly on the plasma parameters, and for typical experimental values it is not always very small and can even become larger than unity. The analysis presented here is therefore limited to parameter regions where it is indeed small. Contrary to the procedure in [49], which uses WKB analysis with the drawback of having to employ a non-rigorous expansion in the trapping parameter κ in order to have tractable results, the method presented here is based on the construction of a boundary layer solution, which avoids this drawback. The result differs only insignificantly by a factor $4/\pi$. Denoting a derivative with respect to κ with a prime and multiplying eq. (3.15) with $iK(\kappa)/(\omega_0 \hat{J}(\kappa))$ yields

$$\hat{\nu} \left(g''_{e0} + (\ln \hat{J})' g'_{e0} \right) + i \frac{K(\kappa)}{\hat{J}\omega_0} (\omega - \langle \omega_{De} \rangle_b) g_{e0} = i \frac{K(\kappa) e \langle \phi \rangle_b}{\hat{J}\omega_0 T_e} (\omega_{*e}^T - \omega) f_{e0}.$$

The outer region outside the boundary coincides with the region far away from the trapped-passing boundary, where collisions can be neglected, and the solution becomes

$$g_{\text{outer}} = \frac{e \langle \phi \rangle_b (\omega_{*e}^T - \omega) f_{e0}}{T_e (\omega - \langle \omega_{De} \rangle_b)}.$$

3.2. EFFECT OF IMPURITIES ON ITG DRIVEN MICROINSTABILITIES

In the inner region, the particles are close to the trapped-passing boundary at $\kappa = 1$, and therefore the elliptic functions can be approximated by their asymptotic limit for $\kappa \rightarrow 1$, yielding $\hat{J}(\kappa \rightarrow 1) \simeq 1$. Assuming for this region that $g_{e0}'' \gg (\ln \hat{J})' g_{e0}'$, the validity of which has been checked *a posteriori*, and changing variables to $t = (1 - \kappa)/\sqrt{\hat{\nu}}$ gives

$$\frac{\partial^2 g_{inner}}{\partial t^2} + i \frac{K(\kappa)}{\omega_0} (\omega - \langle \omega_{De} \rangle_b) g_{inner} = i \frac{e \langle \phi \rangle_b K(\kappa) (\omega_{*e}^T - \omega) f_{e0}}{\omega_0 T_e},$$

with the solution

$$g_{inner} = g_{outer} + \hat{c}_1 \exp \left[-(1 - \kappa) \sqrt{\hat{u} K(\kappa) / \hat{\nu}} \right] + \hat{c}_2 \exp \left[(1 - \kappa) \sqrt{\hat{u} K(\kappa) / \hat{\nu}} \right],$$

where $\hat{u} = -i(y - \langle \omega_{De} \rangle_b / \omega_0)$. The constants c_1 and c_2 can be determined from the boundary condition $g_{e0}(\kappa = 1) = 0$ and the condition that the inner and outer solution must match, $\hat{c}_2 = 0$, in a region where both solutions must be valid. The global solution becomes

$$g_{e0} = g_{outer} \left(1 - \exp \left[-(1 - \kappa) \sqrt{\hat{u} K(\kappa) / \hat{\nu}} \right] \right),$$

which has been shown to agree very well with the numerical solution of eq. (3.15). In order to calculate the quasilinear fluxes, one needs the flux-surface average of the perturbed electron density, given by

$$\left\langle \int g_{e0} d^3 v \right\rangle = 4\sqrt{2\epsilon} \int_0^\infty v^2 dv \int_0^1 K(\kappa) g_{e0} d\kappa,$$

where the κ -integral can be approximated using the identity

$$\int_0^1 \left\{ E(\kappa) + i \frac{4f_s}{3} [(2\kappa - 1)E(\kappa) + (1 - \kappa)K(\kappa)] \right\} d\kappa = \frac{4}{3} \left(1 + i \frac{4f_s}{5} \right).$$

As the equation is still rather complicated to solve analytically, it is necessary to make further approximations. A numerical comparison shows that it is justified to approximate the elliptic integral in the exponent of g_{e0} with a constant, i.e., $K(\kappa) \simeq \int_0^1 K(\kappa) d\kappa = 2$. Furthermore, with the approximation $\langle \omega_{De} \rangle_b \simeq \omega_{D_0}/2$ and

$$\begin{aligned} \int_0^1 K(\kappa) \langle \phi \rangle_b \exp [(\kappa - 1)/\sqrt{n}] d\kappa &\simeq \int_0^1 K(\kappa) \langle \phi \rangle_b d\kappa \int_0^1 \exp [(\kappa - 1)/\sqrt{n}] d\kappa \\ &= 4/3 (1 + i4f_s/5) \sqrt{n}, \end{aligned}$$

3. ASPECTS OF IMPURITY TRANSPORT IN TOKAMAKS

where $n = i\hat{\nu}/(2y - \tilde{\omega}_D)$, the κ -integral becomes

$$\int_0^1 K(\kappa) g_{e0} d\kappa \simeq \frac{4}{3} \left(1 + i \frac{4f_s}{5} \right) \left(1 - \sqrt{\frac{i\hat{\nu}}{2y - \tilde{\omega}_D}} \right),$$

where $\tilde{\omega}_D = \omega_{D0}/\omega$ denotes the normalised magnetic drift frequency. Again, the approximations have been compared with a full numerical solution and shown good agreement. Inserting these terms in the expression for the perturbed electron response yields

$$\begin{aligned} \frac{\hat{n}_e}{n_e} / \frac{e\phi}{T_e} &= 1 - \tilde{\phi} \left\{ \sqrt{2\epsilon} \left[\hat{\omega}_{\eta^*e} - \frac{3}{2} \left(\eta_e \tilde{\omega}_{*e} - \frac{\tilde{\omega}_{Dt}}{2} \hat{\omega}_{\eta^*e} \right) \mathcal{F}_{5/2}^1 \left(\frac{\tilde{\omega}_{Dt}}{2} \right) \right] \right. \\ &\quad \left. - \frac{\Gamma(\frac{3}{4}) \sqrt{\epsilon \hat{\nu}_t}}{\sqrt{-i\pi y}} \left[2\hat{\omega}_{\eta^*e} \mathcal{F}_{3/4}^{3/2} \left(\frac{\tilde{\omega}_{Dt}}{2} \right) - \frac{3\eta_e \tilde{\omega}_{*e}}{2} \mathcal{F}_{7/4}^{3/2} \left(\frac{\tilde{\omega}_{Dt}}{2} \right) \right] \right\}. \end{aligned} \quad (3.17)$$

In this notation, $\tilde{\phi} = (1 + 4if_s/5)4\phi_0/(3\pi\phi)$, $\tilde{\omega}_{Dt} = \omega_{D0}/(\omega x_e^2)$, $\hat{\nu}_t = \hat{\nu}x_e^3$, $\tilde{\omega}_{*a} = \omega_{*a}/\omega$, $\hat{\omega}_{\eta^*a} = 1 - (1 - 3\eta_a/2)\tilde{\omega}_{*a}$ and $\mathcal{F}_b^a(z) = {}_2F_0(a, b; ; z)$, where ${}_2F_0$ denotes the generalised hypergeometric function.

Perturbed ion response

In the ion version of eq. (3.14), collisions can be neglected, and thus the impurities do not influence the solution. Therefore, the pure-plasma solution of [49] can be used, which was derived assuming that $k_{\parallel}v_{Ti} \ll \omega$ and consequently neglecting the parallel dynamics. The solution is

$$\frac{\hat{n}_i}{n_i} / \frac{e\phi}{T_i} = -\tilde{\omega}_{*i} + \left(\frac{3\tilde{\omega}_{Dsi}}{2} - b_i \right) \left[\hat{\omega}_{\eta^*i} - \frac{5}{2} (\eta_i \tilde{\omega}_{*i} - \tilde{\omega}_{Dsi} \hat{\omega}_{\eta^*i}) \mathcal{F}_{7/2}^1(\tilde{\omega}_{Dsi}) \right],$$

where $b_a = b_{a0} [1 + s^2(2\pi^2 - 12 + if_s(2\pi^2 - 3))/(6(1 + if_s))]$, $b_{a0} = (k_{\theta}\rho_{sa})^2$, $\rho_{sa} = v_{th,a}/(\sqrt{2}\Omega_a)$ and

$$\tilde{\omega}_{Dsa} = \frac{6 + (9 + 16if_s)s}{12(1 + if_s)} \frac{\omega_{Da0}}{\omega},$$

with $\omega_{Da0} = -2k_{\theta}v_{th,a}^2/(3\Omega_a R)$. As small-wavelength (comparable to the ion gyroradius) perturbations were not included and only terms linear in b_{i0} were kept, the solution is limited to the fastest growing ITG modes ($k_{\theta}\rho_{si} \sim 0.2$), where these approximations are valid.

Perturbed impurity response

In the impurity version of eq. (3.14), collisions can be neglected as well if the condition

$$(Z^3 m_e / m_i)^{1/2} (n_z Z^2 / n_i) \epsilon \nu_{*e} \ll 1$$

is satisfied. As ϵ and ν_{*e} are ordered small and $Z^2 n_z / n_i = \mathcal{O}(Z_{\text{eff}}) = \mathcal{O}(1)$, this is well satisfied as long as $(Z^3 m_e / m_i)^{1/2} = \mathcal{O}(1)$, which is true for $Z \lesssim 10$. For higher impurity charges, it depends strongly on how small the collisionality really is; in a typical JET discharge with parameters $q = 1.5, R = 3, n \approx 10^{20}/\text{m}^3, T_e \approx 3\text{keV}$ and $\epsilon = 0.1$, the assumption breaks down around $Z \simeq 20$, where the product approaches unity. For higher temperatures, where the collisionality becomes smaller, values up to $Z \simeq 20 - 25$ might be allowed, but for higher charges collisions have to be included. Thus, the analysis presented here is limited to the low and moderate Z region, but thereby nonetheless including some of the most prominent impurities in a fusion reactor, e.g. carbon (C^6) and Helium (He^2). If collisions can be neglected, the impurity density response has exactly the same structure as the ion response (FLR effects which have been neglected in the derivation of the ion equation are even smaller for the impurities, scaling with some fractions of $1/Z$), and thus

$$\frac{\hat{n}_z}{n_z} / \frac{Ze\phi}{T_z} = -\tilde{\omega}_{*z} + \left(\frac{3\tilde{\omega}_{Dsz}}{2} - b_z \right) \left[\hat{\omega}_{\eta*z} - \frac{5}{2} (\eta_z \tilde{\omega}_{*z} - \tilde{\omega}_{Dsz} \hat{\omega}_{\eta*z}) \mathcal{F}_{7/2}^1(\tilde{\omega}_{Dsz}) \right]. \quad (3.18)$$

3.2.2 Quasilinear impurity flux

Using the linear solutions for the perturbed density responses from the previous sections, one can calculate the quasilinear particle fluxes arising from a potential perturbation $\hat{\phi}$. The corresponding perturbed drift velocity $\mathbf{v}_{\hat{E} \times B}$ drives an ambipolar particle flow, averaged over the flux surface,

$$\begin{aligned} \Gamma_a &= \left\langle \int \mathbf{v}_{\hat{E} \times B} \cdot \nabla \psi f_{a1} d^3 v \right\rangle \\ &= \mathcal{R} \left\langle \hat{n}_a \mathbf{v}_{\hat{E} \times B}^* \cdot \nabla \psi \right\rangle, \end{aligned}$$

where an asterisk denotes the complex conjugate. The flux is non-zero only if the potential and density perturbations are out of phase as in-phase contributions cancel during the averaging procedure. Therefore, only the non-adiabatic part of the electron distribution can drive a flow. Noticing that

$$(\mathbf{b} \times \nabla \phi^*) \cdot \nabla \psi = ik_\theta \hat{\phi}^*,$$

3. ASPECTS OF IMPURITY TRANSPORT IN TOKAMAKS

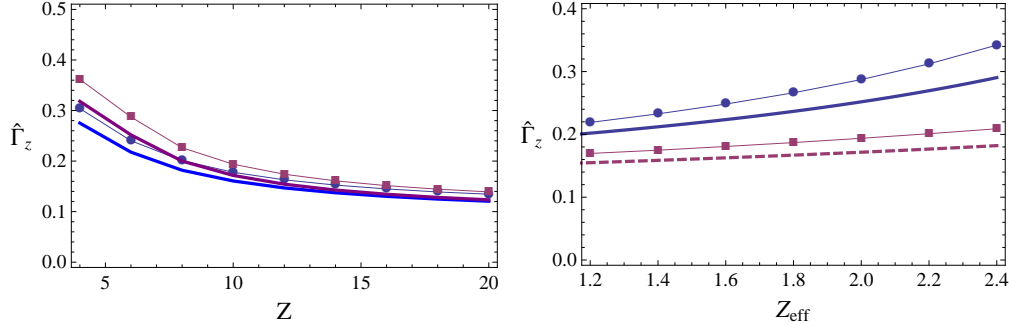


FIGURE 3.6 Left: Normalised impurity flux vs. impurity charge for $Z_{\text{eff}} = 1.5$ (blue) and $Z_{\text{eff}} = 1.5$ (purple). Right: Normalised impurity flux vs. effective charge for $Z = 6$ (solid), $Z = 10$ (dashed). The dots and squares are the corresponding GYRO results.

one can rewrite the expression for the quasilinear particle fluxes as

$$\Gamma_a = -\frac{k_\theta p_a}{eB} \left| \frac{e_a \langle \phi \rangle}{T_a} \right|^2 \Im \left(\frac{\langle \hat{n}_a \rangle / n_a}{e_a \langle \phi \rangle / T_a} \right),$$

where $\langle \phi \rangle = (1 + if_s)\phi_0/2$ and \hat{n}_a/n_a is the nonadiabatic perturbed density response. Fig. 3.6 shows the quasilinear impurity flux obtained from the perturbed impurity density (3.18), together with the results of quasilinear GYRO simulations [48], versus Z and Z_{eff} for a standard case typically used in GYRO simulations (“GA standard case”), $a/L_{Te} = a/L_{Ti} = 3$, $s = 1$, $q = 2$, $a/R = 1/3$, $r/a = 1/2$ and $a/L_{ne} = 1$. The flux is normalised to $k_\theta p_z/(eB) |e \langle \phi \rangle / T_e|^2$. The results for a different scenario can be found in [39], although with different normalisation. For the given input parameters, the figures show that the impurity flux is expected to be outwards. If the other parameters are kept constant, the flux changes sign for $R/L_{n_z} \lesssim 2$. With increasing impurity charge, the resulting flux decreases, and it is higher for higher Z_{eff} . In fig. 3.6, it is obvious that the flux increases nearly linearly with Z_{eff} . The effect is more pronounced for low impurity charge. When the charge gets higher, the increase is only moderate. Fig. 3.7 shows the dependence of the impurity flux on the inverse radial impurity density scale length a/L_{n_z} . Interestingly, the crossover point at which the impurity flux changes from inward to outward is nearly independent of Z and Z_{eff} . Similar results have been obtained previously in fluid simulations of ITG turbulence dominated transport [50].

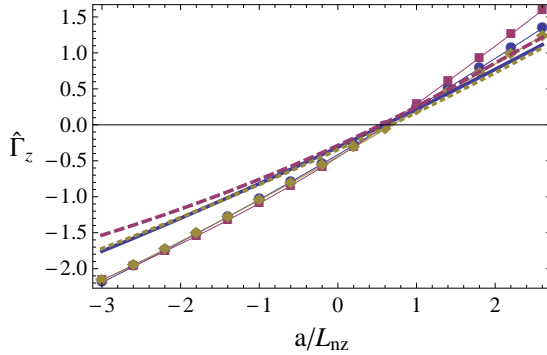


FIGURE 3.7 Normalised impurity flux vs. inverse radial impurity density gradient for the parameters: solid $Z_{\text{eff}} = 1.5$, $Z = 6$, dashed: $Z_{\text{eff}} = 2$, $Z = 6$, dotted: $Z_{\text{eff}} = 2$, $Z = 10$. The dots and squares are the corresponding GYRO results.

3.2.3 Stability

As quasi-neutrality has to be satisfied in every order, i.e. both for the equilibrium densities and for the perturbed densities, the following relation is obtained

$$\frac{\hat{n}_e}{n_e} = (1 - Z f_z) \frac{\hat{n}_i}{n_i} + Z f_z \frac{\hat{n}_z}{n_z}, \quad (3.19)$$

where $f_z \equiv n_z/n_e$ is the fraction of impurities. To simplify the analysis, only the flux-surface averages of the perturbed densities are considered. The dispersion relation was solved numerically for the mode frequency ω and the growth rate γ of ITG modes propagating in the ion diamagnetic direction ($\sigma = -1$) employing the expressions for the perturbed densities from section 3.2.1. Trapped-electron modes (TEM) propagating in the electron diamagnetic direction ($\sigma = 1$) can also be described by (3.19) but will not be addressed here. In the limit of very large aspect ratio, $\epsilon \rightarrow 0$, it is possible to derive an approximate analytical expression for the condition of marginal stability, where γ vanishes, by neglecting the contribution from the trapped part of the perturbed electron density, which is small in this limit. Consequently, the dispersion relation simplifies to

$$\begin{aligned} & \tau_i^*(Z f_z - 1) \left\{ \tilde{\omega}_{*i} - \left(\frac{3\tilde{\omega}_{Dsi}}{2} - b \right) \left[\hat{\omega}_{\eta*i} - \frac{5}{2} (\eta_i \tilde{\omega}_{*i} - \tilde{\omega}_{Dsi} \hat{\omega}_{\eta*i}) \mathcal{F}_{7/2}^1(\tilde{\omega}_{Dsi}) \right] \right\} \\ & - Z^2 f_z \tau_z^* \left\{ \tilde{\omega}_{*z} - \left(\frac{3\tilde{\omega}_{Dsz}}{2} - b_z \right) \left[\hat{\omega}_{\eta*z} - \frac{5}{2} (\eta_z \tilde{\omega}_{*z} - \tilde{\omega}_{Dsz} \hat{\omega}_{\eta*z}) \mathcal{F}_{7/2}^1(\tilde{\omega}_{Dsz}) \right] \right\} \\ & = 1 \end{aligned} \quad (3.20)$$

3. ASPECTS OF IMPURITY TRANSPORT IN TOKAMAKS

where $\tau_a^* = T_e/T_a$. As pointed out in [49], the imaginary parts of $\tilde{\omega}_{Dsa}$ and b_a are much smaller than their real parts if $f_s \ll 1$, which is the case for a broad range of the considered shear region. Then, for $\gamma = 0$, the only terms containing an imaginary part in eq. (3.20) are those containing the functions $\mathcal{F}_{7/2}^1(\tilde{\omega}_{Dsi})$ and $\mathcal{F}_{7/2}^1(\tilde{\omega}_{Dsz})$, which have imaginary parts for all values except $\tilde{\omega}_{Dsi} = \tilde{\omega}_{Dsz} = 0$. Considering the imaginary parts of the ion and impurity hypergeometric functions, one finds that, for moderately high charge numbers and above ($Z \gtrsim 10$), the impurity one peaks outside the considered shear region and nearly vanishes compared with the ion one everywhere else. Therefore, an approximate stability boundary for high impurity charge can be obtained from the condition that the coefficient in front of $\mathcal{F}_{7/2}^1(\tilde{\omega}_{Dsi})$ must vanish. As this coefficient is only dependent on the bulk ion quantities, the eigenfrequency and stability boundary are very weakly affected by the increasing impurity charge, even for a significant fraction of impurities, and approximately equal the corresponding pure-plasma expressions [49],

$$\frac{\omega_{0c}}{\omega_{*e}} = \frac{b_i - 1}{\tau_i^* b_i + 1} + \left(1 + \frac{1}{\tau_i^*}\right) \frac{(2 + 3s)L_{ni}}{(\tau_i^* b_i + 1)2R}, \quad (3.21)$$

and

$$\frac{a}{L_{Tic}} = \frac{\left(1 + \tau_i^{*-1}\right)(2 + 3s)a}{3R(1 - b_i)}. \quad (3.22)$$

Fig. 3.8 shows the mode frequency ω_0 in the case of marginal stability (normalised to c_s/a , where $c_s = \sqrt{T_e/m_i}$ is the ion sound speed) and the critical temperature gradient a/L_{Tic} computed from the full dispersion relation as a function of the impurity charge Z and Z_{eff} , together with the expressions given in eqs. (3.21) and (3.22). The parameters used in the calculations were $s = 1$, $q = 2$, $a/R = 1/3$, $a/R = 2$ and $a/L_{ne} = 1$. For the regions of high impurity charge, where the analytically derived expressions are valid, the agreement with the numerical simulation is very good. There is, as expected, a large discrepancy for lower charges as then the imaginary part of the impurity hypergeometric function becomes comparable to the ion one and thus the impurities can significantly influence the stability condition, especially for impurities like helium or carbon, which have very low Z . In fig. 3.9, the full solutions for the mode frequency and growth rate as obtained from the dispersion relation (3.19) are shown, again together with quasilinear GYRO results, for the standard and hybrid case. Although the absolute values of both quantities decrease with increasing Z_{eff} , reflecting the fact that the impurity terms in the dispersion relation start to play a larger role when the impurity density is increased, which has a stabilising effect, the influence of the charge Z on the frequency and growth rate of the mode is only marginal, except, again, for very small values of Z .

3.2. EFFECT OF IMPURITIES ON ITG DRIVEN MICROINSTABILITIES

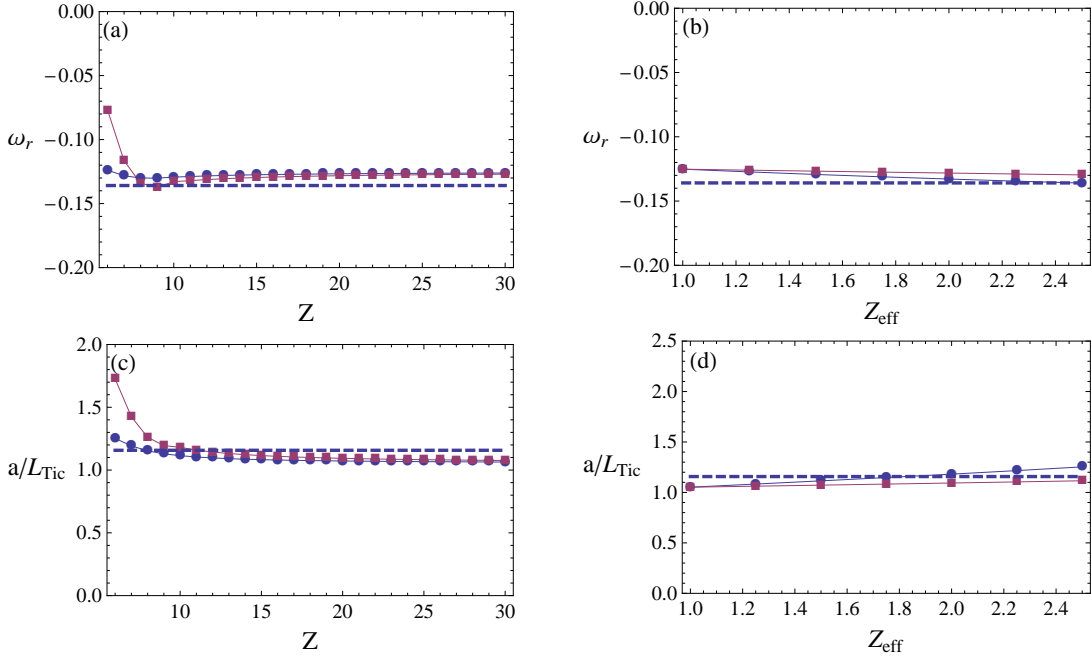


FIGURE 3.8 Upper figures (a, b): Normalised mode frequency (in units of c_s/a) vs. impurity charge (a) and effective charge (b). Lower figures (c, d): Critical ion temperature gradient vs. impurity charge (c) and effective charge (d). Dashed: analytical expression from eqs. (3.21)–(3.22). Left figures (a, c): dots: $Z_{\text{eff}} = 1.5$; squares: $Z_{\text{eff}} = 2$. Right figures (b, d): dots: $Z = 10$; squares: $Z = 20$. The impurity charge and density do not affect the mode frequency and the critical ion temperature gradient significantly for $Z > 10$.

3.2.4 Conclusions of section 3.2

A semi-analytical model for impurity transport driven by ITG turbulence in a large aspect-ratio, weakly collisional tokamak plasma with unshifted circular flux surfaces has been derived and compared with quasilinear simulation results with the GYRO code. A numerically motivated model was employed for the electrostatic potential, but no approximations were made of the magnetic drift frequencies, and collisions were included using a Lorentz operator. The dispersion relation for the mode frequency and growth rate was solved numerically, employing analytical expressions for the perturbed particle densities, which have also been used to derive analytical expressions for the quasilinear fluxes and, in case of high- Z impurities, an approximate stability condition. The quasilinear impurity flux has been found to decrease with increasing impurity charge. It increases with increasing Z_{eff} , and the increase is stronger pronounced for low impurity charge. Depending on the inverse radial impurity density scale

3. ASPECTS OF IMPURITY TRANSPORT IN TOKAMAKS

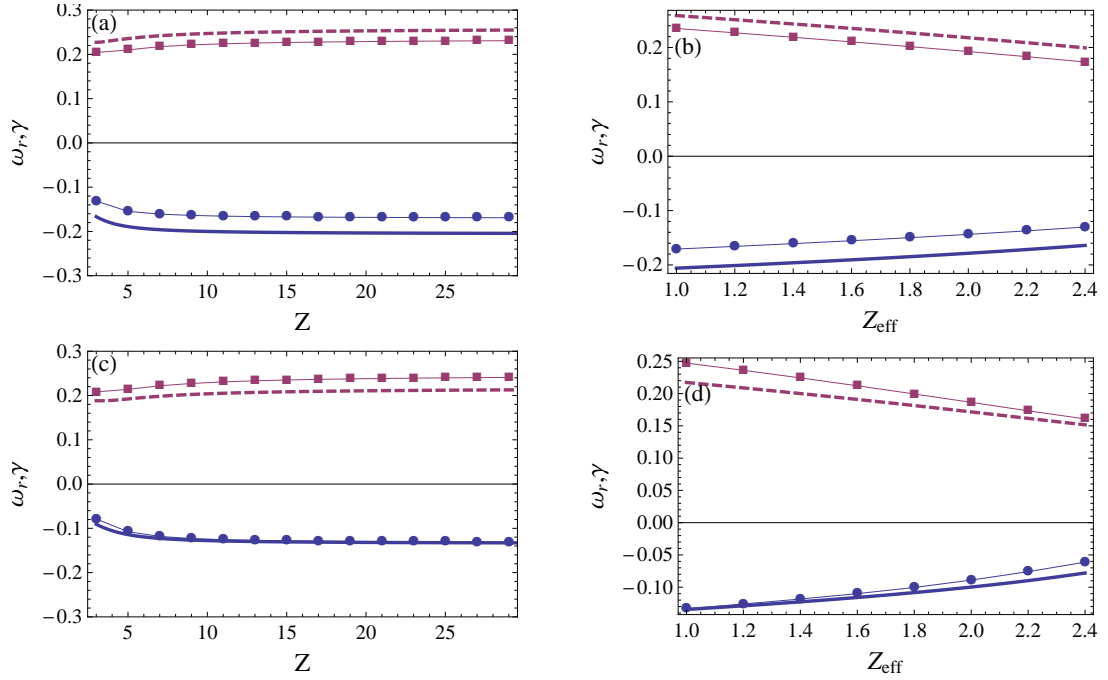


FIGURE 3.9 Left figures (a, c): Normalised mode frequency (solid) and growth rate (dashed) (in units of c_s/a) vs. impurity charge for $Z_{\text{eff}} = 1.5$. Right figures (b, d): Normalised mode frequency (solid) and growth rate (dashed) vs. effective charge for $Z = 6$. The dots and squares are the corresponding GYRO results. Upper figures (a, b): GA standard case, lower figures (c, d): hybrid case.

length, the impurity flux changes sign from inward to outward at $a/L_{n_z} \approx 0.7$ for the given simulation parameters. Interestingly, this value is not influenced much by Z or Z_{eff} . For high impurity charge ($Z \gtrsim 10$), the impurities hardly influence the stability boundary (characterised by the condition that the growth rate vanishes), and the corresponding values for the critical inverse temperature gradient and the mode frequency coincide more or less with the pure-plasma results derived in [49]. However, if the charge is smaller, the impurities do significantly influence these quantities, manifested in a decrease of the mode frequency by up to a factor two and an increase in the critical inverse radial temperature gradient of approximately the same order. Far from marginal stability, the impurity charge hardly influences the mode frequency and growth rate, whereas an increase in the impurity density (increased Z_{eff} at constant Z) leads to a decrease of the absolute values of both quantities, thereby exerting a stabilising effect on the mode. The analytical and semi-analytical results are in good agreement with quasilinear GYRO simulations.

4 Aspects of impurity transport in Stellarators

This chapter is concerned with neoclassical transport of impurities in stellarators. Astonishingly, less research has been performed on this topic than on the corresponding tokamak problems, although neoclassical transport poses a much greater problem in stellarators. Due to the existence of helically trapped particles¹ and other complicated particle orbits, not all of which are intrinsically confined, particles can escape much faster and in greater number from stellarator plasmas than from tokamak plasmas, where all particle orbits stay close to one flux surface to lowest order in δ_a . Consequently, understanding neoclassical stellarator transport is an important issue regarding stellarator optimisation, i.e., the attempt to adjust the magnetic configuration so as to improve the neoclassical confinement, a need which does not occur in tokamaks. The complicated geometry makes both analytical calculations and numerical simulations demanding. Especially in the regimes of low and intermediate collisionality, where effects of particle orbits matter, the variety of different complicated particle trajectories renders any attempt to derive an exact analytic theory taking care of these effects more or less hopeless. There is, however, a possibility to derive analytic equations even in stellarators, and that is in the collisional Pfirsch-Schlüter regime, where particle orbits are permanently interrupted by collisions and thus, effectively, no trapped particles exist. Therefore, a fluid approach can be used (see section 2.5), which disregards particle orbit effects but otherwise keeps the 3D-geometry of the stellarator, and the results can be expressed in terms of the magnetic field strength and various other geometric quantities. Although the applicability is limited to cold edge plasmas, where the plasma is collisional enough to allow for a fluid treatment, analytical theory is nonetheless an important tool for the understanding of basic mechanisms and scalings of the transport. Furthermore, it can provide a useful benchmark for numerical codes and cast light on the accuracy of different approximations on the collision operator usually made in the codes.

Stellarator impurity transport has been considered in the literature before, mainly in the framework of the Hirshman-Sigmar moment formalism [51, 52]. The present calculation, which is based on the direct expansion of the drift kinetic equation by Hazeltine and Hinton [53], retains some terms of geometrical nature that are otherwise neglected, see, e.g., [54], and is used here to calculate explicit transport coefficients.

¹particles trapped in the helical magnetic field ripple

4. ASPECTS OF IMPURITY TRANSPORT IN STELLARATORS

In section 4.1, the impurity transport in arbitrary stellarator geometry is derived in the conventional transport ordering described in section 2.3.3. In the subsequent section 4.2, the transport ordering is modified to allow for large radial gradients that can occur in the plasma edge region. This new ordering leads to various effects, among others to a redistribution of impurities on flux surfaces, which affects the neoclassical transport of the bulk ions, since the friction force is affected by this redistribution.

4.1 Impurity Pfirsch-Schlüter transport in Stellarators

As mentioned in the introduction, impurity accumulation in the centre of fusion plasmas poses a potential threat to fusion performance through radiation losses. As stellarators lack the intrinsic ambipolarity that tokamaks are characterised by, the problem is much more pronounced since the radial electric field plays a major role in the transport. The point is that neoclassical transport is driven by the *thermodynamic forces*

$$\begin{aligned} A_{a_1} &\equiv \frac{d\ln p_a}{d\psi} + \frac{e_a}{T_a} \frac{d\phi}{d\psi}, \\ A_{a_2} &\equiv \frac{d\ln T_a}{d\psi}. \end{aligned}$$

Specifically, in the case of a highly charged impurity ($Z \gg 1$), there is a term in the transport proportional to

$$A_{z_1} = \frac{d\ln p_z}{d\psi} + \frac{Ze}{T_z} \frac{d\phi}{d\psi}.$$

In order to maintain ambipolarity of the transport, the radial electric field adjusts accordingly. In the usual operation scenario (ion-root operation, see section 2.6), it points inwards, and since this term is multiplied by the large factor Z it will cause large inward transport. Interestingly, unlike in a tokamak, two different drives of transport occur in tokamaks, one, in analogy with the tokamak, being friction, and the other one being pressure anisotropy. The latter is multiplied by a geometric factor that vanishes in axisymmetric systems and does not cause any transport in the tokamak. Although, as shown later in this chapter, the friction term dominates at high collisionality, the pressure anisotropy term is nonetheless important as it is the term responsible for setting the radial electric field. The remainder of this section is organised as follows. In section 4.1.1, the drift kinetic equation is solved for both the bulk ions and an impurity species. The corresponding particle and heat fluxes are calculated in sections 4.1.2 and 4.1.4, respectively, while section 4.1.3 deals with the consequences for ambipolarity. The results of this chapter are summarised in section 4.1.5.

4.1.1 Expansion of the kinetic equation

In this section, a plasma in the collisional (Pfirsch-Schlüter) regime is considered consisting of electrons, hydrogenic bulk ions and a single species of highly charged impurities, i.e. the assumption $Z \gg 1$ is made. In order to account for the stellarator geometry and to avoid employing a specific coordinate system, one can express geometry-related quantities in terms of a variable u , defined in the following: Consider the equilibrium current \mathbf{j}_0 satisfying $\mathbf{j}_0 \times \mathbf{B} = \nabla p_0$, where p_0 is the equilibrium pressure. Let u be defined via

$$\begin{aligned}\mathbf{h} &= \frac{\mathbf{j}_0}{p'_0} = \frac{1}{p'_0} \left(\frac{\mathbf{b} \times \nabla p_0}{B} + j_{0\parallel} \mathbf{b} \right) \\ &\equiv \frac{\mathbf{b} \times \nabla \psi}{B} + u \mathbf{B},\end{aligned}$$

where \mathbf{b} is the unit vector along the magnetic field and a prime denotes derivation with respect to the radial spatial coordinate ψ . As the divergence of the equilibrium current must vanish, $\nabla \cdot \mathbf{h} = 0$, and therefore u must satisfy

$$\nabla_{\parallel} u = \frac{1}{p'_0} \nabla_{\parallel} \left(\frac{j_{0\parallel}}{B} \right) = \frac{2}{B^2} (\mathbf{b} \times \nabla \psi) \cdot \nabla \ln B. \quad (4.1)$$

This notation will be employed frequently in the following.

In order to calculate the radial transport of impurities, which is given by [3]

$$\langle \mathbf{T}_z \cdot \nabla \psi \rangle = \left\langle \int f_z \mathbf{v}_d \cdot \nabla \psi d^3 v \right\rangle, \quad (4.2)$$

where the drift velocity \mathbf{v}_d is

$$\mathbf{v}_d = \frac{\mathbf{b} \times \nabla \phi}{B} \cdot \nabla \psi + \left(\frac{v_{\perp}^2}{2} + v_{\parallel}^2 \right) \frac{\mathbf{b} \times \nabla \ln B}{\Omega} \cdot \nabla \psi, \quad (4.3)$$

and $\langle \dots \rangle$ denotes the flux surface average defined in section 2.3.2, one needs to solve the drift kinetic equation for the impurities. Specifically, it is necessary to calculate the friction force and the pressure anisotropy, as the transport term can be rewritten as

$$\langle \mathbf{T}_z \cdot \nabla \psi \rangle = \frac{1}{e_z} \left(\left\langle u B R_{z\parallel} \right\rangle + \left\langle \left(\frac{B}{2} \nabla_{\parallel} u + u \nabla_{\parallel} B \right) (p_{z\parallel} - p_{z\perp}) \right\rangle \right), \quad (4.4)$$

4. ASPECTS OF IMPURITY TRANSPORT IN STELLARATORS

as will be shown in section 4.1.2. Here, $R_{z\parallel}$ is the impurity-ion friction force and terms of second order in $\delta_i \equiv \rho_i/L$ have been neglected. The perpendicular and parallel pressures p_\perp and p_\parallel , respectively, are defined as

$$\begin{pmatrix} p_\parallel \\ p_\perp \end{pmatrix} = \int m \begin{pmatrix} v_\parallel^2 \\ v_\perp^2/2 \end{pmatrix} f d^3v.$$

The flow velocities are, as usual in neoclassical theory, assumed to be one order smaller than the thermal velocities, $V_a \sim \delta_a v_{th,a}$, which is the only possibility in most stellarator configurations [55], where large flows are prohibited. The drift kinetic equation is ordered as usual in δ_a to yield in lowest order

$$C_a(f_{a_0}) = v_\parallel \nabla_\parallel f_{a_0},$$

the solution to which is a stationary Maxwellian as shown in section 2.3.3, and in first order

$$C_a(f_{a_1}) = v_\parallel \cdot \nabla_\parallel f_{a_1} + \mathbf{v}_d \cdot \nabla f_{a_0} + \frac{e_a}{T_a} v_\parallel f_{a_0} \nabla_\parallel \phi. \quad (4.5)$$

The independent coordinates in velocity space are $\varepsilon_a^* = m_a v^2/2 + e_a \phi$ and $\mu_a = m_a v_\perp^2/(2B)$, contrary to the notation introduced in section 2.3.3 where the kinetic energy was used as an independent variable. As this equation is still too complicated to be solved analytically, it is further simplified exploiting the condition that the mean-free path is short in the Pfirsch-Schlüter regime to make a subsidiary expansion in $\Delta_{aa} \equiv \lambda_{aa}/L \ll 1$, where λ_{aa} is the mean free path [3, 56]. Superscript indices correspond to this expansion whereas subscript indices express the ordering in δ_a . In lowest order in this expansion, collisions are dominant, and thus

$$C_a(f_{a_1}^{(-1)}) = 0. \quad (4.6)$$

Note that the expansion starts with -1 as the collision term in lowest order is proportional to Δ_{aa}^{-1} . The homogeneous solution for the general linearised collision operator yields for the -1^{st} order distribution function the shifted Maxwellian

$$f_{a_1}^{(-1)} = \left(\frac{p_{a_1}^{(-1)}}{p_a} + \frac{m_a}{T_a} v_\parallel V_{a\parallel}^{(-1)} + \left(x_a^2 - \frac{5}{2} \right) \frac{T_{a_1}^{(-1)}}{T_a} \right) f_{a_0},$$

with equal flow velocities $V_{i\parallel}^{(-1)} = V_{z\parallel}^{(-1)}$ and temperatures $T_{i_1}^{(-1)} = T_{z_1}^{(-1)}$. More specifically, the -1^{st} order flow velocities must vanish due to the following argument: Integrating

4.1. IMPURITY PFIRSCH-SCHLÜTER TRANSPORT IN STELLARATORS

the zeroth order equation, which becomes

$$C_a(f_{a_1}^{(0)}) = v_{\parallel} f_{a_0} \left(\frac{e_a}{T_a} \nabla_{\parallel} \phi_1^{(-1)} + \frac{\nabla_{\parallel} p_{a_1}^{(-1)}}{p_a} + \left(x_a^2 - \frac{5}{2} \right) \frac{\nabla_{\parallel} T_{a_1}^{(-1)}}{T_a} + \frac{m_a}{T_a} \nabla_{\parallel} \left(v_{\parallel} V_{a_{\parallel}}^{(-1)} \right) \right). \quad (4.7)$$

over velocity space yields

$$\begin{aligned} 0 &= \int C_a(f_{a_0}) d^3v \\ &= \int v_{\parallel} \nabla_{\parallel} \left(\frac{m_a}{T_a} v_{\parallel} V_{\parallel}^{(-1)} \right) d^3v \\ &= \frac{1}{3} \frac{m_a}{T_a} \left(\nabla_{\parallel} V_{\parallel}^{(-1)} - V_{\parallel}^{(-1)} \nabla_{\parallel} \ln B \right) \underbrace{\int v^2 f_{a_0} d^3v}_{\neq 0} \end{aligned}$$

where particle conservation was employed and the other terms vanish as they are odd in v_{\parallel} . Thus, it follows that $V_{\parallel}^{(-1)} = K_{-1}(\psi)B$, where K_{-1} is an arbitrary function of ψ which is constant on a flux surface. Now multiply (4.7) by Bv_{\parallel} , integrate over velocity space and take the flux surface average to find

$$\begin{aligned} \sum_a \left\langle B \int m_a v_{\parallel} C_a(f_{a_1}^{(0)}) d^3v \right\rangle &= - \sum_a \left\langle B \int m_a P_2(\xi) v^2 f_{a_1}^{(-1)} d^3v \nabla_{\parallel} \ln B \right\rangle \\ &= \sum_a \left\langle \left(p_{a_{\parallel}}^{(-1)} - p_{a_{\perp}}^{(-1)} \right) \nabla_{\parallel} B \right\rangle = 0. \end{aligned} \quad (4.8)$$

This term must vanish as momentum is conserved in particle collisions. Defining the Spitzer problem

$$C_a(P_2(\xi) f_{a_0} h_a) = x^2 P_2(\xi) f_{a_0}$$

makes it possible to write the solution $f_{a_1}^{(-1)}$ in terms of h_a ,

$$f_{a_1}^{(-1)}|_{P_2} = \frac{m_a}{T_a} K_{-1}(\psi) P_2(\xi) f_{a_0} h_a \nabla_{\parallel} B.$$

4. ASPECTS OF IMPURITY TRANSPORT IN STELLARATORS

Thus,

$$\sum_a \left\langle \left(p_{a\parallel}^{(-1)} - p_{a\perp}^{(-1)} \right) \nabla_\parallel B \right\rangle = \frac{3}{5} K_{-1}(\psi) \langle (\nabla_\parallel B)^2 \rangle \underbrace{\sum_a m_a n_a \{ h_a \}}_{\neq 0},$$

and it follows that K_{-1} vanishes, and therefore also $V_{i\parallel}^{(-1)}$ and $V_{z\parallel}^{(-1)}$.

In order to rewrite eq. (4.7) in a more compact way, the parallel thermodynamic forces are defined as

$$A_{a_1\parallel}^{(-1)} \equiv \frac{\nabla_\parallel p_{a_1}^{(-1)}}{p_a} + \frac{e_a}{T_a} \nabla_\parallel \phi_1^{(-1)}, \quad A_{a_2\parallel}^{(-1)} \equiv \frac{\nabla_\parallel T_{a_1}^{(-1)}}{T_a},$$

and then

$$C_a \left(f_{a_1}^{(0)} \right) = v_\parallel f_{a_0} \left(A_{a_1\parallel}^{(-1)} + \left(x_a^2 - \frac{5}{2} \right) A_{a_2\parallel}^{(-1)} \right). \quad (4.9)$$

This Spitzer problem, which requires the knowledge of how the collision operator affects the distribution function, can be solved via a moment ansatz decomposing the distribution functions in Sonine polynomials (generalised Laguerre polynomials)

$$L_j^{(m)}(x) \equiv \frac{1}{j!} \frac{e^x}{x^m} \frac{d^j}{dx^j} (x^{j+m} e^{-x})$$

as

$$\begin{aligned} f_{z_1}^{(0)} &= \frac{m_z}{T_z} v_\parallel f_{z_0} \sum_k a_{z_k} L_k^{(3/2)}(x_z^2) \\ f_{i_1}^{(0)} &= \frac{m_i}{T_i} v_\parallel f_{i_0} \sum_k a_{i_k} L_k^{(3/2)}(x_i^2). \end{aligned}$$

As further steps involve taking different moments of the collision operator, it has proven useful to define the following matrix elements

$$\begin{aligned} M_{ab}^{jk} &= \frac{\tau_{ab}}{n_a} \int v_\parallel L_j^{(3/2)}(x_a^2) C_{ab} \left[\frac{m_a}{T_a} v_\parallel L_k^{(3/2)}(x_a) f_{a_0}, f_{b_0} \right] d^3v, \\ N_{ab}^{jk} &= \frac{\tau_{ab}}{n_a} \int v_\parallel L_j^{(3/2)}(x_a^2) C_{ab} \left[f_{a_0}, \frac{m_b}{T_b} v_\parallel L_k^{(3/2)}(x_b^2) f_{b_0} \right] d^3v. \end{aligned}$$

4.1. IMPURITY PFIRSCH-SCHLÜTER TRANSPORT IN STELLARATORS

Analytical expressions for these matrix elements can be found in Braginskii's famous review article [57], and in the explicit form used here in [3]. The Spitzer problem (4.9) can then be rewritten as a matrix problem

$$\sum_{b,k} \frac{m_a}{T_a \tau_{ab}} \left(M_{ab}^{jk} a_{a_k} + N_{ab}^{jk} a_{b_k} \right) = A_{a_1\parallel}^{(-1)} \delta_{j0} - \frac{5}{2} A_{a_2\parallel}^{(-1)} \delta_{j1}$$

where $\tau_{ab} = 3\sqrt{\pi}/(4\hat{\nu}_{ab}) = 3\pi^{3/2}\epsilon_0^2 m_a v_{th,a}^3 / (n_b e_a^2 e_b^2 \ln \Lambda)$ and $\ln \Lambda$ is the Coulomb logarithm. As the Sonine polynomial expansion is well-suited for transport problems and converges quickly, the series is usually truncated after the L_2 component, and this will be done here; note, however, that this is not a full solution of the fluid equations and reflects the problem of the fluid closure addressed in section 2.5, here done by an asymptotic expansion. Solving the matrix problem, one finds that, due to the symmetry properties of the matrix elements, the matrix does not have full rank, and thus a solubility condition exists for the values of the parallel thermodynamic forces on the right-hand side. As the $j = 0$ equations for ions and impurities are linearly dependent, the same must hold for the forces on the right-hand side if a solution is to exist, and therefore the condition

$$\sum_a p_a A_{a_1\parallel}^{(-1)} = 0$$

must hold. This condition follows directly from momentum conservation by multiplying (4.9) by v_{\parallel} , integrating over velocity space and summing over all species. Thus, the problem is always soluble, and $A_{z_1\parallel}^{(-1)}$ can be expressed as $-p_i/p_z A_{i_1\parallel}^{(-1)}$. The electron contribution is small and can safely be neglected. Assuming equal equilibrium temperatures, $T_{i_0} = T_{z_0}$, which is realistic for usual values of Z , and using eq. (4.6), from which follows that the -1^{st} order temperatures in the Δ expansion must be equal as well, one can conclude directly that $A_{z_2\parallel}^{(-1)} = A_{i_2\parallel}^{(-1)}$, which leaves only two unknowns on the right-hand side of the system of equations. The coefficients can then be written as functions of the bulk ion quantities in the form

$$\begin{aligned} a_{i_0} - a_{z_0} &= \frac{T_i}{m_i \hat{\nu}_{ii}} \left(\alpha_0 A_{i_1\parallel}^{(-1)} + \beta_0 A_{2\parallel}^{(-1)} \right) \\ a_{a_j} &= \frac{T_i}{m_i \hat{\nu}_{ii}} \left(\alpha_{a_j} A_{i_1\parallel}^{(-1)} + \beta_{a_j} A_{2\parallel}^{(-1)} \right), j \geq 1. \end{aligned}$$

Note that, as the six-dimensional matrix has only rank five, one of the quantities remains unknown, and therefore $V_{i\parallel}^{(0)}$ can only be expressed through $V_{z\parallel}^{(0)}$ (reflecting Galilean invariance). In the limit of large Z , solving the matrix problem becomes especially easy since the

4. ASPECTS OF IMPURITY TRANSPORT IN STELLARATORS

impurity-ion collision operator can be approximated by

$$C_{zi}(f_{z1}^{(0)}) = -\frac{\mathbf{R}_{zi}}{m_z n_z} \cdot \frac{\partial f_{z1}^{(0)}}{\partial \mathbf{v}} + \frac{m_i n_i}{m_z n_z \tau_{iz}} \frac{\partial}{\partial \mathbf{v}} \cdot \left((\mathbf{v} - \mathbf{V}_z^{(0)}) f_{z1}^{(0)} + \frac{T_i}{m_z} \frac{\partial f_{z1}^{(0)}}{\partial \mathbf{v}} \right).$$

Multiplying by v_{\parallel} and integrating over velocity space yields

$$\begin{aligned} \int m_z v_{\parallel} C_{zi}(f_{z1}^{(0)}) d^3 v &= \frac{R_{iz\parallel}}{n_z} \int v_{\parallel} \frac{\partial f_{z1}^{(0)}}{\partial v_{\parallel}} = -R_{iz\parallel} \\ &= \nabla_{\parallel} p_{z1}^{(-1)} + e_z \nabla_{\parallel} \phi_1^{(-1)}. \end{aligned}$$

Thus,

$$C_{zi}(f_{z1}^{(0)}) = v_{\parallel} f_{z0} A_{z1\parallel}^{(-1)},$$

which cancels the first expression on the right-hand side of eq. (4.9), and the remaining equation

$$C_{zz}(f_{z1}^{(0)}) = v_{\parallel} f_{z0} \left(x_z^2 - \frac{5}{2} \right) A_{2\parallel}^{(-1)}$$

depends only on the impurity parameters. It can be solved analytically for two of the three unknowns, a_{z1} and a_{z2} to yield

$$\begin{aligned} a_{z1} &= \frac{75}{32} \sqrt{\frac{\pi}{2}} A_{z2\parallel}^{(-1)} \frac{T_z}{m_z \hat{\nu}_{zz}} \\ a_{z2} &= -\frac{5}{8} \sqrt{\frac{\pi}{2}} A_{z2\parallel}^{(-1)} \frac{T_z}{m_z \hat{\nu}_{zz}}. \end{aligned}$$

The third coefficient, a_{z0} , equals the parallel impurity flow velocity $V_{z\parallel}^{(0)}$, as will become clear presently. The ion problem can then be solved with the impurity coefficients given. In the *Lorentz limit* of high Z and Z_{eff} (see section 4.1.3), ion self collisions do not matter and the ion collision operator can be approximated with the disparate-mass-ratio ion-impurity collision operator (see section 2.4, which makes it easy to solve the problem analytically). The results for the ion coefficients are given in the appendix of this section. Again, the parallel ion flow velocity is only given in terms of the parallel impurity flow velocity. The Sonine

4.1. IMPURITY PFIRSCH-SCHLÜTER TRANSPORT IN STELLARATORS

polynomials are orthogonal in the sense that

$$\left\{ x_a^{2k-3} L_n^k(x_a^2) L_m^k(x_a^2) \right\} = \delta_{mn} \frac{\Gamma(n+k+1)}{n! \Gamma(5/2)}.$$

Exploiting this property, one can find some useful relations between the coefficients of the distribution functions and the parallel flow velocities $V_{a\parallel}^{(0)}$ and heat fluxes $q_{a\parallel}^{(0)}$, namely

$$\begin{aligned} a_{a_0} &= \frac{1}{n_a} \int v_\parallel f_{a_1}^{(0)} d^3v = V_{a\parallel}^{(0)} \\ a_{a_1} &= \frac{1}{n_a} \int v_\parallel L_1^{(3/2)} f_{a_1}^{(0)} d^3v = -\frac{2}{5} \frac{q_{a\parallel}^{(0)}}{p_a}. \end{aligned}$$

These expressions can now be used to calculate the parallel thermodynamic forces in terms of the radial gradients, yielding in a first step

$$\begin{aligned} A_{i_{1\parallel}}^{(-1)} &= -\frac{m_i \hat{\nu}_{ii}}{T_i} \frac{(2/5)\beta_0 \sum_a q_{a\parallel}^{(0)}/T_a + \beta_{i_1} n_i (V_{i\parallel}^{(0)} - V_{z\parallel}^{(0)})}{(\alpha_{i_1}\beta_0 - \alpha_0\beta_{i_1})n_i} \\ A_{2\parallel}^{(-1)} &= \frac{m_i \hat{\nu}_{ii}}{T_i} \frac{(2/5)\alpha_0 \sum_a q_{a\parallel}^{(0)}/T_a + \alpha_{i_1} n_i (V_{i\parallel}^{(0)} - V_{z\parallel}^{(0)})}{(\alpha_{i_1}\beta_0 - \alpha_0\beta_{i_1})n_i}, \end{aligned}$$

where terms proportional to n_z/n_i have been neglected as impurities are usually rare enough to make this quantity quite small.

The remaining problem is now to relate the flow velocities and heat fluxes to the radial gradients, which can be achieved by taking different moments of the kinetic equation and using conservation properties such as particle and energy conservation. From the particle moment of (4.5), one obtains

$$0 = \int C_a(f_{a_1}^{(1)}) d^3v = \int v_\parallel \nabla_\parallel f_{a_1}^{(0)} d^3v + \int \mathbf{v}_d \cdot \nabla f_{a_0} d^3v.$$

4. ASPECTS OF IMPURITY TRANSPORT IN STELLARATORS

With

$$\begin{aligned}\int v_{\parallel} \nabla_{\parallel} f_{a_1}^{(0)} d^3v &= B \nabla_{\parallel} \left(\int \sum_{\sigma} \frac{\pi v^3}{B_0} f_{a_1}^{(0)} dv d\lambda \right) \\ &= B \nabla_{\parallel} \left(\frac{n_a V_{a_{\parallel}}^{(0)}}{B} \right)\end{aligned}$$

and

$$\begin{aligned}\int \mathbf{v}_d \cdot \nabla f_{a_0} d^3v &= \int \mathbf{v}_d \cdot \nabla \psi \frac{\partial f_{a_0}}{\partial \psi} d^3v \\ &= \int \left(\underbrace{\frac{\mathbf{b} \times \nabla \phi_0}{B} \cdot \nabla \psi}_{=0} + \left(\frac{v_{\perp}^2}{2} + v_{\parallel}^2 \right) \frac{\mathbf{b} \times \nabla \ln B}{\Omega_a} \cdot \nabla \psi \right) \frac{\partial f_{a_0}}{\partial \psi} d^3v \\ &= -\frac{p_a}{e_a} B \nabla_{\parallel} u A_{a_1},\end{aligned}$$

where

$$\begin{aligned}\left. \left(\frac{\partial f_{a_0}}{\partial \psi} \right) \right|_{\varepsilon_a^*} &= f_{a_0} \left(\frac{d \ln p_a}{d \psi} + \frac{e_a}{T_a} \frac{d \phi}{d \psi} + \left(x_a^2 - \frac{5}{2} \right) \frac{d \ln T_a}{d \psi} \right) \\ &= f_{a_0} \left(A_{a_1} + \left(x_a^2 - \frac{5}{2} \right) A_{a_2} \right),\end{aligned}$$

this yields

$$B \nabla_{\parallel} \left(\frac{n_a V_{a_{\parallel}}^{(0)}}{B} - \frac{p_a}{e_a} A_{a_1} u \right) = 0.$$

Analogously, from the energy moment,

$$\sum_a B \nabla_{\parallel} \left(\frac{q_{a_{\parallel}}^{(0)}}{T_a B} - \frac{5}{2} \frac{p_a}{e_a} A_{a_2} u \right) = 0.$$

4.1. IMPURITY PFIRSCH-SCHLÜTER TRANSPORT IN STELLARATORS

as

$$\begin{aligned}
0 &= \sum_a \int \left(x_a^2 - \frac{5}{2} \right) C_a(f_{a1}^{(1)}) d^3 v \\
&= \sum_a \left[\int \left(x_a^2 - \frac{5}{2} \right) v_{\parallel} \nabla_{\parallel} f_{a1}^{(0)} d^3 v \right. \\
&\quad \left. - \frac{m_a}{e_a} B \nabla_{\parallel} u \int v_{\parallel}^2 \left(x_a^2 - \frac{5}{2} \right) f_{a0} \left(A_{a1} + \left(x_a^2 - \frac{5}{2} \right) A_{a2} \right) d^3 v \right] \\
&= \sum_a \left(B \nabla_{\parallel} \left(\frac{q_{a\parallel}^{(0)}}{BT_a} \right) - \frac{p_a}{e_a} B \nabla_{\parallel} u \frac{5}{2} A_{a2} \right).
\end{aligned}$$

Due to the assumption of equal equilibrium temperatures, $A_{i2} \approx A_{z2}$, and thus

$$\begin{aligned}
V_{a\parallel}^{(0)} &= \frac{T_a}{e_a} A_{a1} u B + K_a(\psi) B, \\
\sum_a \frac{q_{a\parallel}^{(0)}}{T_a} &= \frac{5}{2} \sum_a \frac{p_a}{e_a} A_2 u B + L(\psi) B,
\end{aligned}$$

where $K_a(\psi)$ and $L(\psi)$ are integration constants. K_z and L can be obtained from the constraints

$$\left\langle B \sum_a \frac{q_{a\parallel}^{(0)}}{T_a} \right\rangle = 0, \quad \left\langle B \left(V_{i\parallel}^{(0)} - V_{z\parallel}^{(0)} \right) \right\rangle = 0, \quad (4.10)$$

as $\langle B \nabla_{\parallel} M \rangle$ must vanish for all scalars M . Obtaining a third constraint for K_i is a bit more complicated (and unfortunately involves quite some algebra), but is possible from the condition that

$$\sum_a \left\langle \nabla_{\parallel} B \left(p_{a\parallel} - p_{a\perp} \right) \right\rangle = \sum_a \left\langle \nabla_{\parallel} B \int m_a v^2 P_2(\xi) f_{a1}^{(1)} d^3 v \right\rangle = 0, \quad (4.11)$$

where $P_2(\xi)$ is the second Legendre polynomial and $\xi = v_{\parallel}/v$. This condition can be found from taking the flux surface average of B times the velocity moment of the first-order equation, which reads

$$C_a(f_{a1}^{(1)}) = v_{\parallel} \nabla_{\parallel} f_{a1}^{(0)} + \mathbf{v}_d \cdot \nabla f_{a0} + \frac{e_a}{T_a} v_{\parallel} f_{a0} \nabla_{\parallel} \phi_1^{(0)}, \quad (4.12)$$

4. ASPECTS OF IMPURITY TRANSPORT IN STELLARATORS

as in the calculation for obtaining (4.8). Given the fact that the pressure anisotropy of each species is proportional to $p_a/\hat{\nu}_{aa}$, a factor which is smaller for the impurities than for the bulk ions by a factor $Z^{-7/2}$ (if $Z_{\text{eff}} - 1 = \mathcal{O}(1)$), the impurity contribution to (4.11) can be neglected, so that only the ion pressure anisotropy has to be calculated. As the Legendre polynomials are orthogonal in the sense that

$$\int_{-1}^1 P_m(\xi)P_n(\xi)d\xi = \frac{2}{2n+1}\delta_{mn},$$

only the P_2 components of the distribution function contribute in this equation. These first occur in first order in the mean-free path expansion, so eq. (4.12) has to be solved. Unlike the problem of solving the zeroth order equation, where the right-hand side was proportional to $P_1(v_{\parallel}/v)$, in this case Spitzer problems proportional to P_2 must be solved, which involve a different kind of matrix elements than used before. Defining the functions g_{ij} via

$$C_i(P_2(\xi)f_{i_0}g_{ij}) = (-1)^j P_2(\xi)x^2 f_{i_0} L_j^{(3/2)}(x^2),$$

one can express the solution through these functions, which can be determined independently. Conveniently, the pressure anisotropy can be expressed in terms of the velocity space average of the P_2 components of the distribution functions in the following way:

$$\begin{aligned} p_{i_{\parallel}} - p_{i_{\perp}} &= \int m_i v^2 P_2(\xi) f_{i_1}^{(1)} d^3 v \\ &= \frac{4p_i}{\sqrt{\pi}} \int_{-1}^1 P_2^2(\xi) d\xi \int_0^{\infty} e^{-x^2} x^4 \frac{f_{i_1}^{(1)}|_{P_2}}{P_2(\xi) f_{i_0}} dx \\ &= \frac{3}{5} p_i \left\{ \frac{f_{i_1}^{(1)}|_{P_2}}{P_2(\xi) f_{i_0}} \right\}, \end{aligned}$$

and therefore it is convenient to define

$$\{g_{ij}\} \equiv \frac{5}{2} \frac{\gamma_{ij}}{\hat{\nu}_{ii}}. \quad (4.13)$$

The part of the first order ion distribution function which is proportional to P_2 reads

$$f_{i_1}^{(1)}|_{P_2} = -\frac{1}{3\nu_{iz}} \left(v_{\parallel} \nabla_{\parallel} f_{i_1}^{(0)} + \mathbf{v}_d \cdot \nabla f_{i_0} \right) |_{P_2},$$

4.1. IMPURITY PFIRSCH-SCHLÜTER TRANSPORT IN STELLARATORS

where

$$\mathbf{v}_d \cdot \nabla f_{i_0}|_{P_2} = -\frac{m_a}{3e_a} v^2 P_2(\xi) f_{i_0} \left(A_{i_1} - L_1^{(3/2)}(x_i^2) A_{i_2} \right) \frac{B}{2} \nabla_{\parallel} u$$

and from the zeroth order contribution of the ion distribution, which is proportional to v_{\parallel} , one finds the expressions

$$v_{\parallel} \nabla_{\parallel} v_{\parallel}|_{P_2} = \frac{v^2}{3} \nabla_{\parallel} \ln B P_2(\xi)$$

and

$$v_{\parallel}^2|_{P_2} = \frac{2v^2}{3} P_2(\xi).$$

Then,

$$f_{i_1}^{(1)}|_{P_2} = \frac{2}{3} P_2(\xi) f_{i_0} \left[(\nabla_{\parallel} \ln B + 2\nabla_{\parallel}) (a_{i_0} g_{i_0} - a_{i_1} g_{i_1} + a_{i_2} g_{i_2}) - \frac{B}{2} \nabla_{\parallel} u \frac{T_i}{e_i} (A_{i_1} g_{i_0} + A_{i_2} g_{i_1}) \right],$$

and the bulk ion pressure anisotropy becomes

$$p_{i_{\parallel}} - p_{i_{\perp}} = \frac{p_i}{\hat{\nu}_{ii}} \left[(\nabla_{\parallel} \ln B + 2\nabla_{\parallel}) (a_{i_0} \gamma_{i_0} - a_{i_1} \gamma_{i_1} + a_{i_2} \gamma_{i_2}) - \frac{B}{2} \nabla_{\parallel} u \frac{T_i}{e_i} (A_{i_1} \gamma_{i_0} + A_{i_2} \gamma_{i_1}) \right].$$

Using (4.10) and (4.11), one finds the three integration constants to read

$$\begin{aligned} L(\psi) &= -\frac{5}{2} \sum_a \frac{p_a}{e_a} A_{a2} \frac{\langle uB^2 \rangle}{\langle B^2 \rangle}, \\ K_z(\psi) &= \left(\frac{T_i}{e_i} A_{i_1} - \frac{T_z}{e_z} A_{z_1} \right) \frac{\langle uB^2 \rangle}{\langle B^2 \rangle} + K_i(\psi), \\ K_i(\psi) &= - \left(\frac{T_i}{e_i} A_{i_1} G_1(\psi) + \frac{T_i}{e_i} A_{i_2} \frac{\gamma_{i_1}}{\gamma_{i_0}} \left(G_1(\psi) - \frac{\langle uB^2 \rangle}{\langle B^2 \rangle} \right) \right. \\ &\quad \left. + \frac{\gamma_{i_2}}{\gamma_{i_0}} \left(\left(\frac{T_i}{e_i} A_{i_1} - \frac{T_z}{e_z} A_{z_1} \right) \eta_2 + \frac{T_i}{e_i} A_{i_2} \eta_1 \right) \left(G_1(\psi) - \frac{\langle uB^2 \rangle}{\langle B^2 \rangle} + \frac{1}{3} \frac{\langle \frac{B}{2} \nabla_{\parallel} u \nabla_{\parallel} B \rangle}{\langle (\nabla_{\parallel} B)^2 \rangle} \right) \right), \end{aligned}$$

4. ASPECTS OF IMPURITY TRANSPORT IN STELLARATORS

where $G_1(\psi) \equiv \langle \nabla_{\parallel} B(u \nabla_{\parallel} B + B \nabla_{\parallel} u/2) \rangle / \langle (\nabla_{\parallel} B)^2 \rangle$ and

$$\begin{aligned}\eta_1 &= \frac{\alpha_0 \beta_{i_2} - \beta_0 \alpha_{i_2}}{\alpha_{i_1} \beta_0 - \alpha_0 \beta_{i_1}}, \\ \eta_2 &= \frac{\alpha_{i_1} \beta_{i_2} - \beta_{i_1} \alpha_{i_2}}{\alpha_{i_1} \beta_0 - \alpha_0 \beta_{i_1}}.\end{aligned}$$

4.1.2 Radial particle transport

In this section, the radial particle flux of the impurities is calculated. Inserting the expression for the drift velocity in (4.2), one obtains

$$\begin{aligned}\langle \Gamma_z \cdot \nabla \psi \rangle &= \left\langle \int f_z \left(\frac{\mathbf{b} \times \nabla \phi}{B} \cdot \nabla \psi + \left(\frac{v_{\perp}^2}{2} + v_{\parallel}^2 \right) \frac{\mathbf{b} \times \nabla \ln B}{\Omega_z} \cdot \nabla \psi \right) d^3 v \right\rangle \\ &= - \left\langle n_z \frac{\mathbf{b} \times \nabla \psi}{B} \cdot \nabla \phi \right\rangle - \left\langle \frac{1}{e_z} \mathbf{b} \times \nabla \psi \cdot \frac{\nabla B}{B^2} \int m_z f_z \left(\frac{v_{\perp}^2}{2} + v_{\parallel}^2 \right) d^3 v \right\rangle \\ &= \langle n_z (u \mathbf{B} - \mathbf{h}) \cdot \nabla \phi \rangle - \frac{1}{e_z} \left\langle (p_{z\perp} + p_{z\parallel}) \frac{B}{2} \nabla_{\parallel} u \right\rangle.\end{aligned}$$

On the other hand, substituting $e_z/T_z v_{\parallel} f_{z_0} \nabla_{\parallel} \phi$ yields

$$\begin{aligned}\langle e_z n_{z_0} u B \nabla_{\parallel} \phi \rangle &= \left\langle e_z u B \int \frac{m_z}{T_z} v_{\parallel}^2 f_{z_0} d^3 v \nabla_{\parallel} \phi \right\rangle \\ &= - \left\langle e_z u B \int v_{\parallel}^2 \nabla_{\parallel} f_z d^3 v \right\rangle + \left\langle u B R_{z\parallel} \right\rangle \\ &= \left\langle u B R_{z\parallel} \right\rangle + \left\langle e_z p_{z\parallel} B \nabla_{\parallel} u \right\rangle + \left\langle e_z u B (p_{z\parallel} - p_{z\perp}) \nabla_{\parallel} \ln B \right\rangle,\end{aligned}$$

and thus

$$\langle \Gamma_z \cdot \nabla \psi \rangle = \frac{1}{e_z} \left(\left\langle u B R_{z\parallel} \right\rangle + \left\langle \left(\frac{B}{2} \nabla_{\parallel} u + u \nabla_{\parallel} B \right) (p_{z\parallel} - p_{z\perp}) \right\rangle \right)$$

as stated in section 4.1.1. Calculating the impurity pressure anisotropy is extremely tedious, and the result is lengthy and not very enlightening (and therefore not shown here); the most important feature of the result is that, as the pressure anisotropy is inversely proportional to the collision frequency whereas the friction force is proportional to it, the following estimate

4.1. IMPURITY PFIRSCH-SCHLÜTER TRANSPORT IN STELLARATORS

holds:

$$\frac{\text{pressure anisotropy term}}{\text{friction term}} \sim \frac{\Delta_{ii}^2}{Z^4} \ll 1.$$

The friction term thus dominates, and not only in the Δ expansion, as expected from the order in which friction and pressure anisotropy occur, but also by a factor Z^4 , which becomes large even for relatively small values of the impurity charge Z , and thus the exact structure of the impurity pressure anisotropy does not matter.

The friction part can be calculated to be

$$\begin{aligned} \langle uBR_{z\parallel} \rangle &= -\langle uBR_{i\parallel} \rangle = -\langle uBp_i A_{i\parallel}^{(-1)} \rangle \\ &= -\frac{m_i n_i \hat{\nu}_{ii}}{\alpha_{i_1} \beta_0 - \alpha_0 \beta_{i_1}} \left(\langle u^2 B^2 \rangle - \frac{\langle uB^2 \rangle^2}{\langle B^2 \rangle} \right) \left(\beta_{i_1} \left(\frac{T_i}{e_i} A_{i_1} - \frac{T_z}{e_z} A_{z_1} \right) + \beta_0 \frac{T_i}{e_i} A_2 \right). \end{aligned}$$

The entire effect of the magnetic field geometry is contained in the factor

$$\left(\langle u^2 B^2 \rangle - \frac{\langle uB^2 \rangle^2}{\langle B^2 \rangle} \right),$$

which is always positive by the Schwartz inequality. In the limit of large Z and for $Z_{\text{eff}} = 2$, the coefficients can be calculated analytically, and one obtains

$$\langle uBR_{z\parallel} \rangle = -m_i n_i \hat{\nu}_{ii} \left(\langle u^2 B^2 \rangle - \frac{\langle uB^2 \rangle^2}{\langle B^2 \rangle} \right) \left(0.50 \left(\frac{T_i}{e_i} A_{i_1} - \frac{T_z}{e_z} A_{z_1} \right) - 0.41 \frac{T_i}{e_i} A_2 \right).$$

4.1.3 Ambipolarity

Although not contributing much to the radial transport, the pressure anisotropy is nonetheless important as the radial electric field is set by the condition that the transport must be ambipolar. Because the transport due to friction is intrinsically ambipolar, the pressure anisotropy term is the relevant one in this process. Again, the impurity pressure anisotropy contributes only as a small correction to the ion pressure anisotropy and will not be calculated here, but the impurities influence the balance by changing the ion pressure anisotropy in comparison with a pure plasma through ion-impurity collisions. In a pure plasma, the ion pressure anisotropy

4. ASPECTS OF IMPURITY TRANSPORT IN STELLARATORS

has been calculated by Simakov and Helander [54] and is, in the notation adopted here,

$$\begin{aligned} & \left\langle \left(\frac{B}{2} \nabla_{\parallel} u + u \nabla_{\parallel} B \right) (p_{i\parallel} - p_{i\perp}) \right\rangle \\ &= -\frac{3p_i}{\tilde{\nu}_{ii}} \left[\left(1.80 \frac{T_i}{e_i} A_{i1} + 3.21 \frac{T_i}{e_i} A_{i2} \right) (G_2(\psi) - G_1(\psi)) + 0.10 \frac{T_i}{e_i} A_{i2} G_3(\psi) \right]. \end{aligned} \quad (4.14)$$

In an impure plasma, both the P_1 and the P_2 Spitzer problems have to be modified so as to include collisions with impurities. Whereas the results for the P_1 problem have been shown in section 4.1.1, where Braginskii's matrix elements could be used in the calculation, such matrix elements are not as easily available for the P_2 components, and it is tedious to calculate them analytically for arbitrary mass ratio and effective charge. If they are known, the coefficients γ_{ij} defined in (4.13) can easily be determined. However, though the full calculation is lengthy, it is possible to calculate these coefficients analytically without too much effort in the limit of large Z and Z_{eff} , the so-called *Lorentz limit*. Although this limit is not a situation which would occur during usual operation of a machine as impurities are assumed to be so numerous that a burning plasma with a positive energy balance is rendered impossible, it contains useful information when combined with the results of the trace impurity limit, in which $Z_{\text{eff}} \ll 1$. In this limit, the impurities are too rare to influence the radial electric field, and therefore the pressure anisotropy corresponds to that in a pure plasma given by eq. (4.14). Having calculated both the limit of very small and very large Z_{eff} , where the realistic value for Z_{eff} in experiments is expected to lie somewhere in between, one obtains an impression of the effect of the impurities on the radial electric field. For the calculation of the P_2 matrix elements, the ion-impurity collision operator is approximated by pitch-angle scattering and a momentum restoring term (see section 2.4), noting that pitch-angle scattering is the dominant process when the mass ratio is very disparate. As Z_{eff} is assumed to be large, ion self collisions can be neglected compared with ion-impurity collisions, and thus the entire ion collision operator is

$$C_i(f_{i1}^{(1)}) \approx C_{iz}(f_{i1}^{(1)}) = \nu_{iz} \left(\mathcal{L}(f_{i1}^{(1)}) + \frac{m_i}{T_i} v_{\parallel} V_{z\parallel} f_{i0} \right).$$

Expanding the functions g_{ij} as

$$g_{ij} = x_i^2 \sum_k b_{jk} L_k^{(5/2)}(x_i^2),$$

4.1. IMPURITY PFIRSCH-SCHLÜTER TRANSPORT IN STELLARATORS

one finds, as the Legendre polynomials are eigenfunctions of the Lorentz operator,

$$C_i(g_{ij}) = -3\nu_{iz}P_2(\xi)f_{i0}x_i^2 \sum_k b_{jk} L_k^{(5/2)}(x_i^2).$$

With the help of this relation, the coefficients γ_{ij} can be calculated using the orthogonality properties of the Sonine polynomials with respect to the velocity space average; the values are given in the appendix of this chapter. The pressure anisotropy contribution to the radial transport then becomes

$$\begin{aligned} & \left\langle \left(\frac{B}{2} \nabla_{\parallel} u + u \nabla_{\parallel} B \right) (p_{i\parallel} - p_{i\perp}) \right\rangle \\ &= -\frac{3p_i}{(Z_{\text{eff}} - 1)\hat{\nu}_{ii}} \left[\left(0.47 \frac{T_i}{e_i} A_{i1} + 1.93 \frac{T_z}{e_z} A_{z1} + 9.90 \frac{T_i}{e_i} A_{i2} \right) \cdot (G_2(\psi) - G_1(\psi)) \right. \\ & \quad \left. + \left(1.29 \frac{T_i}{e_i} A_{i2} - 0.65 \left(\frac{T_i}{e_i} A_{i1} - \frac{T_z}{e_z} A_{z1} \right) \right) \cdot G_3(\psi) \right], \end{aligned}$$

where

$$\begin{aligned} G_2(\psi) &= \left\langle \left(\frac{B}{2} \nabla_{\parallel} u + u \nabla_{\parallel} B \right)^2 \right\rangle, \\ G_3(\psi) &= \left\langle \frac{B}{2} \nabla_{\parallel} u \left(\frac{B}{2} \nabla_{\parallel} u + u \nabla_{\parallel} B \right) \right\rangle - \left\langle \frac{B}{2} \nabla_{\parallel} u \nabla_{\parallel} B \right\rangle G_1(\psi) \end{aligned}$$

and $G_1(\psi)$ has already been defined in section 4.1.1. Except for the quantitative change in the magnitude of the coefficients, there is no great qualitative change when impurities are present, as the contribution from A_{z1} is proportional to $1/Z$ and thus relatively small. The only qualitative difference is the additional contribution from A_{i1} in front of G_3 . The magnitude of the two geometric terms $G_2 - G_1$ and G_3 is strongly dependent on the exact geometry of the device, but the latter term tends to be slightly smaller than or comparable to the first one. Although the magnitude of the ion distribution function coefficients increases when impurities are present, the overall contribution to the pressure anisotropy decreases due to the large factor $Z_{\text{eff}} - 1$ in the denominator.

4. ASPECTS OF IMPURITY TRANSPORT IN STELLARATORS

4.1.4 Heat flux

The radial heat fluxes are also influenced by the presence of impurities, and are given by

$$\begin{aligned}\langle \mathbf{q}_a \cdot \nabla \psi \rangle &= T_a \left\langle \int f_a \left(x_a^2 + \frac{e_a \phi}{T_a} - \frac{5}{2} \right) \mathbf{v}_d \cdot \nabla \psi d^3 v \right\rangle \\ &= T_a \langle \mathbf{\Gamma}_a \cdot \nabla \psi \rangle - \frac{m_a}{e_a} \left\langle \frac{B}{2} \nabla_{\parallel} u \int f_{a1} \left(v_{\parallel}^2 + \frac{v_{\perp}^2}{2} \right) \left(x_a^2 + \frac{e_a \phi_1}{T_a} - \frac{3}{2} \right) d^3 v \right\rangle.\end{aligned}$$

The particle flux has already been calculated in the last section, and the second term can be rewritten, using the orthogonality properties of the Sonine and the Legendre polynomials and neglecting components proportional to P_2 , which first occur in first order in the Δ_{ii} expansion and are thus two orders smaller than the other terms, as

$$\begin{aligned}&\frac{m_a}{e_a} \left\langle \frac{B}{2} \nabla_{\parallel} u \int f_{a1} \left(v_{\parallel}^2 + \frac{v_{\perp}^2}{2} \right) \left(x_a^2 + \frac{e_a \phi_1}{T_a} - \frac{3}{2} \right) d^3 v \right\rangle \\ &= \frac{m_a}{e_a} \underbrace{\left[\left\langle \frac{B}{2} \nabla_{\parallel} u \int f_{a1} \left(\frac{v_{\perp}^2}{2} - v_{\parallel}^2 \right) \left(x_a^2 - \frac{3}{2} + \frac{e_a \phi_1}{T_a} \right) d^3 v \right\rangle \right]}_{\sim P_2(\xi)} \\ &\quad + \left\langle B \nabla_{\parallel} u \int f_{a1} v_{\parallel}^2 \left(x_a^2 - \frac{5}{2} + 1 + \frac{e_a}{T_a} \phi_1 \right) d^3 v \right\rangle \\ &= \frac{m_a}{e_a} \left[\left\langle B \nabla_{\parallel} u \int \frac{T_{a1}}{T_{a0}} v_{\parallel}^2 \left(x_a^2 - \frac{5}{2} \right)^2 f_{a0} d^3 v \right\rangle + \left\langle B \nabla_{\parallel} u \int v_{\parallel}^2 \frac{p_{a1}}{p_{a0}} f_{a0} d^3 v \right\rangle \right. \\ &\quad \left. + \left\langle B \nabla_{\parallel} u \int f_{a0} v_{\parallel}^2 \frac{e_a}{T_a} \phi_1 d^3 v \right\rangle \right] \\ &= -\frac{p_a}{e_a} \left\langle u B \left(\frac{5}{2} A_{2\parallel}^{(-1)} + A_{a1\parallel}^{(-1)} \right) \right\rangle.\end{aligned}$$

Combining this term with the expression for the particle flux, the total heat flux becomes

$$\begin{aligned}\langle \mathbf{q} \cdot \nabla \psi \rangle &= \frac{5}{2} \sum_a \frac{T_a}{e_a} p_{a0} \left\langle u B A_{2\parallel}^{(-1)} \right\rangle \\ &= \frac{5}{2} \sum_a \frac{T_a}{e_a} p_{a0} \frac{m_i \hat{\nu}_{ii}}{T_i} \left(\langle u^2 B^2 \rangle - \frac{\langle u B^2 \rangle^2}{\langle B^2 \rangle} \right) \frac{\alpha_{i1} \left(\frac{T_i}{e_i} A_{i1} - \frac{T_z}{e_z} A_{z1} \right) + \alpha_0 \frac{T_i}{e_i} A_{i2}}{\alpha_{i1} \beta_0 - \alpha_0 \beta_{i1}}.\end{aligned}$$

4.1.5 Conclusions of section 4.1

The Pfirsch-Schlüter impurity particle and heat fluxes in a stellarator have been calculated. Compared with the axisymmetric case, the particle transport is qualitatively different and consists of two separate terms, one tokamak-like term that is proportional to the friction force, and one term related to the difference between parallel and perpendicular pressures, which is multiplied by a geometric factor that vanishes in axisymmetric systems. The first term is proportional to the collision frequency and the second one is inversely proportional to it. When comparing the magnitude of their contributions in the Pfirsch-Schlüter regime, one therefore finds that the friction term is considerably larger than the pressure anisotropy term, both with respect to the ordering in the shortness of the mean free path and to the ordering of the impurity charge $Z \gg 1$. Since the two terms differ by a factor of Z^4 , even for relatively small impurity charges the friction term will dominate. As the friction term is intrinsically ambipolar, the small pressure anisotropy term, which does not have this property, is nonetheless important for determining the radial electric field. The main contribution comes from the bulk ion pressure anisotropy, which is affected quantitatively by the presence of impurities, but the qualitative effect of the impurities is minor.

The circumstance that the neoclassical pressure anisotropy becomes small at high collisionality may have implications for the conclusion drawn in [27, 58] and [59] that the radial electric field is usually set by neoclassical rather than turbulent transport in stellarators, even if the turbulent fluxes exceed the neoclassical ones. This result was based on the observation that the particle flux produced by gyrokinetic turbulence is intrinsically ambipolar (in leading order) whereas the neoclassical transport is not. Since the neoclassical non-ambipolarity decreases with increasing collisionality, however, one would expect that turbulence could affect the electric field in cool edge plasmas if the small non-ambipolarity of the turbulence can compete with the similarly small one of the neoclassical transport.

The Pfirsch-Schlüter heat flux is unremarkable. The direct contribution from the impurities is smaller than that from the bulk ions, but the latter is affected by the presence of impurities. In a pure plasma, the heat flux exceeds the particle flux by a large factor, but they are comparable when impurities are present.

4.1.6 Appendix: Coefficients of the distribution functions

For fixed Z, Z_{eff} , the coefficients of the distribution functions can easily be calculated numerically. Here, some values are given for different impurity charge and effective charge, assuming equal equilibrium temperatures. The values for $Z_{\text{eff}} \gg 1$ are analytical limits.

4. ASPECTS OF IMPURITY TRANSPORT IN STELLARATORS

TABLE 4.1 Coefficients of $f_{i_1}^{(0)}$

	$Z = 6, Z_{\text{eff}} = 2$	large $Z, Z_{\text{eff}} = 2$	large $Z, Z_{\text{eff}} \gg 1$
α_0	-1.618	-2.591	$-4.51/(Z_{\text{eff}} - 1)$
α_{i_1}	0.520	0.738	$2.71/(Z_{\text{eff}} - 1)$
α_{i_2}	-0.005	0.084	$-0.39/(Z_{\text{eff}} - 1)$
β_0	-1.301	-1.843	$-6.77/(Z_{\text{eff}} - 1)$
β_{i_1}	1.673	2.205	$11.28/(Z_{\text{eff}} - 1)$
β_{i_2}	-0.613	-0.781	$-6.77/(Z_{\text{eff}} - 1)$

TABLE 4.2 Coefficients of $f_{z_1}^{(0)}$

	$Z = 6, Z_{\text{eff}} = 2$	large $Z, Z_{\text{eff}} = 2$
α_0	-1.618	-2.591
α_{z_1}	0.006	0.000
α_{z_2}	0.000	0.000
β_0	-1.301	-1.843
β_{z_1}	0.029	0.000
β_{z_2}	-0.006	0.000

TABLE 4.3 Coefficients γ_{i_j}

	large $Z, Z_{\text{eff}} \gg 1$
γ_{i_0}	$-2.41/(Z_{\text{eff}} - 1)$
γ_{i_1}	$-6.02 / (Z_{\text{eff}} - 1)$
γ_{i_2}	$-4.51 / (Z_{\text{eff}} - 1)$

4.2 Pfirsch-Schlüter transport in the presence of large gradients

Toroidal edge plasmas are often characterised by large radial gradients of the bulk ion density and temperature. In fusion relevant experiments, these gradients can easily become larger than allowed for by conventional neoclassical theory based on a small-gyroradius expansion, $\delta_a \equiv \rho_{a_\theta}/L_\perp \ll 1$, of the kinetic equation, which was treated in the section 4.1 (hereafter referred to as “conventional theory”) and where ρ_{a_θ} is the poloidal gyroradius and L_\perp the radial scale length of the density and temperature gradients. Note that, as soon as large gradients are involved, the parallel and perpendicular scale lengths have to be treated separately, which leads to the refinement in the definition of δ_a involving L_\perp and ρ_{a_θ} . This problem may be of particular interest in the context of the H-mode (see section 1.2.4), one characteristic of which is the formation of sharp edge pedestals acting as a transport barrier. Although it is fundamentally difficult to construct a rigorous neoclassical transport theory if δ_a is not a small parameter, it is possible to extend conventional theory to include the cases of larger gradients. In this new ordering, δ_i is still treated as small, though not as the *smallest* expansion parameter any more, as is implicitly assumed in conventional theory. The other particle species’ quantities are then expressed in terms of δ_i . Products of δ_i with large parameters, such as, in the Pfirsch-Schlüter regime, the collisionality $\bar{\nu}_{ii} \equiv \lambda_{ii}/L_\parallel$, where λ_{ii} is the ion mean free path and L_\parallel the connection length, and the impurity charge Z , e.g. $\Delta_i \equiv \delta_i \bar{\nu}_{ii} Z^2$, can easily be of order unity in the plasma edge, and this is taken into account in the new ordering. The consequence is that in this new ordering the lowest order impurity distribution function is only locally Maxwellian, contrary to the conventional case where all lowest order quantities are flux functions. In practice, as a consequence of the large gradients, the impurities start developing density variations *within* the flux surface, which, depending on the plasma conditions, can lead to an accumulation of impurities at certain points on the flux surface. In tokamaks, this redistribution has previously been predicted to lead to impurity accumulation of the order of up to 30% of the total density at the high-field side of the torus [60, 61], a result which is in qualitative agreement with experimental results of present machines such as Alcator C-mod or MAST. However, there has been no work at all on how this effect is affected by stellarator geometry, and the calculations presented in this section are aiming at calculating this effect. As a stellarator plasma, contrary to the tokamak case, cannot rotate freely [27] but instead has a radial electric field which adjusts itself so as to make the radial transport ambipolar (see section 2.6), the effect of the impurity redistribution is fundamentally different in a stellarator due to effects from the radial electric field which cancel in axisymmetric systems. The remainder of this section is organised as follows. In section 4.2.1, the kinetic theory is described and a differential equation for the impurity density variation is derived. This equation is solved, first in different analytical limits in section 4.2.2, and then fully with the help of numerical tools in section 4.2.3. The results are discussed and summarised in sections 4.2.4 and 4.2.5.

4. ASPECTS OF IMPURITY TRANSPORT IN STELLARATORS

4.2.1 Kinetic equations

As in the previous section, we consider a stellarator plasma in the collisional regime consisting of hydrogenic bulk ions and a single species of heavy, highly charged impurities with charge $Z \gg 1$. The effect of electron collisions on the other species is small and therefore neglected, and the impurities are assumed to be not too numerous, so that the assumption $Z^2 n_z / n_i \ll 1$ holds (trace impurities). The drift kinetic equation for each species,

$$C_a(f_a) = v_{\parallel} \nabla_{\parallel} f_a + \mathbf{v}_d \cdot \nabla f_a + \frac{e_a}{T_a} v_{\parallel} \nabla_{\parallel} \phi f_a, \quad (4.15)$$

where \mathbf{v}_d is given by (4.3), is now solved employing the ordering mentioned above, namely $\delta_i \ll 1, \Delta_i = \mathcal{O}(1)$. As the impurity charge Z does not enter the ion equation except in the collision term, where it does not alter the magnitude because C_{iz} is smaller than C_{ii} by a factor Z_{eff} , the ion problem is not affected by the new ordering, and thus the solution for the ion distribution function is the same as in the previous section. This implies in particular that all lowest-order ion quantities are flux functions and thus do not vary on the flux surface. In the impurity equation, however, the new ordering implies that collisions dominate the dynamics, whereas the term containing the parallel derivative of f_a drops to next order, and therefore the lowest order impurity equation becomes

$$C_z(f_z^{(0)}) = 0. \quad (4.16)$$

The solution to this homogeneous collision operator problem is a *perturbed Maxwellian*,

$$f_z^{(0)} = \left(\frac{p_z^{(0)}}{p_{z0}} + \frac{m_z}{T_z} v_{\parallel} V_{z\parallel}^{(1)} + \left(x_z^2 - \frac{5}{2} \right) \frac{T_z^{(1)}}{T_{z0}} \right) f_{z0}, \quad (4.17)$$

leaving the lowest order density $n_z^{(0)}$, temperature $T_z^{(0)}$ and parallel flow velocity $V_{z\parallel}^{(0)}$ free to vary on the flux surface as they are functions of θ and ϕ as well as ψ . Perturbed quantities are indicated by superscript indices whereas subscript indices symbolise the expansion in the conventional ordering $\delta_i \ll 1, \Delta_i \ll 1$. Quantities with a subscript 0 are always flux functions. However, (4.16) implies equal temperatures and flow velocities of all involved particle species, thereby making the lowest order impurity temperature a flux function, $T_z^{(0)} \approx T_{i0}(\psi)$, and the lowest order flow velocity vanishes since this has been shown in the previous section to hold for the ion flow velocity. Therefore, the first quantity to vary on the flux surface when the gradients get larger is the impurity density n_z . The variations of the impurity temperature and flow velocity are therefore one order smaller in δ_i than the density variation (without loss of generality or changing the structure of eq. (4.17), $f_z^{(0)}$ and $n_z^{(0)}$ can be understood to include

4.2. PFIRSCH-SCHLÜTER TRANSPORT IN THE PRESENCE OF LARGE GRADIENTS

the first order variations as well such as to formally keep the ordering valid in this notation). In next order in the impurity equation, parallel dynamics have to be included,

$$C_z(f_z^{(1)}) = v_{\parallel} \nabla_{\parallel} f_z^{(0)} + \frac{e_z}{T_z} v_{\parallel} \nabla_{\parallel} \phi^{(0)} f_z^{(0)}.$$

Due to the trace impurity assumption $Z_{\text{eff}} - 1 \ll 1$, the electrostatic potential is not influenced much by the varying impurity density and is therefore constant on flux surfaces to lowest order, so that the last term vanishes. In a theory where the impurity ions are more numerous, or the plasma is not in the high-collisional regime any more, the contributions from this term cannot be neglected and may lead to substantial changes in the solution, especially as the term contains the large factor Z . Again, for convenience, the quantity u defined by (4.1),

$$\nabla_{\parallel} u \equiv \frac{1}{p'_0} \nabla_{\parallel} \left(\frac{j_{0\parallel}}{B} \right) = \frac{2}{B^2} (\mathbf{b} \times \nabla \psi) \cdot \nabla \ln B,$$

is used frequently in the calculation.

Taking the particle moment of the impurity version of (4.15), one can exploit particle conservation to find

$$B \nabla_{\parallel} \left(\frac{n_z^{(0)} V_{z\parallel}^{(1)}}{B} \right) = - \frac{d\phi}{d\psi} \left(\frac{\mathbf{b} \times \nabla \psi}{B} \cdot \nabla n_z^{(0)} - B \nabla_{\parallel} u n_z^{(0)} \right),$$

where

$$\int v_{\parallel} \nabla_{\parallel} f_z^{(1)} d^3v = B \nabla_{\parallel} \left(\frac{n_z^{(0)} V_{z\parallel}^{(1)}}{B} \right)$$

as in the previous section and

$$\begin{aligned} \int \mathbf{v}_d \cdot \nabla f_z^{(0)} d^3v &= \frac{\mathbf{b} \times \nabla \psi}{B} \cdot \left[\frac{\nabla p_z^{(0)}}{T_{z0}} - \frac{n_{z0} \nabla T_z^{(1)}}{T_{z0}} \right] + \frac{\mathbf{b} \times \nabla \ln B}{\Omega_z} \cdot \nabla n_z^{(0)} v_{th,z}^2 \\ &+ 2 \frac{\mathbf{b} \times \nabla \ln B}{\Omega_z} \cdot \nabla \psi \int v_{\parallel}^2 \left(\frac{p_z^{(0)}}{p_{z0}} + \left(x_z^2 - \frac{5}{2} \right) \frac{T_z^{(1)}}{T_{z0}} \right) f_{z0} \left(A_{z1} + \left(x_z^2 - \frac{5}{2} \right) A_{z2} \right) d^3v \\ &\approx - \frac{d\phi}{d\psi} \left(\frac{\mathbf{b} \times \nabla \psi}{B} \cdot \nabla n_z^{(0)} - B \nabla_{\parallel} u n_z^{(0)} \right), \end{aligned}$$

4. ASPECTS OF IMPURITY TRANSPORT IN STELLARATORS

were used, keeping only the terms of leading order in Z . This equation contains the two unknown quantities $n_z^{(0)}$ and $V_z^{(1)}$, so another equation is needed. As these are the leading order contributions, the superscripts will be suppressed in the following, and the impurity density will be normalised to its flux-surface averaged value, i.e. $n_z \equiv n_z^{(0)}/\langle n_z^{(0)} \rangle$. The second condition can be obtained from the v_{\parallel} -moment of (4.15), which shows that the friction force is related to the impurity density variation via

$$\begin{aligned} \int m_z v_{\parallel} C_z(f_z^{(1)}) &= R_{zi_{\parallel}} = \int m_z v_{\parallel}^2 \nabla_{\parallel} f_z^{(0)} = \nabla_{\parallel} p_z^{(0)} \\ \Rightarrow \nabla_{\parallel} n_z &= -\frac{1}{T_i} R_{iz_{\parallel}}, \end{aligned}$$

where momentum conservation was employed for the last equation as it is easier to solve for the ion-impurity friction. In the trace impurity limit, the impurities do not affect the ion distribution function, and the resulting equation

$$C_{ii}(f_{i_1}) = v_{\parallel} f_{i_0} \left(A_{i_{1\parallel}} + \left(x_i^2 - \frac{5}{2} \right) A_{i_{2\parallel}} \right)$$

has been solved before [54] and has the solution

$$f_{i_1} = -\frac{2}{5} \frac{m_i}{p_i T_i} q_{i\parallel} v_{\parallel} f_{i_0} \left(L_1^{(3/2)}(x_i^2) - \frac{4}{15} L_2^{(3/2)}(x_i^2) \right) + \left(\frac{p_{i_1}}{p_{i_0}} + \frac{m_i}{T_i} v_{\parallel} V_{i\parallel} + \left(x_i^2 - \frac{5}{2} \right) \right) f_{i_0}.$$

This corresponds to the pure plasma solution of the problem treated in the previous section, leading to the following expressions for the ion flow velocity and heat flux,

$$\begin{aligned} n_i V_{i\parallel} &= n_i \frac{T_i}{e_i} A_{i_1} uB + K_i(\psi) B \\ \frac{q_{i\parallel}}{p_i} &= \frac{5}{2} \frac{T_i}{e_i} A_{i_2} \left(uB - \frac{B \langle uB^2 \rangle}{\langle B^2 \rangle} \right), \end{aligned}$$

where the integration constant $K_i(\psi)$ has been determined to be

$$\begin{aligned} K_i(\psi) = -\frac{T_i n_i}{e_i} \left((A_{i_1} + 1.82 A_{i_2}) \frac{\langle u(\nabla_{\parallel} B)^2 + 1/4 \nabla_{\parallel} u \nabla_{\parallel} B^2 \rangle}{\langle (\nabla_{\parallel} B)^2 \rangle} - 0.05 A_{i_2} \frac{\langle u(\nabla_{\parallel} B)^2 \rangle}{\langle (\nabla_{\parallel} B)^2 \rangle} \right. \\ \left. - 1.77 A_{i_2} \frac{\langle uB^2 \rangle}{\langle B^2 \rangle} \right). \end{aligned}$$

4.2. PFIRSCH-SCHLÜTER TRANSPORT IN THE PRESENCE OF LARGE GRADIENTS

As highly charged impurities are considered, the ion-impurity collision operator can be approximated by the disparate mass ratio operator from section 2.4,

$$C_{iz}(f_{i_1}) = \nu_{iz} \left(\mathcal{L}(f_{i_1}) + \frac{m_i}{T_i} v_{\parallel} V_{z_{\parallel}} f_{i_0} \right).$$

Inserting the solution for f_{i_1} yields

$$\begin{aligned} R_{zi_{\parallel}} &= - \int m_i v_{\parallel} C_{iz}(f_{i_1}) d^3v = \frac{4}{3\sqrt{\pi}} m_i n_i \hat{\nu}_{iz} \left(V_{i_{\parallel}} - V_{z_{\parallel}} - \frac{2}{5} \frac{q_{i_{\parallel}}}{p_i} \right) \\ &= \frac{4}{3\sqrt{\pi}} m_i n_i \left\langle \frac{\hat{\nu}_{iz}}{n_z} \right\rangle \left[\frac{T_i}{e_i} \left(\frac{d \ln p_i}{d\psi} + \frac{e_i}{T_i} \frac{d\phi}{d\psi} - \frac{d \ln T_i}{d\psi} \right) u B n_z \right. \\ &\quad \left. + \left(\frac{K_i(\psi)}{n_i} + \frac{d \ln T_i}{d\psi} \frac{\langle u B^2 \rangle}{\langle B^2 \rangle} \right) B n_z - V_{z_{\parallel}} n_z \right]. \end{aligned}$$

Here, $\nu_{iz} = \hat{\nu}_{iz}/x^3$. Introducing the notation

$$\begin{aligned} \tilde{v}(\psi) &\equiv \frac{4}{3\sqrt{\pi}} \frac{m_i n_i}{e_i} \left\langle \frac{\hat{\nu}_{iz}}{n_z} \right\rangle \\ K_i^*(\psi) &\equiv \frac{K_i(\psi)}{n_i} + \frac{d \ln T_i}{d\psi} \frac{\langle u B^2 \rangle}{\langle B^2 \rangle} \\ \gamma &\equiv u + (A_{i_1} - A_{i_2})^{-1} K_i^*(\psi), \end{aligned}$$

one obtains the two equations

$$\nabla_{\parallel} n_z = \tilde{v} \left((A_{i_1} - A_{i_2}) \gamma B n_z - n_z V_{z_{\parallel}} \right) \quad (4.18)$$

and

$$B \nabla_{\parallel} \left(\frac{n_z V_{z_{\parallel}}}{B} \right) = - \frac{d\phi}{d\psi} \left(\frac{\mathbf{b} \times \nabla \psi}{B} \cdot \nabla n_z - B n_z \nabla_{\parallel} \gamma \right). \quad (4.19)$$

Depending on the exact situation, it can be easier to solve a combination of these two first-order nonlinear (in n_z and $V_{z_{\parallel}}$) partial differential equations, resulting in the following second-

4. ASPECTS OF IMPURITY TRANSPORT IN STELLARATORS

order linear equation

$$B\nabla_{\parallel} \left((A_{i_1} - A_{i_2})\gamma n_z - \frac{1}{\tilde{v}} \frac{\nabla_{\parallel} n_z}{B} \right) = -\frac{d\phi}{d\psi} \left(\frac{\mathbf{b} \times \nabla\psi}{B} \cdot \nabla n_z - B n_z \nabla_{\parallel} \gamma \right). \quad (4.20)$$

Remark:

If the impurities are more numerous, they influence the ion solution as in the problem treated in the previous section; however, as the impurity density is no longer a flux function, it cannot be taken out of the flux surface average any more, and then the integration constant K_i becomes dependent on n_z via various flux surface averages of n_z with other functions. Consequently, the two-variable problem treated here has to be extended by a third nonlinear equation for K_i , and the problem becomes extremely complicated, far too complicated for any analytical solution.

4.2.2 Analytical limits

In general, it is not possible to solve eqs. (4.18) and (4.19), or alternatively (4.20), analytically, as they form a set of partial differential equations and the functions B and γ , although known in principle, do not have an analytical representation but are only available in numerical form. However, it is possible to gain some useful information on how the different terms affect the impurity redistribution by considering different limits, i.e. strong or weak radial gradients or radial electric field, which will be done in the subsequent sections.

Weak radial gradients

In the case of weak radial gradients, i.e. $d\phi/d\psi \ll 1$ and $A_{i_1} - A_{i_2} \ll 1$, eq. (4.19) yields

$$B\nabla_{\parallel} \left(\frac{n_z V_{z\parallel}}{B} \right) \ll \frac{n_z V_{z\parallel}}{L_{\parallel}},$$

which can easily be integrated up and leads to

$$V_{z\parallel} \approx \frac{B}{n_z} K_z(\psi).$$

The constant $K_z(\psi)$ can be determined from the constraint that $\langle B\nabla_{\parallel} n_z \rangle$ must vanish, and reads $K_z(\psi) = (A_{i_1} - A_{i_2}) \langle \gamma B^2 n_z \rangle / \langle B^2 \rangle$. The right-hand side of the remaining equation

for n_z ,

$$\nabla_{\parallel} n_z = \tilde{\nu}(A_{i1} - A_{i2}) \left(\gamma n_z B - B \frac{\langle \gamma B^2 n_z \rangle}{\langle B^2 \rangle} \right), \quad (4.21)$$

is small as well, and thus

$$\nabla_{\parallel} n_z \ll \frac{n_z}{L_{\parallel}}$$

with the solution $n_z \approx n_z(\psi)$. Thus, the conventional limit of weak gradients, leading to the densities being constant on flux surfaces, is correctly reproduced.

Large radial gradients, vanishing radial electric field

In the opposite limit of large gradients, (4.20) is still too complicated for an analytical treatment, but a very interesting and analytically tractable limit is the case of small radial electric field, $e_i/T_i d\phi/d\psi \ll d\ln n_i/d\psi$, in which the terms containing the perpendicular derivative become negligible and the partial differential equation simplifies to an ordinary one. Although this case would not occur in a realistic experimental equilibrium, where density gradient and radial electric potential tend to cancel each other (ion root operation) and are thus of comparable magnitude, it is nonetheless enlightening to study this case as it has the appealing property of mathematically resembling the tokamak case and giving some fundamental insight into the different mechanisms involved in the redistribution process. In this limit, the right-hand side of (4.19) is approximately equal to zero, and thus the impurity flow velocity can be calculated in terms of the impurity density, leading to eq. (4.21) as in the opposite limit. The solution to this equation depends fundamentally on the properties of the function γ , especially on whether γ has any zeroes. If this is not the case, the left-hand side of (4.21) is negligible due to the large multiplier $A_{i1} - A_{i2}$ on the right-hand side. The solution then becomes rather easy,

$$n_z \approx \left\langle \frac{1}{\gamma} \right\rangle^{-1} \frac{1}{\gamma}.$$

Employing the value for γ in the axisymmetric limit,

$$\gamma|_{axisym} = -\frac{I(\psi)}{B^2(1 + 2.77 d\ln T_i/d\psi)},$$

where $I(\psi)$ is the toroidal current, reproduces the tokamak result found in [60] correctly.

4. ASPECTS OF IMPURITY TRANSPORT IN STELLARATORS

However, if γ does have zeros, the problem is fundamentally different. As there are points at which the left-hand side vanishes whereas the right-hand side does not, it is not possible to neglect the parallel gradient in these regions, in which a boundary layer forms. The calculation for this case, based on the method of integrating factors and an expansion around the points where γ vanishes, is given in the following. The result is that, in the limit of very large gradients, the impurities become strongly localised around these zeros, an effect which can physically be understood by noticing that the friction force, which is the drive for the redistribution, is proportional to γ and thus vanishes as well at these points. Due to periodicity, there must exist points from where all impurity ions are carried away, but also points at which they accumulate. In the limit $A_{i_1} - A_{i_2} \rightarrow \infty$, the impurity density becomes a delta distribution at the accumulation points.

This situation can in principle also occur in a tokamak, but parametric dependencies of $\gamma|_{axisym}$ show that this is only possible if the radial temperature and density gradients have opposite signs, which is not the case for usual operation scenarios.

In Boozer coordinates (ψ, α, φ) , where the magnetic field can be represented as $B = \beta \nabla \psi + I \nabla \theta + J \nabla \varphi = \nabla \psi \times \nabla \alpha$ for some functions β, I, J (see section 2.7.2), the parallel gradient becomes

$$\nabla_{\parallel} = \frac{B}{\sqrt{g}} \frac{\partial}{\partial \varphi},$$

where $1/\sqrt{g}$ is the Jacobian, and (4.21) can be represented as

$$\frac{\partial n_z}{\partial \varphi} = h \left(\gamma n_z - \frac{\langle \gamma B^2 n_z \rangle}{\langle B^2 \rangle} \right)$$

with

$$h(\psi) \equiv \tilde{v}(A_{i_1} - A_{i_2}) \sqrt{g}/B^2 \gg 1.$$

Using the method of integrating factors, this can be solved to yield

$$n_z(\varphi) = e^{hf(\varphi)} \left[c - h \frac{\langle \gamma B^2 n_z \rangle}{\langle B^2 \rangle} \int_0^{\varphi} e^{-hf(\varphi')} d\varphi' \right]$$

where c is an integration constant and $f(\varphi) \equiv \int_0^{\varphi} \gamma(\varphi') d\varphi'$. Suppose $f'(\varphi) = \gamma(\varphi)$ has

4.2. PFIRSCH-SCHLÜTER TRANSPORT IN THE PRESENCE OF LARGE GRADIENTS

$2k$ zeros in $\varphi \in [0, 2\pi)$, whereof k maxima and k minima at $\varphi_0, \dots, \varphi_{2k-1}$. As, due to the exponential decay, most of the contribution to the integral comes from the area around the zeros, we can approximate

$$\int_0^\varphi e^{-hf(\varphi')} \approx \begin{cases} k \int_{\varphi_0-\varepsilon(k)}^{\varphi_0+\varepsilon(k)} e^{-hf(\varphi')} d\varphi' & \text{for } h < 0 \\ k \int_{\varphi_1-\varepsilon(k)}^{\varphi_1+\varepsilon(k)} e^{-hf(\varphi')} d\varphi' & \text{for } h > 0 \end{cases},$$

where, without loss of generality, φ_0 (φ_1) has been shifted to the origin. Replacing $f(\varphi)$ with its Taylor expansion around $\varphi_i, i \in \{0, 1\}$, and extending the range of integration again to $\varphi \in [0, 2\pi)$ leads to an expression involving an error function with the expansion parameter in the argument, and can therefore be approximated with its asymptotic limit for small values. Note that the integral always exists as always $hf''(\varphi_i) > 0$. The final result is

$$n_z(\varphi) = c^* e^{\int_0^\varphi \gamma d\varphi'} - hk \frac{\langle \gamma B^2 n_z \rangle}{\langle B^2 \rangle} \sqrt{\frac{\pi}{2h\gamma'(\varphi)}} e^{\int_{\varphi_i}^\varphi \gamma d\varphi'},$$

where c^* can be determined from the normalisation constraint $\langle n_z \rangle = 1$.

4.2.3 Numerical solution of the full problem

To study realistic scenarios, in which the pressure gradient and the radial electric field are of comparable magnitude and approximately cancel each other, one has to resort to a numerical solution of (4.20). This has been done via a Fourier decomposition using the MConf library, which has been developed for transport analyses in stellarators [62]. MConf uses Boozer coordinates, which have been introduced in section 2.7.2. In this set of coordinates, the parallel and radial derivatives can be represented as

$$\mathbf{B} \cdot \nabla = \frac{B^2}{\iota I + J} \left(\iota \frac{\partial}{\partial \theta} + \frac{\partial}{\partial \varphi} \right)$$

and

$$\mathbf{B} \times \nabla \psi \cdot \nabla = \frac{B^2}{\iota I + J} \left(J \frac{\partial}{\partial \theta} - I \frac{\partial}{\partial \varphi} \right).$$

4. ASPECTS OF IMPURITY TRANSPORT IN STELLARATORS

For numerical reasons, it is convenient to use $w = n/B^2$ as a variable instead of $n \equiv n_z/\langle n_z \rangle$, for then

$$\frac{\int \int w d\varphi d\theta}{\int \int 1/B^2 d\varphi d\theta} = \langle n \rangle = 1.$$

In order to relate the magnitude of the radial electric field to the magnitude of the radial density gradient, the quantity

$$\mu \equiv \frac{e_i}{T_i} \frac{d\phi/d\psi}{A_{i_1} - A_{i_2}}$$

is used as a control parameter for the radial electric field instead of $d\phi/d\psi$ itself. Eq. (4.20) can then be rewritten in Boozer coordinates as

$$\left(\iota \frac{\partial}{\partial \theta} + \frac{\partial}{\partial \varphi} \right)^2 w + g(\theta, \varphi, \psi) \frac{\partial w}{\partial \theta} + h(\theta, \varphi, \psi) \frac{\partial w}{\partial \varphi} + f(\theta, \varphi, \psi) w = 0, \quad (4.22)$$

where

$$\begin{aligned} g(\theta, \varphi, \psi) &= 4\iota \frac{\partial \ln B}{\partial \alpha} - \tilde{v}(\iota I + J)(A_{i_1} - A_{i_2}) \left(\iota \gamma + \mu \frac{J}{B^2} \right) \\ h(\theta, \varphi, \psi) &= 4 \frac{\partial \ln B}{\partial \alpha} - \tilde{v}(\iota I + J)(A_{i_1} - A_{i_2}) \left(\gamma - \mu \frac{I}{B^2} \right) \\ f(\theta, \varphi, \psi) &= 2 \left(\left(\frac{\partial \ln B}{\partial \alpha} \right)^2 + \frac{1}{B} \frac{\partial^2 B}{\partial \alpha^2} \right) - \tilde{v}(\iota I + J)(A_{i_1} - A_{i_2}) \left(\frac{2\gamma}{B} \frac{\partial B}{\partial \alpha} + \frac{\partial \gamma}{\partial \alpha} \right) \end{aligned}$$

and $\partial/\partial\alpha \equiv \iota\partial/\partial\theta + \partial/\partial\varphi$. Note that

$$g = \underbrace{\iota h - \frac{\mu}{B^2} (\iota I + J)^2 \tilde{v} (A_{i_1} - A_{i_2})}_{\text{normally } \neq 0},$$

and therefore, away from rational flux surfaces (i.e., surfaces on which ι has a rational value), it cannot happen that the coefficients g and h vanish simultaneously. After a decomposition in Fourier components, eq. (4.22) has the form

$$-(\iota k + l)^2 w_{kl} + \sum_{m',n'} (i(k-m')g_{m'n'} + (l-n')h_{m'n'} + f_{m'n'}) w_{k-m',l-n'} = 0.$$

4.2. PFIRSCH-SCHLÜTER TRANSPORT IN THE PRESENCE OF LARGE GRADIENTS

If a solution to this problem is to exist, the resulting matrix must be (and is) singular; one obtains a unique solution by adding the normalisation constraint

$$w_{00} - (\iota k + l)^2 w_{kl} + \sum_{m'n'} (i(k - m')g_{m'n'} + (l - n')h_{m'n'} + f_{m'n'}) w_{k-m',l-n'} = b_{00},$$

where b_{mn} are the Fourier coefficients of $1/B^2$. The matrix problem was implemented with two different matrix solvers, one direct one and one iterative one, yielding the same results. In the simulations, the Fourier series was typically truncated after 54 components. With the numerical data provided by a configuration data bank created for use in international collaborations (*IEA Implementing Agreement for Cooperation in Development of the Stellarator Concept*), it is possible to study the redistribution process in different devices. Fig. 4.1 shows the results for W7-AS for different values of $\tilde{v}(A_{i1} - A_{i2})a^2$, where a is the average minor radius. The values for the plasma parameters were chosen to match experimental values found in W7-AS during H-mode operation. For a bulk ion density of $5 \cdot 10^{19} - 1 \cdot 10^{20}$, a bulk ion temperature of 100 eV and a radial density scale length of 2cm in the pedestal, realistic values for $\tilde{v}(A_{i1} - A_{i2})a^2$ lie between 0.01, corresponding to weak gradients, and 10 for very large gradients and high impurity charge. As an upper limit and to show what happens qualitatively in the limit of very large gradients and very high impurity charge, values of up to 100 have been included in the simulation. The ratio between the radial temperature and density gradients was set $T'/n' = 2$, and μ was chosen accordingly to make A_{i1} vanish, which corresponds to ion-root operation. The flux surface was chosen to be $s = 0.9$, where s is the magnetic flux normalised to the flux at the separatrix. As visible from fig. 4.1, for weak radial gradients the impurity density is nearly constant on the flux surface, and thus the limit of conventional theory is correctly recovered. A slight in-out asymmetry shows, with the impurities accumulating at the inboard side of the torus, but the overall density variation is moderate with only 5% variation. When the gradients get larger, the impurities accumulate at a certain toroidal angle, the more the larger the gradients get. In the limit of very large gradients, the distribution function approaches a delta distribution at these points. When looking at the pattern of the function γ for these plasma parameters, one finds that γ crosses zero, and thus points of vanishing friction force exist, which explains the very strong accumulation of the impurities (hereafter referred to as “strong localisation”). In fig. 4.2, the corresponding radial impurity flux is plotted as a function of the largeness of the gradients. It is easy to show that, in leading order, the particle flux across the field is still given by

$$\langle \mathbf{\Gamma}_z \cdot \nabla \psi \rangle = \frac{1}{e_z} \left\langle u B R_{z\parallel} \right\rangle,$$

even when the impurity density is no longer a flux function. In comparison with a conventional calculation, where the flux increases linearly with increasing gradients, it is reduced due to

4. ASPECTS OF IMPURITY TRANSPORT IN STELLARATORS

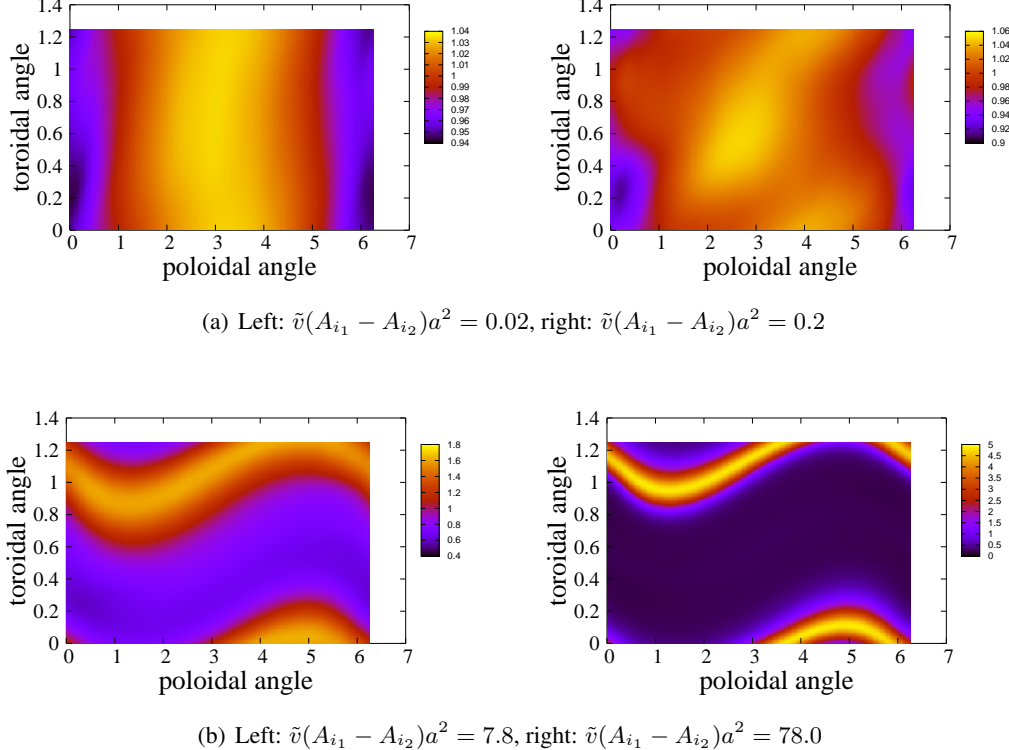


FIGURE 4.1 Normalised impurity density in W7-AS for different magnitude of the radial gradients.

the redistribution. However, even for extreme values of $\tilde{v}(A_{i_1} - A_{i_2})a^2$, the flux is still a monotonically increasing function of the gradients.

Qualitatively different results are obtained for W7-X and LHD. Since the order of magnitude of the radial gradients in these devices can be expected to be comparable to that found in W7-AS, the same range of simulation parameters should be appropriate. In this parameter regime, one finds that in both devices γ does not have any zeros. The impurity accumulation is thus not as strong as in W7-AS, leading to up to 15% density variation in W7-X and to up to 30% in LHD as shown in figs. 4.3 and 4.4, again for different radial gradients. The patterns of the redistribution show some similarity, with two regions of accumulation separated by elongated regions with reduced density. The corresponding impurity fluxes are shown in fig. 4.5. Interestingly, although the density variation is much smaller than in W7-AS, the effect on the radial transport is much more pronounced, leading to a considerable reduction of the impurity flux and thus making it a non-monotonic function of the magnitude of the radial gradients. In LHD, the flux is reversed from inward to outward for very large gradients.

4.2. PFIRSCH-SCHLÜTER TRANSPORT IN THE PRESENCE OF LARGE GRADIENTS

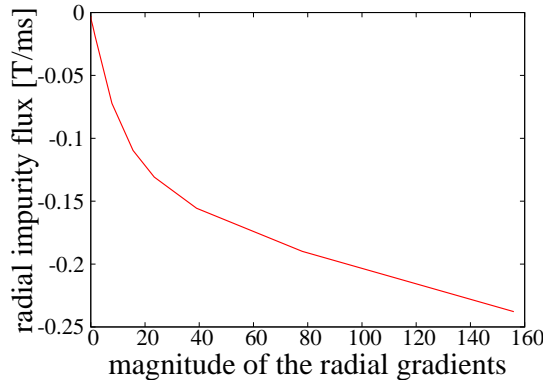


FIGURE 4.2 Impurity flux in W7-AS for $T'/n' = 2$, $\mu = 1.5$.

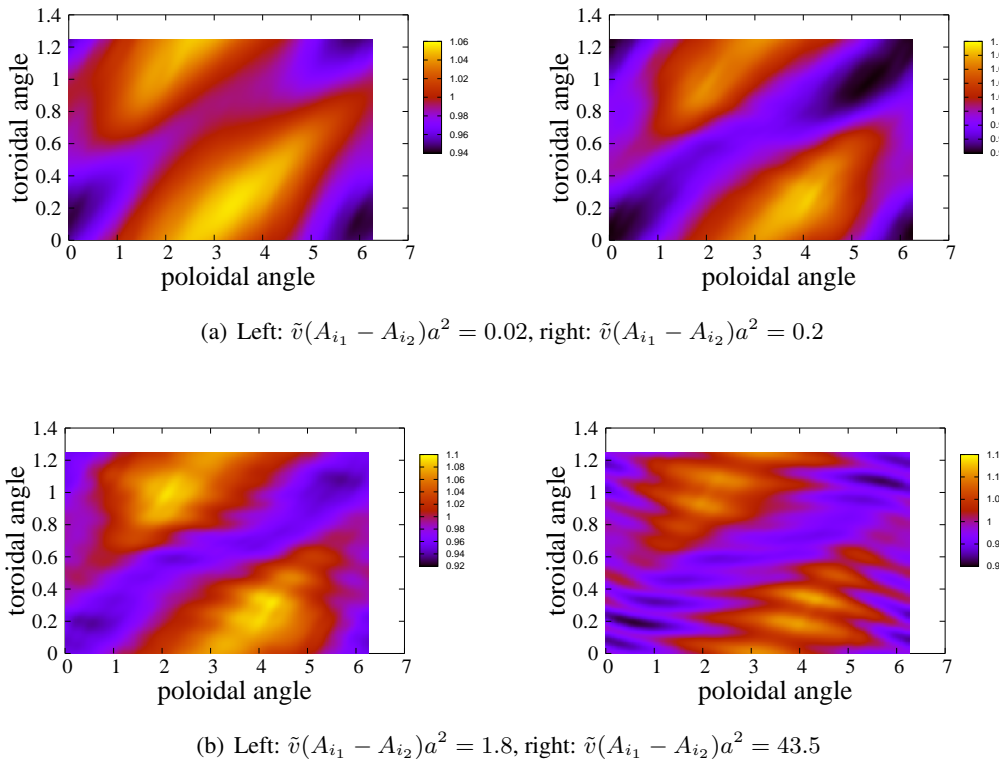


FIGURE 4.3 Normalised impurity density in W7-X for different magnitude of the radial gradients.

4. ASPECTS OF IMPURITY TRANSPORT IN STELLARATORS

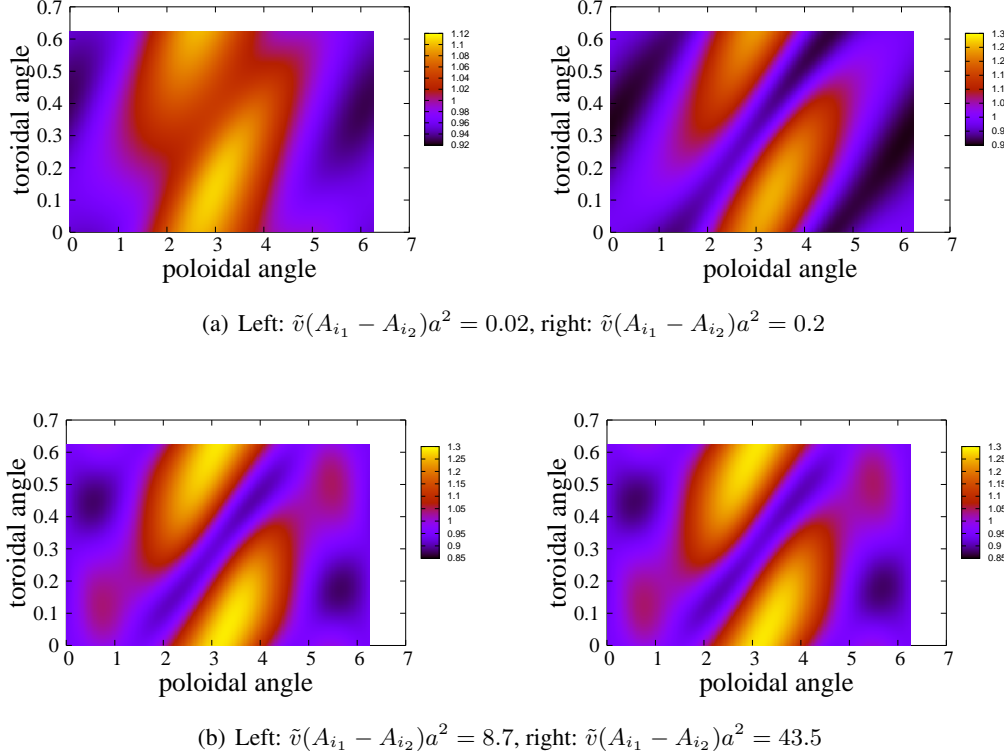


FIGURE 4.4 Normalised impurity density in LHD for different magnitude of the radial gradients.

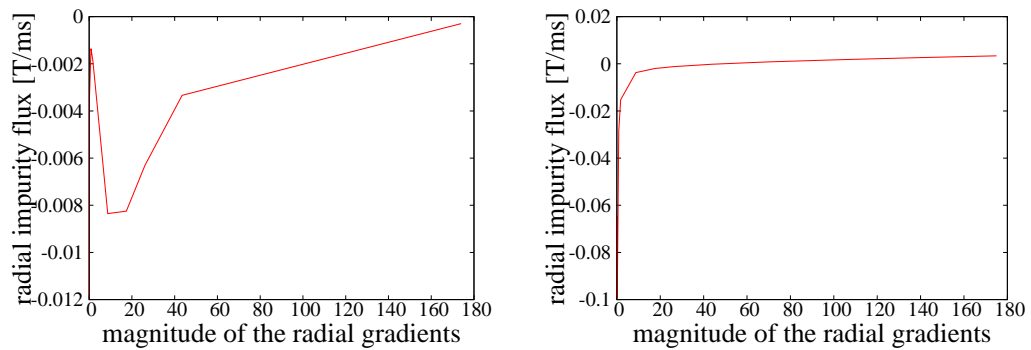


FIGURE 4.5 Impurity fluxes for $T'/n' = 2$, $\mu = 1.5$; left: W7-X, right: LHD.

4.2. PFIRSCH-SCHLÜTER TRANSPORT IN THE PRESENCE OF LARGE GRADIENTS

Running the code for tokamak devices leads to the results found previously of impurity density peaking on the high-field side of the torus [60], with an overall variation between 10–30%, depending mainly on the aspect ratio of the device.

From both simulations and the analytic formulas, it is obvious that the drive of the redistribution is parallel friction between the bulk ions and the impurities, as in a tokamak. However, the way in which the impurities are redistributed is qualitatively influenced by, on the one hand, the radial ion temperature gradient, and, on the other hand, the radial electric field, which does not play a role in axisymmetric configurations. The effect of the radial temperature gradient comes from its entering the constant $K_i^*(\psi)$. Thereby, it influences the magnitude and possibly even the sign of the friction force, which has a large impact on the redistribution if γ is modified from being entirely positive (negative) to a state where both signs occur. The radial electric field influences the redistribution in two different ways. Since it also enters the constant $K_i^*(\psi)$, it can directly influence the friction force in this way. Additionally, it drives an $\mathbf{E} \times \mathbf{B}$ rotation, which varies on the flux surface and thereby changes the pattern of the redistribution. Therefore, the dependence of the impurity density on the radial electric field is rather complicated and analytically not tractable.

However, the numerical results suggest that, even when a radial electric field is included, the impurity redistribution and consequently also the radial particle transport are strongly affected by whether or not γ , which is proportional to the friction force, has zeros. If this is not the case, the density variations are moderate. The exact redistribution pattern depends on the magnetic geometry of the device. Regarding the radial impurity transport, as long as the gradients are weak, the relation between the gradients and the radial impurity flux is approximately linear. When the gradients get larger, the impurities are redistributed in such a way that they experience less friction. Therefore, the radial flux is reduced and becomes very small for large gradients. Mathematically, this is manifested by the fact that the left-hand side of (4.21), which is proportional to the friction force and thus to the particle flux, becomes negligible when the gradients are large enough.

If γ has zeros, the friction force vanishes at certain points and drives the impurity distribution function towards a delta distribution at “half” the zeros, namely, at those towards which the friction force is directed. If the radial electric field is strong, this process can be counteracted by the $\mathbf{E} \times \mathbf{B}$ rotation, which carries the impurities away from these points. However, in the simulation for W7-AS, the ambipolar electric field seems to be too weak so that friction is the dominant process and strong accumulation occurs. Although the redistribution slightly reduces the friction force, since the impurity flux now increases less rapidly than linear with increasing magnitude of the radial gradients, it is still a monotonic function. Unlike the case when γ does not have any zeros, there exist regions where the left-hand side of (4.21) is not negligible (namely, where γ vanishes). Thus, the radial flux cannot become as small as in the cases when γ does not have any zeros. Again, whether or not this is the case depends on the magnetic geometry.

4. ASPECTS OF IMPURITY TRANSPORT IN STELLARATORS

4.2.4 Discussion

A possible objection against the applicability of the theory is that both particle species were assumed to be in the Pfirsch-Schlüter regime, which, at least for the bulk ions, is not realistic in a fusion plasma. Unfortunately, in a stellarator, this regime is the only one where a completely analytic theory is possible. However, for the main aspects of the theory to be valid, only the impurities need be collisional, which is a much more realistic assumption. The ion distribution function enters the calculation only through the friction force, and could in principle be calculated numerically in a less collisional regime and then substituted into the equation for the friction. Whether this affects the redistribution in a qualitative way remains to be seen. In principle, it should not be difficult to detect the redistribution experimentally with the appropriate diagnostics. In the tokamak case, impurity accumulation at the high-field side was found experimentally in various devices, with even higher absolute density variation than predicted by the theory. During the operation of W7-AS, no such redistribution was found, but one has to keep in mind that there was no attempt to find such an effect, and there might also be some question as to whether the diagnostics available would have been sensitive enough to resolve density variations within a flux surface. Currently operating smaller experiments, such as WEGA or TJ-K, have the intrinsic problem that the achieved maximum temperatures are far too low to get a high enough ionisation level of the impurities (they cannot achieve much more than $Z = 2$ or $Z = 3$). At LHD, no attempts in this direction appear to have been performed, either.

4.2.5 Conclusions & Summary of section 4.2

The presence of large gradients in the plasma edge region has a significant influence on heavy impurity ions. Their density develops variations within the flux surface of the order of up to 10–100%, depending on the device. The effect is qualitatively different from that previously found in tokamaks as the radial electric plays a major role in the redistribution process, on the one hand by driving a non-constant (on the flux surface) $\mathbf{E} \times \mathbf{B}$ flow, which may carry particles away from regions of accumulation, and on the other hand by influencing the magnitude and even the sign of the friction force, which is the driving mechanism for the redistribution. The exact pattern of the impurity density on the flux surface depends sensitively on the exact geometry of the device. A crucial aspect for the redistribution process is whether there exist points at which the friction force vanishes. If this is the case, the redistribution can become much more strongly pronounced than otherwise. The radial impurity transport is greatly affected by the redistribution. Whereas it becomes very small when the gradients are large if there are no such points, it might still be a monotonically increasing function of the radial gradients when such points do exist, as in W7-AS, although the flux is still reduced in comparison with a situation without impurity redistribution. Apart from the effects due to the radial electric field, the main difference between tokamaks and stellarators with respect to impurity

4.2. PFIRSCH-SCHLÜTER TRANSPORT IN THE PRESENCE OF LARGE GRADIENTS

redistribution is the occurrence of strong localisation and the corresponding consequences for the transport. In tokamaks, this is in principle also possible, but only if the radial density and temperature gradients have opposite signs, which is usually not the case. The numerical solution of the full impurity density differential equation reproduces the analytical limits correctly, but a comparison with experimental results is lacking, due to reasons discussed in section 4.2.4.

4. ASPECTS OF IMPURITY TRANSPORT IN STELLARATORS

5 Summary & Outlook

Several problems arising in the context of impurities in fusion plasmas have been studied in this thesis. The first one, described in section 3.1, concerns the effect of highly charged impurities on collisional zonal-flow damping. It is shown that the presence of such impurities speeds up the damping of the flows by a factor exceeding Z_{eff} due to an enhancement of the effective bulk ion collision frequency in combination with a more subtle geometric effect. Because the damping is caused by friction between trapped and passing particles, it is dependent on the fraction of trapped particles and thereby on the geometric properties of the device. However, since the impurities collide on a much faster time scale than the bulk ions do, impurity self-collisions effectively slow down the passing impurity population very quickly on the ion collision time scale, and therefore the ions experience friction against the *whole* - trapped and passing - impurity population once this has come to rest. This mechanism explains the enhancement of the damping when heavy impurities are present, which is more pronounced in large-aspect-ratio devices where the fraction of trapped particles is generally lower than at tighter aspect ratio. Another application of these results is related to the question of how quickly the plasma reacts to sudden changes of the pressure profile, which is of particular interest in connection with the LH-transition. Since the mathematical structure of the resulting equations is exactly the same as in the problem studied in connection with the zonal flows, the time scale on which a new equilibrium is established corresponds to the zonal flow damping time (3.11).

In section 3.2, the effect of impurities on ITG-mode turbulence is studied. The resulting quasilinear impurity flux is found to decrease with increasing impurity charge and to increase with increasing Z_{eff} . Depending on the radial impurity density scale length, the flux changes sign from inward to outward at a critical a/Ln_z , which is dependent on the simulation parameters but rather insensitive to Z and Z_{eff} . Regarding the stability of the underlying ITG mode, an increase of the impurity density tends to have a stabilising effect by reducing both the growth rate and the frequency of the mode. The impurity charge plays only a minor role in this process. However, the impurity charge does have an influence on the stability boundary, where the growth rate vanishes. For heavier impurities ($Z \gtrsim 10$), the impurity contribution to the dispersion relation becomes negligible compared with the bulk ion one, and the resulting stability boundary is similar to that in a pure plasma. For lighter species, such as, e.g., carbon or helium, the situation is different as the bulk ion and impurity contributions become comparable, and the critical value of a/Ln_z is shifted upward considerably with rising impurity charge.

5. SUMMARY & OUTLOOK

The subsequent two stellarator problems addressed in chapter 4 are concerned with neoclassical impurity transport. In the first part (section 4.1), the Pfirsch-Schlüter transport of a species of heavy, highly charged impurities is calculated. Stellarator neoclassical transport is qualitatively different from tokamak transport due to the occurrence of a term related to pressure anisotropy in addition to the friction term, which is also present in the tokamak. Although the anisotropy term is found to be much smaller than the friction term, both in an ordering of the smallness of the mean free path and an expansion in the impurity charge, it is nonetheless important since it is not ambipolar, in contrast to the friction contribution. Therefore, it sets the value of the ambipolar electric field. The impurity pressure anisotropy itself is negligible in this context, but impurities influence this mechanism by changing the bulk ion pressure anisotropy via ion-impurity collisions. The fact that the pressure anisotropy term becomes small in the Pfirsch-Schlüter regime might be of importance for previous results showing that the radial electric field is set by neoclassical effects rather than turbulence since the ensuing flows are ambipolar to lowest order.

Finally, section 4.2 is based on these calculations and addresses the topic of impurity redistribution on the flux surface in the presence of large radial gradients. It is shown that the redistribution is driven by parallel friction between the bulk ions and the impurities, and the pattern of the redistribution is qualitatively influenced by the radial ion temperature gradient and the radial electric field. The exact way in which they do so is rather complicated.

In principle, two different situations can occur, characterised by whether or not there are points at which the friction force vanishes. If there are, the impurities start accumulating at these friction-free points if the $\mathbf{E} \times \mathbf{B}$ rotation due to the radial electric field is not sufficiently strong to counteract this mechanism. If no such points exist, the redistribution is less pronounced and is typically of the order of 10–30% of the overall density in the magnetic configurations studied here. In the cases where the friction force is non-zero everywhere, the transport is strongly reduced in comparison with that from conventional neoclassical theory. The impurity flux even becomes a non-monotonic function of the magnitude of the radial gradients, initially increasing with increasing gradients but then falling again to very small values. In the case where impurities accumulate at the zeros of the friction force, the transport is also reduced compared with the predictions of conventional theory, but to a lesser extent. Even for very large gradients, the transport is still a monotonically increasing function of the radial gradients.

The main restriction of this theory is the assumption of both the impurities and the bulk ions being in the collisional Pfirsch-Schlüter regime. Whereas this is often true for heavy impurities in the plasma edge region, the bulk ions are usually much less collisional. However, the main points of the theory remain valid if only the impurities are collisional. The bulk ion distribution must then be calculated by other means. Whereas analytical calculations of the distribution functions are in stellarators restricted to the Pfirsch-Schlüter regime (hence the assumption of collisional bulk ions), it is in principle not a problem to obtain them from numerical simulations for much lower collisionality. Implementing such numerical ion dis-

tribution functions in the theory, thereby making it applicable for a much broader range of experimentally relevant parameters, may be the content of future work.

Bibliography

- [1] K. R. Lang. *Astrophysical Formulae*, volume 2. Springer-Verlag Berlin Heidelberg New York, 3rd edition, 1999.
- [2] U. Schumacher. *Fusionsforschung - Eine Einführung*. Wissenschaftliche Buchgesellschaft Darmstadt, 1993.
- [3] P. Helander and D. J. Sigmar. *Collisional Transport in Magnetized Plasmas*. Cambridge University Press, 2002.
- [4] H. W. Müller and M. Hirsch. Script: IPP Summer University for Plasma Physics, 2007.
- [5] F. Wagner. Regime of Improved Confinement and High Beta in Neutral-Beam-Heated Divertor Discharges of the ASDEX Tokamak. *Phys. Rev. Lett.*, 49:1408, 1982.
- [6] J. Wesson. *Tokamaks*. Oxford Science Publications, 3rd edition, 2004.
- [7] J. Sánchez et al. Confinement transitions in TJ-II under Li-coated wall conditions. *Nucl. Fusion*, 49:104018, 2009.
- [8] F. Wagner. A quarter-century of H-mode studies. *Plasma Phys. Contr. Fusion*, 49:B1, 2007.
- [9] A. H. Boozer. Physics of magnetically confined plasmas. *Rev. Mod. Phys.*, 76:000, 2004.
- [10] P. H. Diamond, S.-I. Itoh, K. Itoh, and T. S. Hahm. Zonal flows in plasma - a review. *Plasma Phys. Contr. Fusion*, 47:R35–R161, 2005.
- [11] Z. Lin, T. S. Hahm, W. W. Lee, W. M. Tang, and R. B. White. Gyrokinetic simulations in general geometry and applications to collisional damping of zonal flows. *Physics of Plasmas*, 7:5, 2000.
- [12] P. H. Diamond, S-I. Itoh, K. Itoh, and T. S. Hahm. Zonal flows in plasma - a review. *Plasma Phys. Control. Fusion*, 47:R35–R161, 2005.
- [13] L. D. Landau. On the vibrations of the electronic plasma. *J. Physics, USSR*, 10:25, 1946.
- [14] J. B. Taylor. Diffusion of Plasma Ions across a Magnetic Field. *Phys. Fluids*, 4:1142, 1961.

- [15] E. A. Belli and J. Candy. Kinetic calculation of neoclassical transport including self-consistent electron and impurity dynamics. *Plasma Phys. Control. Fusion*, 50:095010, 2008.
- [16] R. G. Littlejohn. Variational principles of guiding centre motion. *J. Plasma Phys.*, 29:111–125, 1983.
- [17] J. W. Connor, R. J. Hastie, and J. B. Taylor. Stability of general plasma equilibria, III. *Plasma Physics*, 22:757, 1980.
- [18] J. W. Connor, R. J. Hastie, and J. B. Taylor. High Mode Number Stability of an Axisymmetric Toroidal Plasma. *Proc. R. Soc. Lon. A*, 1:365, 1979.
- [19] R. D. Hazeltine and J. D. Meiss. *Plasma confinement*. Dover Publications, Inc., Mineola, New York, 2003.
- [20] F. Romanelli and S. Briguglio. Toroidal semicollisional microinstabilities and anomalous electron and ion transport. *Phys. Fluids B*, 2:754, 1990.
- [21] T. S. Hahm. Nonlinear gyrokinetic equations for tokamak microturbulence. *Phys. Fluids*, 31:2670, 1988.
- [22] J. W. Connor. The neo-classical transport theory of a plasma with multiple ion species. *Plasma Physics*, 15:765, 1973.
- [23] S. Chapman and T. G. Cowling. *The Mathematical Theory of Non-Uniform Gases*. Cambridge University Press, 3rd edition, 1970.
- [24] S. Chapman. The Kinetic Theory of Simple and Composite Monatomic Gases: Viscosity, Thermal Conduction, and Diffusion. *Proc. R. Soc. Lond. A*, 93:1, 1916.
- [25] D. Enskog. *Kinetische Theorie der Vorgänge in mäßig verdünnten Gasen*. (Almqvist & Wiksell, Uppsala, 1917), Inaugural dissertation, Uppsala University; Arkiv för matematik, astronomi och fysik, 1916.
- [26] S. I. Braginskii. Transport properties in a plasma. *Rev. Plasma Phys.*, 1:205, 1965.
- [27] P. Helander and A. N. Simakov. Intrinsic Ambipolarity and Rotation in Stellarators. *Phys. Rev. Lett.*, 101:145003, 2008.
- [28] S. Braun, P. Helander, E. A. Belli, and J. Candy. Effect of impurities on collisional zonal flow damping in tokamaks. *Plasma Phys. Contr. Fusion*, 51:065011, 2009.
- [29] M. N. Rosenbluth and F. L. Hinton. Poloidal Flow Driven by Ion-Temperature-Gradient Turbulence in Tokamaks. *Phys. Rev. Lett.*, 80:724–727, 1998.

- [30] A. M. Dimits, T. J. Williams, J. A. Byers, and B. I. Cohen. Scalings of Ion-Temperature-Gradient-Driven Anomalous Transport in Tokamaks. *Phys. Review Letters*, 77:71–74, 1996.
- [31] G. W. Hammett, M. A. Beer, W. Dorland, S. C. Cowley, and S. A. Smith. Developments in the gyrofluid approach to Tokamak turbulence simulations. *Plasma Phys. Control. Fusion*, 35:973–985, 1993.
- [32] R. E. Waltz, G. D. Kerbel, and J. Milovich. Toroidal gyro-Landau fluid model simulations in a nonlinear ballooning mode representation with radial modes. *Physics of Plasmas*, 1:2229–2244, 1994.
- [33] F. L. Hinton and M. N. Rosenbluth. Dynamics of axisymmetric ($E \times B$) and poloidal flows in tokamaks. *Plasma Phys. Control. Fusion*, 41:A653–A662, 1999.
- [34] Y. Xiao, P. J. Catto, and K. Molvig. Collisional damping for ion temperature gradient mode driven zonal flow. *Physics of Plasmas*, 14:032302, 2007.
- [35] C. T. Hsu, P. J. Catto, and D. J. Sigmar. Neoclassical transport of isotropic fast ions. *Physics of Fluids B2*, 2:0899–8221/90/020280–11, 1990.
- [36] S. P. Hirshman and D. J. Sigmar. Neoclassical transport of impurities in tokamak plasmas. *Nucl. Fusion*, 21:1079, 1981.
- [37] S. P. Hirshman and D. J. Sigmar. Approximate Fokker-Planck collision operator for transport theory applications. *Phys. Fluids*, 19:1532–1540, 1976.
- [38] F. L. Hinton. Collisional transport in plasma. In *Basic Plasma Physics*, volume 1. North-Holland Publishing Company, 1983.
- [39] T. Fülöp, S. Braun, and I. Pusztai. Impurity transport driven by ion temperature gradient turbulence in tokamak plasmas, accepted for publication. *Phys. Plasmas*, 17:000, 2010.
- [40] C. Estrada-Mila, J. Candy, and R. E. Waltz. Gyrokinetic simulations of ion and impurity transport. *Phys. Plasmas*, 12:022305, 2005.
- [41] C. Angioni and A. G. Peeters. Direction of Impurity Pinch and Auxiliary Heating in Tokamak Plasmas. *Phys. Rev. Lett.*, 96:095003–1, 2006.
- [42] C. Angioni et al. Gyrokinetic simulations of impurity, He ash and α particle transport and consequences on ITER transport modelling. *Nucl. Fusion*, 49:055013, 2009.
- [43] R. Guirlet et al. Parametric dependences of impurity transport in tokamaks. *Plasma Phys. Control. Fusion*, 48:B63–B74, 2006.

- [44] N. Dubuit, X. Garbet, T. Parisot, R. Guirlet, and C. Bourdelle. Fluid simulations of turbulent impurity transport. *Phys. Plasmas*, 14:042301, 2007.
- [45] T. Hein and C. Angioni. Electromagnetic effects on trace impurity transport in tokamak plasmas. *Phys. Plasmas*, 17:012307, 2010.
- [46] H. Nordmann, T. Fülöp, J. Candy, P. Strand, and J. Weiland. Influence of magnetic shear on impurity transport. *Phys. Plasmas*, 14:052303, 2007.
- [47] A. Casati et al. Validating a quasi-linear transport model versus nonlinear simulations . *Nucl. Fusion*, 49:085012, 2009.
- [48] J. Candy and R. E. Waltz. An Eulerian gyrokinetic Maxwell solver. *J. Comput. Phys.*, 186:545, 2003.
- [49] I. Pusztai, T. Fülöp, J. Candy, and J. R. Hastie. Collisional model of quasilinear transport driven by toroidal electrostatic ion temperature gradient modes. *Phys. Plasmas*, 16:072305, 2009.
- [50] T. Fülöp and H. Nordman. Turbulent and neoclassical impurity transport in tokamak plasmas. *Phys. Plasmas*, 16:032306, 2009.
- [51] K. C. Shaing and J. D. Callen. Neoclassical flows and transport in nonaxisymmetric toroidal plasmas. *Phys. Fluids*, 26:3315, 1983.
- [52] M. Coronado and H. Wobig. The ambipolar electric field and neoclassical heat and particle flows in nonaxisymmetric toroidal multispecies plasmas with sources. *Phys. Fluids*, 30:3171, 1987.
- [53] R. D. Hazeltine and F. L. Hinton. Collision-dominated plasma transport in toroidal confinement systems. *Phys. Fluids*, 16:1883, 1973.
- [54] A. N. Simakov and Helander. Neoclassical momentum transport in a collisional stellarator and a rippled tokamak. *Phys. Plasmas*, 16:042503, 2009.
- [55] P. Helander. On rapid plasma rotation. *Phys. Plasmas*, 14:104501, 2007.
- [56] R. D. Hazeltine. Rotation of a toroidally confined, collisional plasma. *Phys. Fluids*, 17:961, 1974.
- [57] S. I. Braginskii. Transport phenomena in a completely ionized two-temperature plasma. *Sov. Phys. JETP*, 6:358, 1958.
- [58] H. Sugama, M. Okamoto, W. Horton, and H. Wakatani. Transport processes and entropy production in toroidal plasmas with gyrokinetic electromagnetic turbulence. *Phys. Plasmas*, 3:2379, 1996.

- [59] P. Helander and A. N. Simakov. Gyrokinetic theory of rotation in Stellarators, accepted for publication. *Contr. Plasma Phys.*, 0:0000, 2010.
- [60] T. Fülöp and P. Helander. Nonlinear neoclassical transport in toroidal edge plasmas. *Phys. Plasmas*, 8:3305, 2001.
- [61] P. Helander. Bifurcated neoclassical particle transport. *Phys. Plasmas*, 5:3999, 1998.
- [62] Y. Turkin, H. Maaßberg, C. D. Beidler, J. Geiger, and N. B. Marushchenko. Current control by ECCD for W7-X. *Fusion Science and Technology*, 50:387, 2006.

List of Figures

1.1	Schematic sketch of the plasma and coils of a tokamak.	3
1.2	Plasma and non-planar coils of the future stellarator W7-X.	4
1.3	Nested flux surfaces plus separatrix and scrape-off layer in a tokamak.	5
1.4	Magnetic island formation in a stellarator.	5
1.5	Illustration of the geometric quantities.	6
1.6	Evolution of the electron density profile during L-H transition in TJ-II.	7
1.7	Trapped and passing orbits in a tokamak.	11
1.8	Neoclassical diffusion coefficient vs. collisionality in a tokamak.	13
1.9	Neoclassical diffusion coefficient vs. normalised collision frequency in a stellarator.	14
1.10	GYRO simulation of zonal flows.	16
3.1	PIC simulation (EUTERPE) of the collisionless pure-plasma potential response.	43
3.2	Damping time: interpolation formula and exact solution.	65
3.3	Normalised damping time vs. effective charge.	66
3.4	Normalised damping time vs. ν_{*i}	66
3.5	Normalised damping time vs. ϵ	68
3.6	Normalised impurity flux vs. impurity charge and effective charge.	82
3.7	Normalised impurity flux vs. inverse radial impurity density gradient.	83
3.8	Normalised mode frequency and critical ion temperature gradient vs. impurity charge and effective charge.	85
3.9	Normalised mode frequency and growth rate vs. impurity charge and effective charge.	86
4.1	Normalised impurity density in W7-AS for different magnitude of the radial gradients.	118
4.2	Impurity flux in W7-AS.	119
4.3	Normalised impurity density in W7-X for different magnitude of the radial gradients.	119
4.4	Normalised impurity density in LHD for different magnitude of the radial gradients.	120
4.5	Impurity fluxes in W7-X and LHD.	120

List of Symbols

α	pitch angle; Boozer angle (chapter 4)
α_c	critical pitch angle
α_{a_j}, α_0	coefficient of the distribution function
\bar{A}	gyroaverage of the quantity A
β_n	normalisation constant of the eigenvalue problem in section 3.1
β_{a_j}, β_0	coefficient of the distribution function
χ_n	n'th eigenvalue of the eigenvalue problem in section 3.1
Δ_a	ratio between the collision frequency and the gyrofrequency; expansion parameter
δ_a	ratio of the Larmor radius to the macroscopic scale length
Δ_{aa}	expansion parameter
δ_{ij}	Kronecker symbol
ϵ	inverse aspect ratio
ϵ_0	electric constant
η_a	ratio of the radial temperature and density scale length of species a
η_j	constant
γ	growth rate of the mode (chapter 3); parameter proportional to the friction force (chapter 4)
Γ_a	particle flux of species a
γ_{a_j}	coefficient of g_{a_j}
$\hat{\gamma}$	normalised growth rate
$\hat{\nu}$	collisionality (expansion parameter)
$\hat{\omega}_{\eta*a}$	frequency appearing in section 3.2
ι	rotational transform
κ	trapping parameter
λ	pitch-angle variable
λ_c	value of the pitch-angle variable at the trapped-passing boundary
λ_D	Debye length

λ_L	Landau length
Λ_n	n'th eigenfunction of the eigenvalue problem in section 3.1
$\langle \dots \rangle$	flux-surface average
$\langle \dots \rangle_b$	bounce average
\mathcal{L}	Lorentz operator
\mathcal{F}_i^j	hypergeometric function
μ	parameter
μ_0	vacuum magnetic permeability
μ_a	magnetic moment of particle species a
∇_{\parallel}	gradient along the magnetic field
ν^*	collisionality
ν	collision frequency
ν_D^{ab}	collision (deflection) frequency for collisions between particle species a and b
ν_{ab}	collision frequency for collisions between particles of species a and b
ω_b	bounce frequency
ω	mode frequency
ω_0	absolute value of the real part of the mode eigenfrequency
Ω_a	gyrofrequency of particle species a
ω_{*a}	diamagnetic frequency
ω_{D_a}	magnetic drift frequency
$\omega_{D_{a_0}}$	frequency appearing in section 3.2
ϕ	electric potential
$\pi_{a_{jk}}$	components of the viscosity tensor of particle species a
ψ	poloidal magnetic flux function
ρ	normalised minor radius
ρ_a	gyroradius of particle species a
ρ_{a_θ}	poloidal gyroradius
ρ_{s_a}	normalised gyroradius of particle species a
σ	sign of the parallel velocity; sign of the real part of the eigenfrequency
\sqrt{g}	Jacobian
τ_a	collision time of particle species a
τ_a^*	ratio of the temperature of particle species a to the electron temperature
τ_b	bounce time

τ_D	diffusion time
τ_E	energy confinement time
τ_p	zonal-flow damping time
τ_{ab}	collision time for collisions between particles of species a and b
θ_b	bounce angle
θ	poloidal angle; ballooning angle
$\tilde{\omega}_{D_a}$	normalised magnetic drift frequency
$\tilde{\omega}_{D_{sa}}$	frequency appearing in section 3.2
$\tilde{\phi}$	perturbed electric potential
\tilde{v}	constant
ε	small parameter
ε_a^*	total energy of particle species a
ε_a	kinetic energy of particle species a
φ	toroidal angle
φ_i	Boozer angle of minimum (maximum) γ
ϑ	gyroangle
κ	magnetic curvature
Π_a	momentum flux tensor of particle species a
\mathbf{A}	vector potential of the magnetic field
\mathbf{a}	acceleration
\mathbf{B}	magnetic field strength
\mathbf{b}	unit vector along the magnetic field
\mathbf{E}	electric field
\mathbf{e}_i	unit vector
\mathbf{h}	equilibrium current divided by p'_0
j_0	equilibrium current
Q_a	energy flux of particle species a
\mathbf{q}_a	heat flux of particle species a
\mathbf{R}	guiding-centre position
\mathbf{r}	particle position
\mathbf{R}_a	friction force of particle species a
\mathbf{R}_{ab}	friction force between particle species a and b
\mathbf{v}	particle velocity
\mathbf{v}_d	drift velocity

v_E	gyroaveraged $\mathbf{E} \times \mathbf{B}$ velocity
v_\perp	velocity perpendicular to the magnetic field
z	phase-space variable
$\hat{\dots}$	ensemble average
ξ	ratio of the parallel velocity to the total velocity
$\{\dots\}$	velocity-space average
a	minor radius of the device
A'	derivative of a quantity A with respect to the radial coordinate ψ
A_{a_i}	thermodynamic forces
a_{a_j}	coefficient of the distribution function
$A_{a_i\parallel}$	parallel thermodynamic force
B_0	reference magnetic field strength
b_a	parameter in section 3.2
b_{a_0}	parameter in section 3.2
b_{a_j}	coefficient of the distribution function
B_{max}	maximum magnetic field strength
B_{min}	minimum magnetic field strength
c^*	integration constant
$C_a(f_a)$	collision operator of particle species a
c_s	ion sound speed
$C_{ab}(f_a, f_b)$	collision operator for collisions between particles of species a and b
D_{ab}	diffusion coefficient for collisions between particles of species a and b
$E(k)$	complete elliptic integral of the first kind
e_a	charge of particle species a
E_r	radial electric field
F_a	distribution function of particle species a
f_a	reduced distribution function of particle species a
f_c	effective fraction of circulating particles
f_s	constant used in model potential
f_z	fraction of impurities
F_{mirror}	mirror force
$G(x)$	Chandrasekhar function
g_a	nonadiabatic part of the perturbed distribution function of particle species a

G_i	geometric constant
g_{a_j}	part of the distribution function, defined by a Spitzer problem
H	Heaviside function
h	parameter in section 4.2
h_a	part of the distribution function, defined by a Spitzer problem
I	toroidal current
J	poloidal current
J_n	n 'th Bessel function
K	integration constant
k	trapping parameter
$K(k)$	complete elliptic integral of the second kind
K_a^*	constant
k_{\parallel}	parallel wavenumber
k_{\perp}	perpendicular wave number
k_{θ}	poloidal wave number
K_a	integration constant
L	macroscopic scale length; angular momentum
L_a	operator in section 3.1
$L_j^{(m)}$	generalised Laguerre polynomial
L_{\parallel}	scale length parallel to the magnetic field
L_{\perp}	scale length perpendicular to the magnetic field
L_{n_a}	inverse radial density scale length of particle species a
L_{T_a}	inverse radial temperature scales length of particle species a
M_a	operator in section 3.1
m_a	mass of particle species a
M_{ab}^{jk}	matrix element of the collision operator
N_a	guiding-centre density
n_a	particle density of species a
N_{ab}^{jk}	matrix element of the collision operator
P	neoclassical polarisation
p	Laplace transformation variable
p_0	equilibrium pressure
p_a	pressure of particle species a
P_n	n 'th Legendre polynomial

P_{heating}	heating power
q	safety factor
R	local major radius
r	local minor radius
R_0	major radius of the device
R_a	friction force of particle species a
S	variable appearing in eikonal representation
s	magnetic shear
s_a	entropy density
t	time
T_a	temperature of particle species a
u	geometric quantity
u_a	momentum-restoring quantity in the model collision operator
U_{kl}	tensor components appearing in the collision operator
$V(\psi)$	volume within the flux surface labelled with ψ
V_a	flow velocity of particle species a
v_{\parallel}	velocity along the magnetic field
$v_{th,a}$	thermal velocity of particle species a
w	impurity density, normalised to the square of the magnetic field strength
W_{Plasma}	plasma energy
x_a	normalised velocity of particle species a
y	normalised eigenfrequency
Z	impurity charge number
z_a	FLR parameter
Z_{eff}	effective ion charge
$\text{Erf}(x)$	error function
$\ln \Lambda$	Coulomb logarithm

Eidesstattliche Erklärung

Hiermit erkläre ich, dass diese Arbeit bisher von mir weder an der Mathematisch-Naturwissenschaftlichen Fakultät der Ernst-Moritz-Arndt-Universität Greifswald noch einer anderen wissenschaftlichen Einrichtung zum Zwecke der Promotion eingereicht wurde. Ferner erkläre ich, dass ich diese Arbeit selbständig verfasst und keine anderen als die darin angegebenen Hilfsmittel benutzt habe.

(Stefanie Braun)

Curriculum Vitae

Personal information

Name: Stefanie Braun *née* Mahlberg
Address: Marsweg 10, 70565 Stuttgart
Email: stefanie.braun@ipp.mpg.de
Nationality: German
Date of Birth: 07.04. 1983
Place of Birth: D-52062 Aachen

Education

August 2007 - August 2010	Max Planck Institute for Plasma Physics, Stellarator Theory division, Greifswald, Germany PhD in Plasma Physics “Effect of impurities on neoclassical transport in fusion plasmas” Scientific supervisor: Prof. Dr. Per Helander
October 2002 - March 2007	University of Stuttgart, Germany Diploma Mathematics “Griffith’s fracture criterion in piezoelectric ceramics” Major subject: Mathematics Minor subject: Physics
September 1993 - July 2002	Oscar-Paret-Schule Freiberg a.N., Germany Abitur

Awards

Prize “Best Diploma in Mathematics in the academic year 2006/2007”
awarded by “Verein Freunde der Mathematik an der Universität Stuttgart e.V.”

Miscellaneous

June 2010	Participation in the 60 th Lindau Nobel Laureate Meeting, Lindau, Germany
August 2007 - August 2010	Member of the International Max Planck Research School on Bounded Plasmas
April 2008 - July 2010	Max Planck Institute for Plasma Physics, Greifswald, Germany PhD representative
September 2009 - October 2009 and May 2008 - June 2008	Chalmers University of Technology, Dep. of Applied Physics / Dep. of radio and Space Sciences, Gothenburg, Sweden Research visits
August 2005 - December 2005	Uppsala University, Uppsala, Sweden Academic exchange semester within the ERASMUS programme
September 2003	University of Stuttgart, Germany Teaching assistant for a mathematics course for study beginners

(Stefanie Braun)

Publications

Papers in Refereed Journals

- S. Braun, P. Helander
“Pfirsch-Schlüter impurity transport in stellarators”
Phys. Plasmas **17**, 072514 (2010)
- T. Fülöp, S. Braun and I. Pusztai
“Impurity transport driven by ion temperature gradient turbulence in tokamak plasmas”
Phys. Plasmas **17**, 062501 (2010)
- S. Braun, P. Helander, E.A. Belli, J. Candy
“Effect of impurities on collisional zonal flow damping in tokamaks”
Plasma Phys. Control. Fusion **51**, 065011 (2009)

Conference Contributions

- T. Fülöp, S. Braun, I. Pusztai
“Impurity transport driven by electrostatic turbulence in tokamak plasmas”
37th EPS conference on Plasma Physics, Dublin, Ireland (2010)
- S. Braun, P. Helander, E. A. Belli, J. Candy
“Collisional zonal-flow damping in an impure tokamak plasma”
36th EPS conference on Plasma Physics, Sofia, Bulgaria (2009)
- S. Braun, P. Helander
“Collisional zonal-flow damping in an impure tokamak plasma”
Spring Meeting of the German Physical Society, Greifswald (2009)

Acknowledgements

When I came to Greifswald nearly three years ago, someone told me that everyone cries twice in this town: once when coming and once when leaving. I had no problems believing the first part; to my surprise, the latter has come true as well, and this is mainly due to the people I have met there.

First, I'd like to thank Per Helander, whom I had the great luck to have as supervisor. His brilliance and never-ending enthusiasm for physics were always of help with problems and a source of motivation and, no matter how busy, he never hesitated to take the time to answer my questions. Not even the severe winter weather and its consequences could stop him from being the world's best supervisor.

Furthermore, I'd like to thank the whole Stellarator Theory division for the always friendly and welcoming atmosphere. In particular, special thanks to Ralf Kleiber and Axel Könies for many helpful clarifications and discussions, Alexey Mishchenko and Yuriy Turkin for their help with the numerics, Matthias Borchardt and Henry Leyh for the support with everything related to computers, Andrea Pulss for many a fixed LaTex problem and the nice figures, Jutta Gauger for all the hours she had to fight with the "Reisekostenstelle" because my business trips all went via Stuttgart, and Jörg Riemann for making me laugh.

I gratefully acknowledge Tünde Fülöp for inviting me to Gothenburg and giving me the chance to work with her, and for all the other support she has given me. Thank you as well to Jeff Candy and István Pusztaí, with whom I also had the pleasure to work in Gothenburg.

A big thank you also goes to my friends Peter Drewelow, Tamás Fehér, Karla Kauffmann and Håkan Smith, for making life in Greifswald so much more worth living, and for all the funny, sad, thoughtful and cheerful hours we spent together. And for bearing me either whistling - when I was in a good mood - or complaining - when I wasn't - all the time, I don't know which was harder.

I'd also like to thank my family, who haven't seen too much of me during these three years, and especially my parents, who have always encouraged my interest in science. Since they also financially supported the first 23 years of my life and I haven't thanked them properly before, I'd like to do so now.

Finally, my greatest thanks go to my husband Flo for dryly commenting my crazy plans to move to the other end of Germany right after our wedding with the words 'Well, I guess this means we have to buy a BahnCard...'. Thank you so much for your understanding and for going with me through these three difficult years of long-distance relationship. Without your support I wouldn't have managed it.

